Università degli Studi di Padova

Dipartimento di Ingegneria Industriale

Corso di Laurea Magistrale in Ingegneria Meccanica

Tesi di laurea

Structural analysis of a rugby wheelchair frame during field and laboratory tests

Relatore: **Prof. Nicola Petrone**
Dipartimento di Ingegneria Industriale

Correlatore: **Ing. Daniela D'Onofrio**
OffCarr s.r.l.

Laureando: **Francesco Bettella**

Anno Accademico 2015/2016

Summary

INTRODUCTION

Wheelchair Rugby was born to give an opportunity to play at high level to many people with disabilities. People with disabilities as tetraplegia struggled to find place in basketball's team for their difficulties in throwing the ball. In wheelchair rugby they are the protagonists. In this sport there is an upper limit of disability level and that allows everyone to feel part of the team.

Every player can find his role. Who has less problems to the upper limbs (high points) can be a striker and carry the ball and who has many problems to catch the ball (low points) can be a defender. It seems that defenders may have a marginal role; instead they are the fulcrum of the team. They have to block the opposing strikers and all the attack actions of the opposing team. But they have also to protect the team mates from the opposing defenders. To do this all contacts between the wheelchairs are allowed.

The blocks and the hits are the essence of the play. A failed block can give a point to the other team and a good block can transform a defensive action in offensive one. The players have to be strong to stop the opponent or to keep him far from the action. In the same time, they have to be agile to escape the opposing block.

The wheelchair must have the same characteristics of the players. They have to be strong and resistant to very hard collisions, every part of the frame and its connection may be studied for prevent any breakings or damages. But in the same time they must be lightest as possible and mostly they have to be manoeuvrable. So its construction isn't so simple and it represent a synthesis of these two characteristics.

The aim of this study is to purpose a method to analyse the behaviour of its frame in different load conditions and give many useful elements to improve the existing model, in parallel with biomechanical evaluations and performance measurements.

CHAPTER 1: WHEELCHAIR RUGBY

1.1 Introduction to Wheelchair Rugby

Wheelchair Rugby is a mixed team sport for male and female tetraplegics. A unique sport created by athletes with a disability, it combines elements of basketball, rugby and ice hockey. Players compete in teams of four to carry a ball across the opposing team's goal line.

Contact between wheelchairs is permitted, and it is an integral part of the sport as players use their chairs to block and hold opponents.

Wheelchair rugby players compete in manual wheelchairs specifically designed for the sport. Players must meet minimum disability criteria and be classifiable under the sport classification rules.

Wheelchair Rugby is a Paralympic sport, with twenty-six countries competing in international competition and more than ten others developing national programs.

1.2 History of Wheelchair Rugby

Wheelchair Rugby was invented in 1977 in Winnipeg, Canada, by a group of quadriplegic athletes who were looking for an alternative to wheelchair basketball. They wanted a sport which would allow players with reduced arm and hand function to participate equally. The sport they created, originally called Murderball, is now known as Wheelchair Rugby.

The sport first appeared outside of Canada in 1979, at a demonstration at Southwest State University in Minnesota. The first Canadian National Championship was held that same year. The first team in the United States was formed in 1981, and the first international tournament, bringing together teams from the United States and Canada, was held in 1982. Throughout the 1980's, other local and national tournaments took place in various countries. The first international tournament with a team from outside North America was held in 1989 in Toronto, Canada. With teams from Canada, Great Britain and the United States, this was a breakthrough for developing international competition and cooperation.

In 1990, Wheelchair Rugby appeared at the World Wheelchair Games as an exhibition event, which helped fuel the sports rapid growth and popularity internationally.

In 1993 with 15 countries actively participating, the wheelchair rugby was recognized as an official sport for athletes with a disability, and the International Wheelchair Rugby Federation (IWRF) was established as a sport section of the International Stoke Mandeville Wheelchair Sports Federation. That same year seven countries participated at the Stoke Mandeville International World Wheelchair Games.

In 1994, Wheelchair Rugby was officially recognized by the International Paralympic Committee (IPC) as a Paralympic sport. The first Wheelchair Rugby World Championships were held the following year in Nottwil, Switzerland with eight teams competing. In 1996 Wheelchair Rugby was included as a demonstration sport in the Atlanta Paralympic Games with 6 countries competing. In 1998, Toronto, Canada hosted the second IWRF Wheelchair Rugby World Championship, and 12 countries attended.

Wheelchair Rugby was recognized as a full medal sport for the first time at the 2000 Paralympic Games in Sydney, Australia. It has since been featured at the Paralympic Games in Athens in 2004, Beijing in 2008, London in 2012 and is included in the competition program for the 2016 Paralympic Games in Rio de Janeiro. World Championships and the Paralympics are held every 4 years.

Currently there are more than forty countries that actively participate in the sport of wheelchair rugby, or who are developing programs within their nation. The IWRF includes three zones: The Americas, with six active countries; Europe, with fourteen active countries; and Asia-Oceania, with six active countries.

1.3 Classification

To be eligible to play Wheelchair Rugby, individuals must have a disability which affects the arms and legs. Most players have spinal cord injuries with full or partial paralysis of the legs and partial paralysis of the arms. Other disability groups who play include cerebral palsy, muscular dystrophy, amputations, polio, and other neurological conditions. Men and women compete on the same teams and in the same competitions.

Players are assigned a sport classification based on their level of disability; teams must field players with a mix of classification values, allowing players with different functional abilities to compete together.

In the beginning of Wheelchair Rugby, according to its classification rules, athletes were divided into three sport classes, largely determined by medical diagnosis and neurological level of spinal cord injury. In 1991 a sport-focused classification system for Wheelchair

Rugby was started. Although the spinal cord injury examination was used as a guideline in classifying the physical assessment, the classification rules were expanded to include, in the determination of the sport class, fundamental activities of Wheelchair Rugby. This change was made, on the other hands, to accommodate the growing number of athletes with different disabilities from spinal cord injury. People with diseases as poliomyelitis, cerebral palsy, muscular dystrophy, multiple sclerosis, multiple amputations and other conditions with impairment in muscle strength similar to tetraplegia, started to be classified and compete in Wheelchair Rugby.

Classification is a continuous updating progress: the last review of the classification rules, by the International Wheelchair Rugby Federation (IWRF), dates to February 2015. All athletes are under regular observation by classifiers, to ensure two important goals:

- to determine eligibility to competition;
- to divide athletes into classes, assigning them a point (0.5, 1.0, 1.5,...3.5). The highest point values are given to players with the least movement restrictions. The lowest point are assigned to those players with the most severe impairments.

People who want to compete in Wheelchair Rugby have to perform different tests and evaluations, to determine the point of classification:

- physical assessment by bench test;
- technical assessment, including a range of sport specific tests and novel non-sport tests;
- observation assessment, consisting of observation of sport-specific activities on court.

A system of classification is necessary both for the athlete and for the team: the assigned point often determines the role of the athlete on court and the type of wheelchair he uses; moreover, according to Wheelchair Rugby rules, the classification point has to be taken into account in the formation of the team playing on court [1].

1.4 The game

Wheelchair Rugby combines elements of rugby, basketball, football and ice hockey and it is played indoor in a basketball court, with a soft-cover volleyball ball. Each team is composed by 4 players and 8 substitutes. For each team, the sum of athletes' classification points playing on court cannot pass 8. During the match, each athlete is assigned a defensive or offensive role.

The field of play is a 15 x 28 m (Figure 1.1), marked by end and side lines and is divided into two halves by the centre line on which the centre circle is also located. On the end lines two cones mark the goal line. At a distance of 1.75 m from the end lines, the key areas are signed. Only 3 defenders are allowed to remain inside these areas while no player is allowed to remain in the opponent's key area for more than 10 seconds when their team is in possession of the ball. On the sides of the court near the side lines penalty areas are marked out.

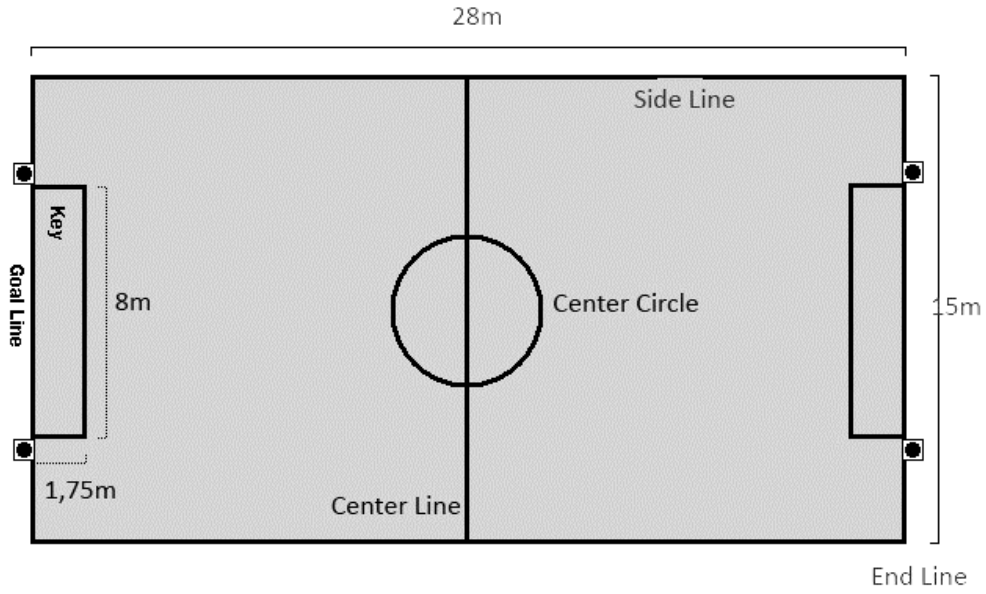

***Figure 1**.1: Wheelchair rugby field.*

The aim of the game is to score a goal by passing or touching the opponent's goal line with two wheels while holding the ball: the team with the highest score at the end of the match, wins. A match is played in 4 quarters of 8 minutes each, with 1 minute break at the end of the first and third quarter and a 5 minute break at the end of the second one. In the case of a tie, 3 minutes extra time is provided. Each team is entitled to 4 time-outs of one minute during the normal length of the game, and one time-out during extended time. If not all the time-outs are used, they can be transferred to extra time.

The game starts in the centre circle of the court: a referee launches the ball vertically between two opponent players. The remaining players take position outside the circle. The ball can be carried, dribbled, passed or stolen in any way, avoiding physical contact between athletes. When moving, players can hold the ball on their thighs, pass it to a team mate or bounce it, but it must be bounced or passed at least once every 10 seconds. Moreover, the team in possession of the ball must pass it to the other half of the court within 15 seconds. After a goal, foul or time-out, the ball is brought back into the game from the end line (when a goal is scored) or from the side lines.

Many unfair sportive behaviours are interrupted by the referees commanding the game. An offensive foul is punished by the loss of the ball, while a defensive foul is punished with

one minute out of the game (in the penalty area). A player under the penalty of leaving the game cannot substitute an injured player. Instead of the one-minute penalty, the referee can award a penalty goal when a player is fouled while in possession of the ball and in position to score a goal [2,3].

Finally, it is worth to remember that Wheelchair Rugby would not exist without the great number of people that help athletes in their primary necessities, inside and outside the game: referees, staff members and volunteers.

1.5 Wheelchairs

The wheelchair is considered part of the player. It is the mean to move ad to express the athletes' specific talents and abilities within the game. At a first sight, it is possible to identify two types of chair: offensive and defensive, as shown in Figure 1.2. Nevertheless, the chair does not automatically determine the role of the athlete during the match.

Figure 1.2: *Offcarr Go Try Rugby Wheelchair. Left: Offensive model; right: defensive model.*

An offensive chair is set up for speed and mobility, and equipped with a front bumper and wings to prevent other wheelchairs from hooking it. In most cases, players with higher points (more than 2.0) use this type of chair. Defensive wheelchairs contain bumpers set up to hook and hold opponents players. These wheelchairs are most often used by players with lower points (less than 1.5).

According to the sport rules, wheelchairs must meet some specifications, for reasons of equality and safety: the athlete is responsible of respecting them. The player who does not meet these specifications, is automatically banned from the game, until he returns on the established standards. The main specifications coming from IWRF Rugby International Rules.

1.6 Rules and regulations

Below there is an extract of the official Rules and Regulations drawn up by the International Wheelchair Rugby Federation (IWRF) [2]. All the wheelchair constructors have to follow these rules for realize a regular wheelchair.

SECTION 4. Wheelchair

Article 23. Compliance with specifications

The wheelchair is considered to be part of the player. Each player is responsible for ensuring that his wheelchair meets all specifications for the duration of the game. If a wheelchair does not meet these specifications it shall be barred from the game until it is brought into compliance.

Article 24. Width

There is no maximum width of wheelchair. No point on the wheelchair may extend in width beyond the widest point of the push rims.

Article 25. Length

The length of the wheelchair as measured from the front-most part of the back wheel to the front-most part of the wheelchair cannot exceed 46 centimeters. (See Wheelchair diagram B)

Article 26. Height

The height of the wheelchair, as measured from the floor to the midpoint of the seat side rail tubing halfway between the front and back of the side rail, cannot exceed 53 centimeters. (See Wheelchair diagram B)

Article 27. Wheels

The wheelchair shall have four wheels. The two large wheels at the back that are used to propel the wheelchair are referred to as the main wheels; the two small wheels at the front are referred to as the casters. (See Wheelchair diagram A)

a. The main wheels shall have maximum diameter of 70 centimeters. Each main wheel must be fitted with a spoke guard that protects the area contacted by another wheelchair, and a push rim. There shall be no bars or plates extending around the main wheels. The rearmost part of the main wheel shall be considered the back of the wheelchair and nothing can extend past this point. (See Article 28)

b. The casters must be on separate axles positioned a minimum of 20 centimeters apart, measured center to center. The housing that holds the caster must be positioned no more than 2.5 centimeters away from the main frame of the wheelchair, measured from the inside edge of the housing to the outside edge of the mainframe.

Article 28. Anti-tip devices

The wheelchair shall be fitted with an anti-tip device attached at the rear of the wheelchair which must contain 2 wheels a minimum of 40cm apart. If the wheels of the anti-tip device are fixed, they cannot project further to the rear than the rearmost point of the main wheels. If the wheels of the anti-tip device swivel, the housing that holds them cannot project further to the rear than the rearmost point of the main wheels. The bottom of the wheels of the anti-tip device must be no more than 2 centimeters above the floor. (See Wheelchair diagram B)

Article 29. Bumper

The wheelchair may be equipped with a bumper projecting from the front of the wheelchair. The bumper, or the front-most part of the wheelchair if no bumper is present, must conform to the following requirements:

a. The front-most part of the bumper, measured to the midpoint of the rod or tubing with the casters in a forward-rolling position, must be exactly 11 centimeters from the floor. (See Wheelchair diagram B)

b. The front-most part of the bumper must be a minimum of 20 centimeters wide measured side to side and must span straight across.

c. At its front-most point, the bumper must not extend more than 20 centimeters beyond the forward edge of the caster housings. (See Wheelchair diagram B)

d. At its widest point, the bumper must not extend more than 2 centimeters beyond the outside edges of the caster housings on each side of the wheelchair. (See Wheelchair diagram A)

e. The lowest point of the bumper must be a minimum of 3 centimeters from the floor. (See Wheelchair diagram B)

f. The highest point of the bumper must be no more than 20 centimeters from the floor. (See Wheelchair diagram B)

g. The rod or tubing used for the bumper must be a minimum of 0.635 centimeters in diameter. (See Wheelchair diagram C)

h. The rod or tubing used for the bumper must be rounded and can have no edges or protrusions that could give a player an unfair mechanical advantage.

i. All rods or tubing used for the bumper should be bent on a bender so that all corners are round. The bends shall not cause the tube to wrinkle, flatten, or flare.

j. The inside curvature of all bends must be a minimum of 2 centimeters in diameter.

k. The minimum outside measurement of any portion of the bumper, measured from outer edge to outer edge, is 3.27 centimeters. (See Wheelchair diagram C)

l. There must be a bar connecting the bumper to the main frame of the wheelchair extending from the widest point of the bumper. This connection must be straight, and must be made at an angle of 45° or greater to the bumper and to the main frame, measured in the horizontal plane as viewed from above.

Article 30. Wings

The wheelchair may be equipped with wings on either side in the area between the front of the wheelchair and the main wheels. Each wing must conform to the following requirements:

a. The outer-most point of contact of the wing must be exactly 11 centimeters from the floor.

b. The lowest point of the wing must be a minimum of 3 centimeters from the floor. (See Wheelchair diagram B)

c. The highest point of the wing must be no more than 20 centimeters from the floor. (See Wheelchair diagram B)

d. The rod or tubing used for the wing must be a minimum of 0.635 centimeters in diameter.

e. The wing cannot extend laterally beyond the center of the tire on the main wheel.

f. The wing may stop at the rear wheel or it may continue past the rear wheel with a connection to the main frame. A wing that stops at the main wheel must conform to the following additional requirements:

   i. It must be rounded at the end without any sharp edges.

   ii. It must end within 1 centimeter of the main wheel. (See Wheelchair diagram B)

g. The space above the wing, extending from the top edge of the wing to 10 centimeters above the top edge of the wing and from the front of the wing to 1 centimeter behind the tire of the main wheel, must be obstacle free.

Article 31. Comfort and safety

The wheelchair must conform to the following additional specifications:

a. All protrusions from the wheelchair, such as push-bars, crossbars, or hooks, must be padded. Note: Handles for pushing the chair are not permitted.

b. No steering devices, brakes, gears, or other mechanical devices are permitted to help operate the wheelchair. If the wheelchair is equipped with such devices, they must be modified so they are not operational and must be repositioned so they do not represent a safety hazard.

c. The wheelchair may be fitted with a device under the front end to prevent it from tipping forward. This device must conform to the following specifications:

d. It cannot be the front-most point of the wheelchair.

e. There is no minimum height above the floor, but it may not be in constant contact with the floor

f. It cannot damage the floor.

   i. Any contact between this device and the floor will be governed by the Physical Advantage rule (Article 79).

   ii. Tires must not leave noticeable marks on the playing surface.

   iii. No counterweights may be added to the wheelchair.

   iv. One cushion, with a maximum thickness of 10 centimeters, is permitted on the seat of the wheelchair.

g. A player may use padding between his knees. This padding must not protrude above the top of the knees.

h. A player may be strapped to the wheelchair.

i. If there is a possibility of a player's feet slipping off the footrest of the wheelchair, a strap or elastic must be used to behind the legs or around the feet to prevent this from occurring.

j. Players may use additional devices to support the ball. This support must be level with or higher than the seat frame. No part of the ball can rest within the seat frame. Straps may be used to secure the ball as long as 75% of the ball is available to be played and only make contact within the bottom 25% of the ball.

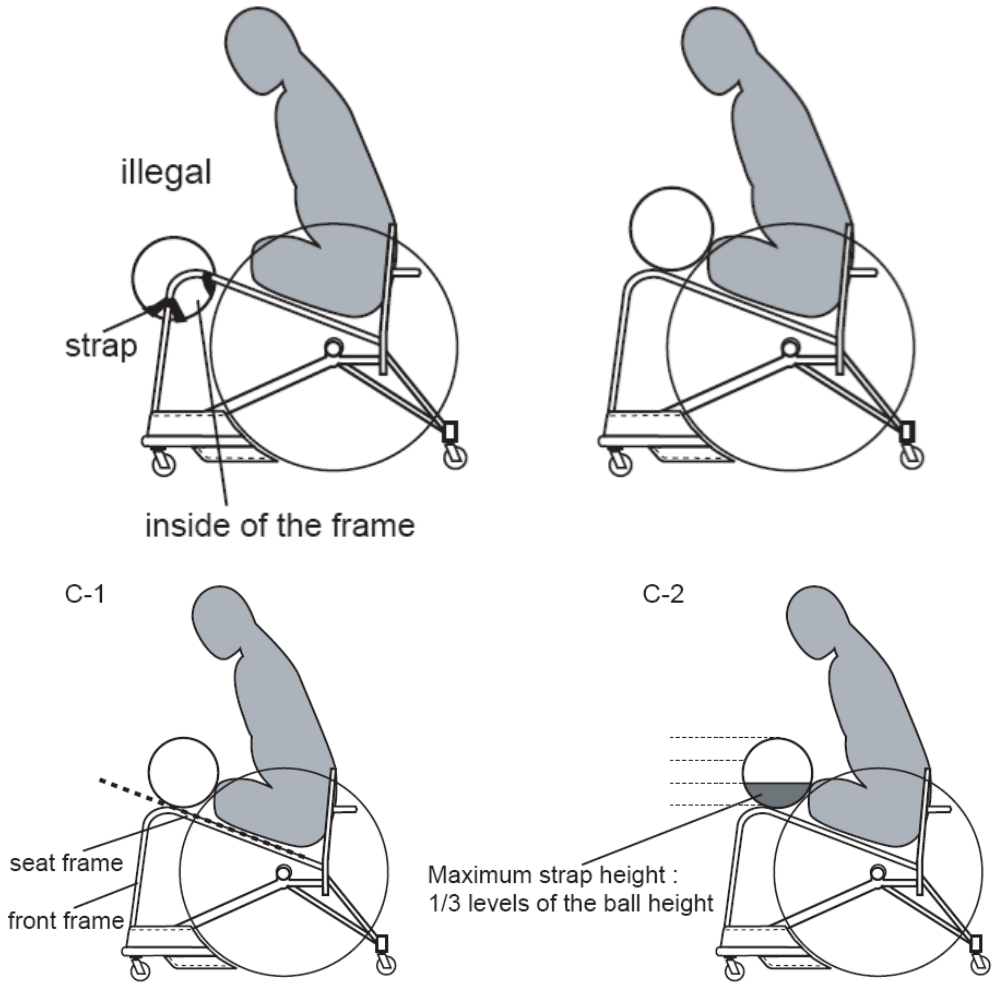

***Figure 1.3**: Position of the ball*

Article 32. Modifications:

Any part of the wheelchair or player equipment may be modified to improve comfort or safety or for medical reasons. These modifications must be safe, must conform to all the wheelchair specifications in these Rules, and may not create any mechanical advantage. Modifications made for medical reasons must be listed on the player's classification card.

Innovative changes that give a mechanical advantage or that do not conform to the presently accepted norms for a wheelchair, as detailed in these Rules, may not be made without prior approval from the IWRF. Such changes must be presented to and approved by the Technical Commission of the IWRF, in writing.

Approval must be received no less than two months prior to the commencement of World Championship, Zone Championship, or Paralympic Games, and one month prior to any other sanctioned event. As the IWRF requires one month to properly process a request and render a decision, requests should be made three months prior to World

Championship, Zone Championship, or Paralympic Games, and two months prior to other sanctioned events.

The commencement of such events is the date of the opening ceremonies, or if there are no opening ceremonies, the date of the first day of competition.

Section 4:

WHEELCHAIR

Diagrams

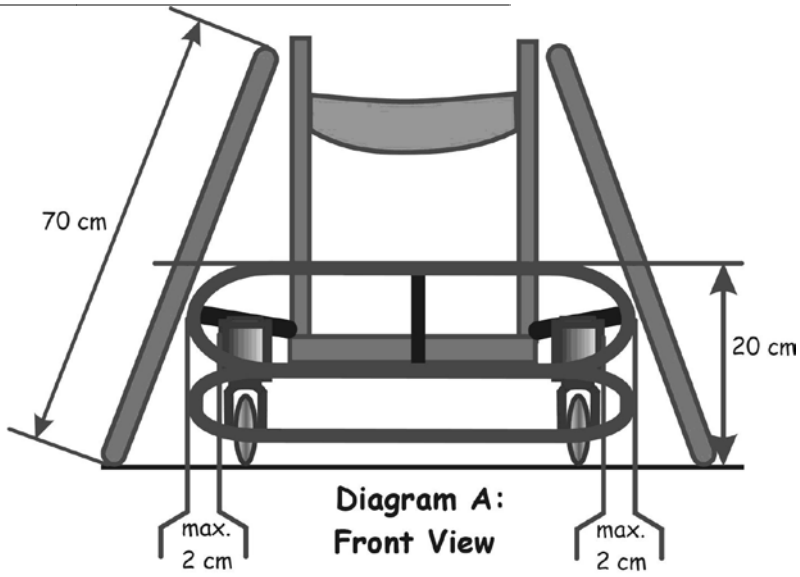

Diagram A: Front View

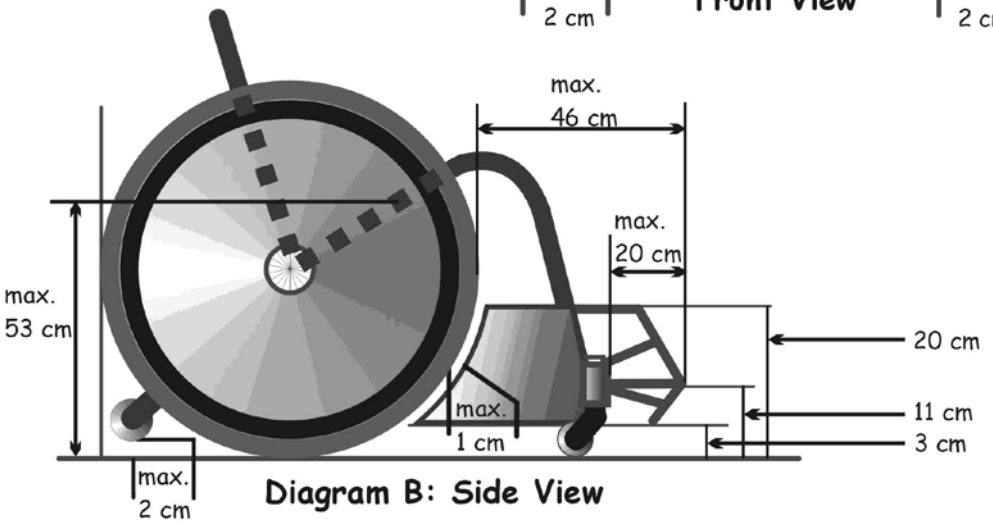

Diagram B: Side View

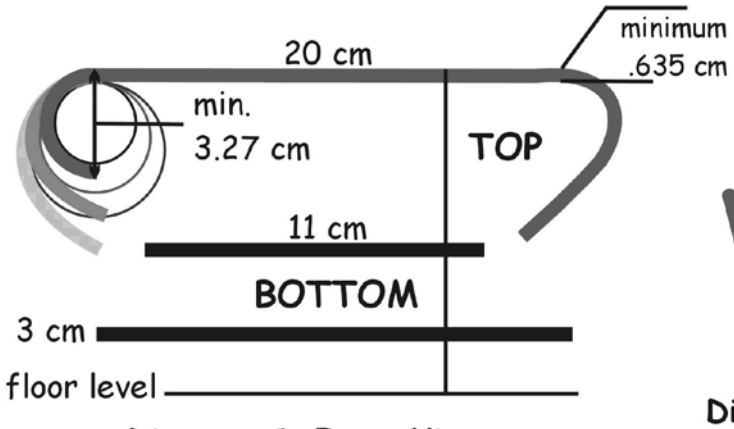

Diagram C: Front View bends in bumper construction

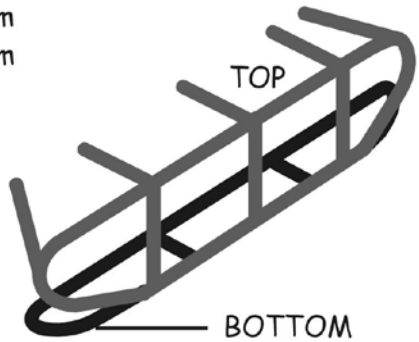

Diagram D: Diagonal View side connections of bumper

SECTION 10. Principles of contact

Although wheelchair rugby is a contact sport, all types of contact are not permitted under all circumstances. Other factors such as the position, location, speed, and vulnerability of players must be considered.

Unsportsmanlike conduct cannot be excused in the name of legal, aggressive play. Referees must consider safety without detracting from the game. Each situation must be judged on its own merits.

This section will detail principles that must be considered by referees when applying the rules. These principles permit contact while protecting players and giving them the opportunity to defend themselves, their positions, and the ball. They allow the referees to judge each situation without interfering with the flow of the game.

Article 86. Safety

While contact between wheelchairs is permitted in Wheelchair Rugby, players should not exceed the reasonable force required when challenging an opponent for position or for possession of the ball. Players are responsible if they initiate contact in a way that places another player at risk. They are expected to make an effort to avoid dangerous contact by slowing down, stopping, or changing direction if necessary.

Referees will judge reasonable force based on a number of factors, including:

a. The relative size, speed, and positions of the players.

b. The angle at which contact occurs.

c. The ability of the player being hit to see and anticipate the contact.

d. The status of the player at time of contact, including whether he is stationary or moving, maintaining his balance, or in the act of falling.

The safety features of a wheelchair, such as the anti-tip devices, cannot be exploited by an opponent to gain an advantage involving contact.

Article 87. Position on the court

A player is entitled to occupy a legal position that is not already occupied by another player. A player who is occupying a position cannot be made to give up that position by means of illegal force. However, a player cannot passively claim a position if challenged by an opponent. A player who has possession of the ball will be given more latitude because he has the added responsibility to protect the ball.

A player attempting to move to a new position may be blocked by one or more opposing players.

Opposing players may use contact against one another in an attempt to occupy a position that is not already clearly occupied by another player.

Article 88. Vertical space

A player is entitled to his immediate vertical space, determined when the player is in an upright, seated position as follows:

a. Measured side-to-side, from the outside edge of one shoulder to the outside edge of the other.

b. Measured front-to-back, from the forward edge of his knees to the inside of his backrest.

c. Measured top-to-bottom, from the top of his head to his legs.

When a player has possession of the ball, illegal contact within this space will be charged to the opposing player if it is initiated by the opposing player, or if it is initiated by the player who has possession of the ball as a result of the normal motions required to protect or pass the ball.

Article 89. Advantage

Situations that result in violations or fouls must be judged within the context of the play. An action or situation that has no effect on the play, or that does not create an advantage or a disadvantage for a player or players, should be ignored and play should be allowed to continue. The flow of the game should not be interrupted by trivial violations of the rules.

Contact that occurs with no effect on the players involved can be judged to be incidental and play can be allowed to continue.

When applying this principle, the advantage or disadvantage caused must be the result of a player's actions, and not the result of a referee's decisions to make or not to make a call.

SECTION 12. Technical fouls

Article 103. Equipment technical foul

A player may not play with a wheelchair that does not conform to the specifications detailed in these rules. If at any time during the game a player is found to be playing with an illegal wheelchair, he shall be charged with a technical foul.

A coach may make a request to the referee for an inspection of an opposing player's wheelchair during a stoppage in play. If the referee finds that the wheelchair is legal, a sixty second time-out and a technical foul shall be charged to the coach who made the request. If no sixty second time-out remains then a second technical foul shall be charged

to the coach. If two technical fouls are charged to the coach they are to be served consecutively by the same player.

If activity during the game has resulted in a previously legal wheelchair failing to conform to the rules, the player shall be given an opportunity to correct the problem before being charged with a technical foul.

CHAPTER 2: PROJECT: “Improvement of the residual neuromuscular capacities in Wheelchair Rugby athletes”

In October 2015 a scientific project started in Padova, with the aim to assess how Wheelchair Rugby can improve the residual neuromuscular capacities in people with different physical disabilities. A scientific team composed by engineers, doctors, physiotherapists and motor scientists collaborates with the Italian Wheelchair Rugby National Team to perform physical, sportive and metabolic measures, in order to get information about their physical state from a medical and biomechanical point of view. These measures are collected to enhance their sportive performance, with the final goal of entering in the international rankings and participate to the Paralympic Games (Tokyo 2020).

2.1 Partners

Several partners finance and support the project:

- HPNR (Human Potential Network Research Onlus Via Toblino 53, Padova) the proposer company, managing the financial and organizational aspects;
- Fondazione Cassa di Risparmio di Padova e Rovigo
- Industrial Engineering Department (DII) of University of Padova;
- Physiology Department of University of Padova;
- FISPES (Italian Federation for Paralympic and Experimental Sports) providing a representation of the Wheelchair Rugby Italian National Team and its supporting staff;
- Offcarr SRL (Via dell’Artigianato 29, Villa del Conte, Padova), the main provider of Italian rugby wheelchairs, also interested in the investigation of biomechanical properties of movement and posture and on the improvement of the structural frame of wheelchairs.

- OIC foundation (Opera Immacolata Concezione, via Toblino 53, Padova), providing the structures, and the equipment for the athletic preparation.
- Microgate (Via Stradivari 4, Bolzano) providing instruments for the biomechanical study;
- Tecnogym (Via Calcinaro 2861, Cesena, FC) providing instruments for the personal training;
- DJO Italia SRL (Via Leonardo da Vinci 97, Trezzano sul Naviglio MI)
- CIP (Italian Paralympic Committee).

2.2 Aims of the project

The project has a 2 years duration (from October 2015) and within this time, there are three main goals that it aims to achieve:

- improving the motor-functional sportive abilities of Wheelchair Rugby athletes, trying to promote at best their residual capacities;
- identifying individual rehabilitation programs;
- producing scientific protocols in order to classify athletes and supervise their performances during the rehabilitation programs.

Once the project is concluded, the results will be used with spinal unities and other related associations, in order to exploit at best the collected information. The results may be extended for other sports for people with disabilities. Moreover, two or more official classifiers, formed during the project duration, may work together with FISPES and IWRF (International Wheelchair Rugby Federation). Finally, the project may bring to the creation of an Italian reference centre for study and training of Paralympic sports, in the University of Padova, with an official role given by CIP. The project aims at an evaluation of players under different points of view: biomechanical, medical and physiological investigations are able to create a general overview of the athletes. A sport engineering research group works for biomechanical measures, a group of doctors and physiotherapists investigates different medical and physiological aspects, and a sport medicine group works for the athletic training. At the same time it’s conducted a study on the wheelchair frame. In particular, these aims are divided into three main aspects, described in the following lines.

- Biomechanical evaluations.
    1. Study of the athletic performance:
        - measuring of dynamic forward push force and braking;
        - measurement of the ability to spin;
        - evaluation of the effectiveness in applying and sustain blocks;
        - evaluation of the strength of delivering the ball.
    2. Study of the properties of the wheelchair:
        - In field load measurement;
        - Maximum stress detection.
        - FEM simulation with 3D model
    3. Study of posture and stability:
        - pressure distribution on cushion;
        - calculation of the 3D position of the center of gravity;
        - calculation of stability indexes.
- Medical evaluations.
    1. Study of the metabolic consumption:
        - measurement of the metabolic capacity thresholds;
        - estimation of body composition;
        - evaluation of muscle activation.
    2. Study of joint mobility:
        - ROM evaluation of shoulder joint;
        - ultrasound detection of muscle structure in the shoulder.
- Sport medicine evaluations.
    1. Identification of individual training schemes:
        - exercises during the team meetings;
        - exercises to individually perform outside the team training;
    2. Study of physiological variables:
        - Ability of isometric shoulder and elbow flexion/extension;
        - measuring of VO2max in ergometer tests;
        - measuring of RR and REE;
        - measuring of lactate and ventilator threshold (IAT);
        - recording of HR in different training situations;
        - EMG recording for different muscle groups.
    3. Study of an appropriate individual diet:

- Daily calories uptake related to individual consumption and workloads.

2.3 Aims of this work

The aims of this work is to make a structural analysis of the rugby wheelchair's frame and to analyse the performance of the Italian wheelchair rugby athletes. It develops according the following points:

- Prepare the wheelchair with strain gauges and accelerometers and realize some calibrations and infield tests
- Evaluate the athletes' performance using three dynamic tests (conducted with eng. Maria Laura Magrini)
- Make a FEM simulation for:
    - Validating the infield measurement with results' comparison
    - Finding the most critical points of the frame to perform a fatigue life prediction

CHAPTER 3: INSTRUMENTATION

In this chapter we will describe the instrumentation used for the infield test (wheelchair, strain gauges, accelerometer, acquisition system) and its setup.

3.1 Wheelchair

The wheelchair object of the study is the offensive model of the wheelchair Go Try for rugby made by the company Off.Carr s.r.l., based in Villa del Conte, Padova, Italy, as shown in Figure 3.1.

The frame and the wheels are custom made to satisfy the anthropometrical needs of the athlete.

***Figure 3.1**: Offensive GoTry by OffCarr rugby wheelchair*

This offensive version weighs 17,20 kg, the rear wheels have a diameter of 25 inches. All the wheelchair is composed by welded tubes of 7020 Aluminium alloy and for the plates of the bumper 5754 Aluminium alloy is used.

7020 Aluminium alloy is a binary Aluminium – Zinc alloy, with addition of magnesium. This type of alloy, Al-Zn-Mg, after a heat treatment has the highest tensile strength between the aluminium alloys. They can easily soldered. The 5754 Aluminium alloy has lower mechanical properties but the plates haven't structural functions, they are only for protection. The properties of the two material are reported in the following Table 3.1.

Properties	Aluminium 7020	Aluminium 5754
Young Modulus	73 GPa	70 GPa
Poisson's Ratio	0,33	0,33
Ultimate Tensile Stress	190 to 390 MPa	210 to 330 MPa
Yield Tensile Stress	120 to 310 MPa	92 to 280 MPa
Elongation at break	5,8 to 14 %	2 to 17 %

***Table 3.1**: Mechanical characteristics of 7020 and 5754 Aluminium Alloy*

For the infield tests, the wheelchair was set up with four strain gauge bridges in four points of the frame to measure nominal load component. Moreover, a triaxial accelerometer was applied to the main axle tube joint, below the seat.

The second problem faced was to build a safe allocation for the acquisition system and the battery power due to protect them during impacts.

3.2 Strain gauge

The strain gauge is a measuring instrument used to detect small dimensional deformations of a body subjected to mechanical or thermal loads. They can reveal the deformation of a body to which they are attached.

3.2.1 Introduction to strain gauge

3.2.1.1 Strain

The strain is the amount of deformation of a body due to an applied force. More specifically, strain ε is defined as the fractional change in length, as shown in Figure 3.2.

$$\varepsilon = \frac{\Delta L}{L}$$

***Figure 3.2**: Definition of strain*

Strain can be positive (tensile) or negative (compressive). Although dimensionless, strain is sometimes expressed in units such as mm/mm and its magnitude is very small. Therefore, strain is often expressed as microstrain (me), which is e x 10^{-6}.

When a bar is strained with a uniaxial force, as in Figure 1, a phenomenon known as Poisson Strain causes the girth of the bar, D, to contract in the transverse, or perpendicular, direction. The magnitude of this transverse contraction is a material property indicated by its Poisson's Ratio. The Poisson's Ratio ν of a material is defined as the negative ratio of the strain in the transverse direction (perpendicular to the force) to the strain in the axial direction (parallel to the force). $\upsilon = {}^{-\varepsilon_T}/_{\varepsilon}$.

3.2.2.2 The Strain Gauge method

While there are several methods of measuring strain, the most common is with a strain gauge, a device whose electrical resistance varies in proportion to the amount of strain of the device. The most widely used gauge is the bonded metallic strain gauge. The name "bonded gauge" is given to strain gauges that are glued to a larger structure under stress, called the test specimen.

The metallic strain gauge consists of a very fine wire or, more commonly, metallic foil arranged in a grid pattern. The grid pattern maximizes the amount of metallic wire or foil subject to strain in the parallel direction (Figure 2). The cross-sectional area of the grid is minimized to reduce the effect of shear strain and Poisson's Strain. The grid is bonded to a thin backing, called the carrier, which is attached directly to the test specimen. Therefore, the strain experienced by the test specimen is transferred directly to the strain gauge, which responds with a linear change in electrical resistance. In fact, the electrical resistance is directly proportional to the resistivity of the material and to the length of the conductor and inversely proportional to the cross section area of the conductor.

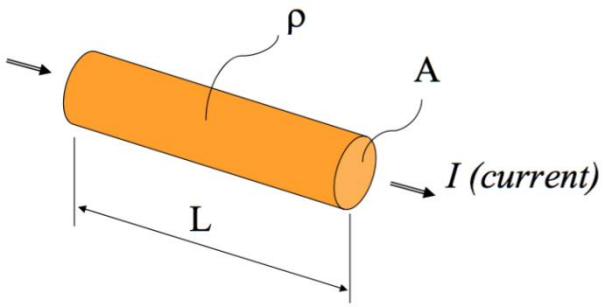

$$R = \frac{\rho L}{A}$$

***Figure 3.3**: Definition of resistance*

with R electrical resistance, ρ resistivity, L length and A cross section area of the conductor.

If a wire or a foil of conductive metal is stretched, it will become skinnier and longer, causing an increase of electrical resistance. Conversely, when it is subjected to a compressive force, it will be broaden and shorten.

$$\frac{\Delta R}{R} = \frac{\Delta \rho}{\rho} + \frac{\Delta L}{L} + \frac{\Delta A}{A}$$

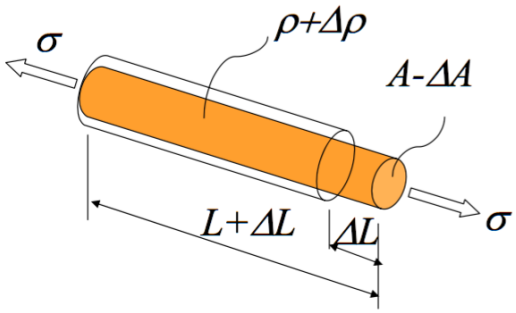

***Figure 3.4**: Deformed conductor*

Strain gauges are available commercially with nominal resistance values from 30 to 3000 Ω, with 120, 350 and 1000 Ω being the most common values and dimensions from few microns to some centimeters.

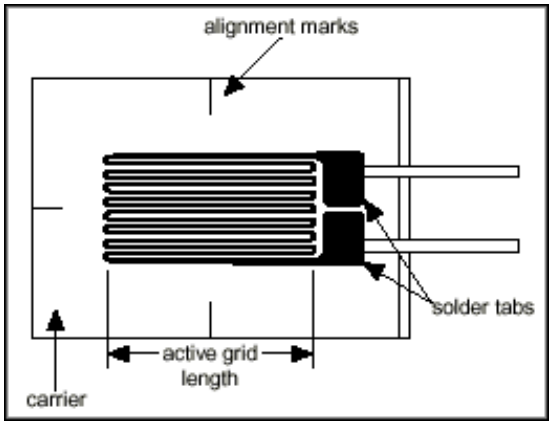

***Figure 3.5**: Bonded metallic strain gauge*

It is very important that the strain gauge is properly mounted onto the surface of the test specimen so that the strain is accurately transferred from the surface, through the adhesive and strain gauge backing to the foil itself.

A fundamental parameter of the strain gauge is its sensitivity to strain, expressed quantitatively as the gauge factor (K). Gauge factor is defined as the ratio of fractional change in electrical resistance to the fractional change in length (strain):

$$K = \frac{\Delta R/R}{\Delta L/L}$$

The gauge factor for metallic strain gauges is typically around 2.

3.2.2.3 Strain Gauge Measurement

In practice, strain measurements rarely involve quantities larger than a few millistrain (e x 10^{-3}), therefore, to measure the strain, it's required accurate measurement of very small changes in resistance. For example, for a test specimen undergone a strain of 500 mε, a strain gauge with a gauge factor of 2 will exhibit a change in electrical resistance of only 2 (500 x 10^{-3}) = 0.1%. For a 120 Ω gauge, this is a change of only 0.12 Ω.

To measure such small changes in resistance, strain gauges are almost used in a bridge configuration with a voltage excitation source. The general Wheatstone bridge, illustrated in Figure 3.6, consists of four resistive arms with an excitation voltage, V_s, that is applied across the bridge.

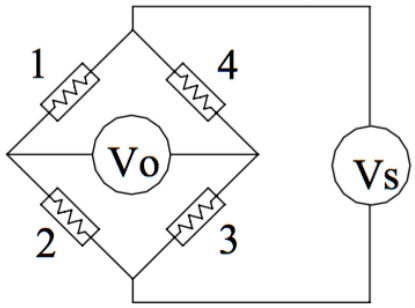

***Figure 3.6**: Wheatstone bridge*

The output voltage of the bridge, V_o, is equal to:

$$V_O = \left[\frac{R_1}{R_1 + R_2} - \frac{R_4}{R_4 + R_3}\right] \cdot V_S$$

From this equation, it is clear that when $R_1/R_2 = R_4/R_3$, the voltage output V_o is zero. Under these conditions, the bridge is said balanced. Any change in resistance in any arm of the bridge results in a nonzero output voltage.

Therefore, if R_i represent active strain gauges, any changes in their resistances will unbalance the bridge and produce a nonzero output voltage. If the nominal resistance of the strain gauge is designated as R, then the strain-induced variation in resistance, ΔR, can be expressed as $\Delta R = R \cdot K \cdot \varepsilon$, from the previously defined Gauge Factor equation.

Assuming that $R_1 = R_2 = R_3 = R_4 = R$, the bridge equation above can be rewritten

$$V_O = \left[\frac{R + \Delta R_1}{R + \Delta R_1 + R + \Delta R_2} - \frac{R + \Delta R_4}{R + \Delta R_4 + R + \Delta R_3}\right] \cdot V_S$$

To express V_O/V_S as a function of strain:

$$\frac{V_O}{V_S} = \frac{K(\varepsilon_1 - \varepsilon_2 + \varepsilon_3 - \varepsilon_4 + \varepsilon_1\varepsilon_3 - \varepsilon_2\varepsilon_4)}{4 + K[2(\varepsilon_1 + \varepsilon_2 + \varepsilon_3 + \varepsilon_4) + (\varepsilon_1 + \varepsilon_3)(\varepsilon_2 + \varepsilon_4)]}$$

and after neglecting the strain products

$$\frac{V_O}{V_S} = \frac{K}{4}(\varepsilon_1 - \varepsilon_2 + \varepsilon_3 - \varepsilon_4)$$

$$V_O = V_S\frac{K}{4}(\varepsilon_1 - \varepsilon_2 + \varepsilon_3 - \varepsilon_4)$$

Measuring the variations of voltage V_0, it's possible to calculate the strain.

3.2.2.4 Wheatstone Bridge Connection

There are three type of connection in the Wheatstone Bridge. It's important to define the bridge factor, that is the amplification factor and gives an information of the bridge's sensitivity.

The quarter bridge connection consists in only one strain gauge, as shown in Figure 3.7.

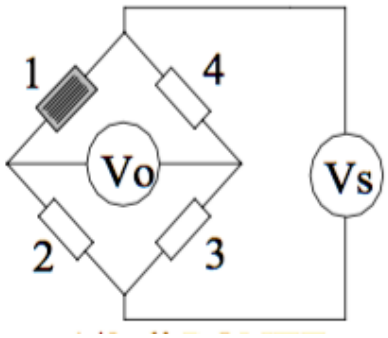

$$V_O = V_S\frac{K}{4}(\varepsilon_1)$$

***Figure 3.7**: Quarter Wheatstone bridge connection*

If ε1=ε, $V_O = V_S\frac{K}{4}(\varepsilon)$ and the bridge factor is 1, the measure is direct.

The other two connections are half and full bridge. There are many different type of configuration depending on the load applied and which is the aim of the measure. The signs of the deformations depend on how the strain gauges are connected and how they are positioned on the object.

In the half bridge connection, they are two strain gauges.

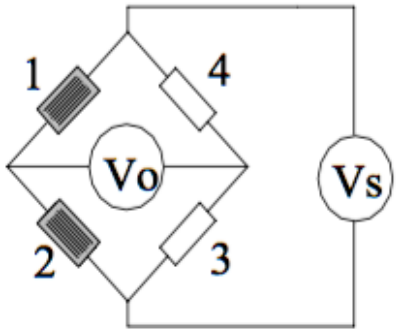

$$V_O = V_S \frac{K}{4}(\varepsilon_1 - \varepsilon_2)$$

***Figure 3.8**: Half Wheatstone bridge connection*

If ε_1=ε and ε_2=-ε, $V_O = V_S \frac{K}{4}(2\varepsilon)$ and the bridge factor is 2.

In full bridge connection, four strain gauges are present.

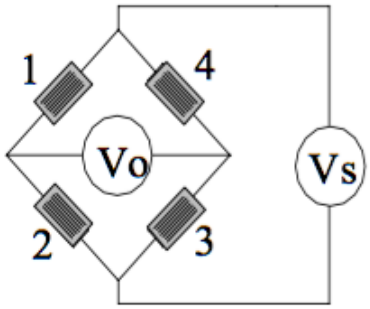

$$V_O = V_S \frac{K}{4}(\varepsilon_1 - \varepsilon_2 + \varepsilon_3 - \varepsilon_4)$$

***Figure 3.9**: Full Wheatstone bridge connection*

If ε1=ε3=ε and ε2=ε4=-ε, $V_O = V_S \frac{K}{4}(4\varepsilon)$ and the bridge factor is 4.

The number of the strain gauges used and their disposition are chosen according to the type of load which the part to be analysed is subjected to.

3.2.2 Strain Gauges

The strain gauges used for the acquisition of the deformations of the frame are produced by the company HBM, Germany, of Y Series (Figure 3.10). These are the principal characteristic of the Y series:

- Linear strain gauge with 1 measuring grid
- Measuring grid foil of Constantan

- Carrier of Polyimide
- Encapsulated measuring grid and Integrated solder tabs
- Maximum permissible effective bridge excitation voltage: 15V

Two different types of strain gauge were used.

- 1-LY43-3/120: nominal resistance 120 Ohm; measuring grid length 3 mm
- 1-LY43-6/350: nominal resistance 350 Ohm; measuring grid length 6 mm

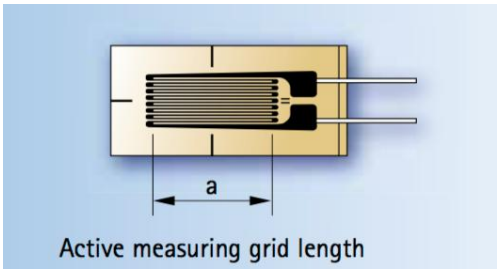

***Figure 3.10**: Strain gauges Y Series*

The HBM strain gauges catalogue with all the details is in the appendix.

3.3 Accelerometer

The accelerometer used is the ICP (integrated circuit piezoelectric) Triaxial Accelerometer model number SAPE-HLS-3010 by HBM company.

The piezoelectric accelerometer uses, as a principle for the detection of the displacement of the mass, the electrical signal generated by a piezoelectric crystal when it is subjected to a compression. In these accelerometers, the mass is suspended on the piezoelectric crystal, which, in this case, acts as a sensor and elastic element. In the presence of an acceleration the mass (which has a certain inertia) compresses the crystal, which generates an electrical signal proportional to the compression. They have a relatively low sensitivity and they can detect high acceleration without damage (even 1000 g).

The ICP accelerometer includes an integrated micro-electronic circuit for signal conditioning, which provides a clean output signal, low impedance and capable of being transmitted over long cables.

Sensitivity @ 100 Hz:

- X axis: 10,40 mV/g
- Y axis: 10,46 mV/g
- Z axis: 10,46 mV/g

3.4 Acquisition system

The acquisition system used is the Somat eDAQLite by HBM, with a 12 V battery. All the cables are Somat Extension Cable (SAC-EXT-MF-2), high-quality 2 meter pre-molded cords set with Male/Female Somat M8 connectors.

This system was chosen because it's very compact, light and reliably. It's made by different layers and it's possible to remove the unused ones, in order to minimize the weight. It's represented in Figure 3.11.

***Figure 3.11**: Somat eDAQlite*

3.5 Wheelchair Setup

In this paragraph, we will describe the location of the instrumentation on the wheelchair. It's fundamental to define the names of the single part and in Figure 3.12 they are described.

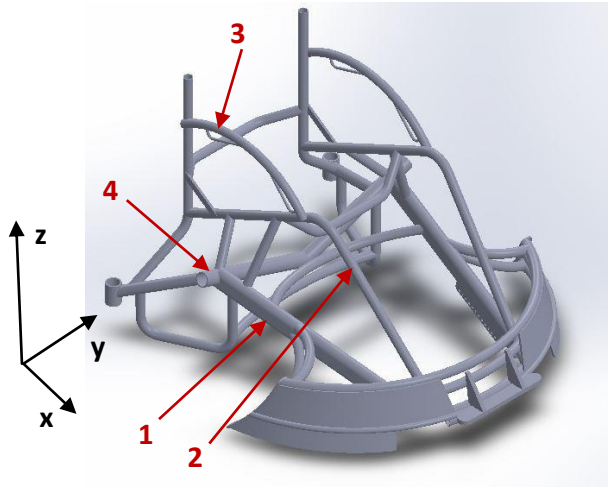

1: Main Tube 2: Front tube 3: Side Tube 4: Axle Tube

***Figure 3.12**: Definition of frame's elements*

3.5.1 Strain gauge bridges position

The position of the four strain gauges bridges is shown in Figure 3.13.

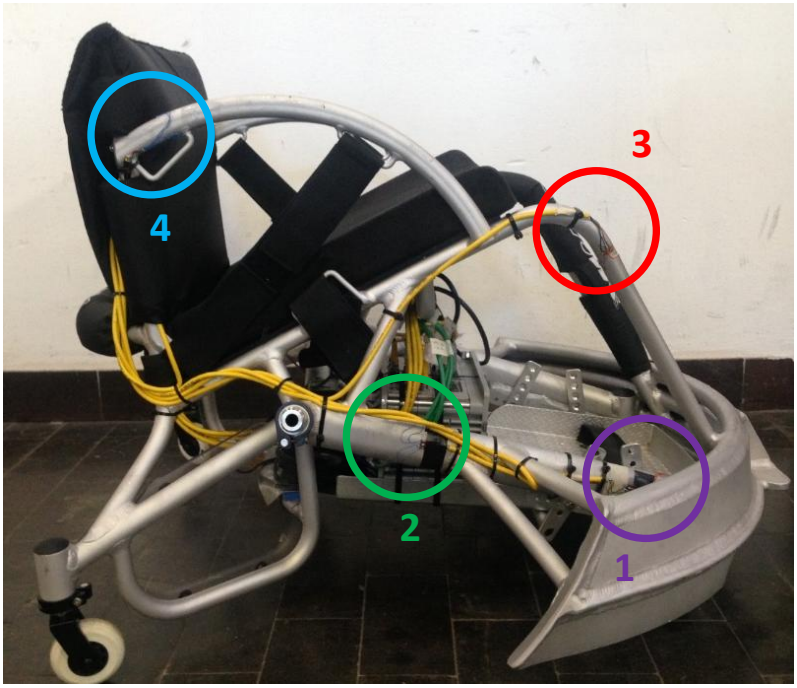

***Figure 3.13**: Position of strain gauges on the frame*

In particular:

- Bridge 1 RMT_AX (Right Main Tube Axial) is a full Wheatstone bridge configuration: four strain gauges of the type HBM 1-LY43-6/350 were used. It's located on the main tube, near the housing of the front small wheel (caster), in the right side of the frame, as shown in Figure 3.14.

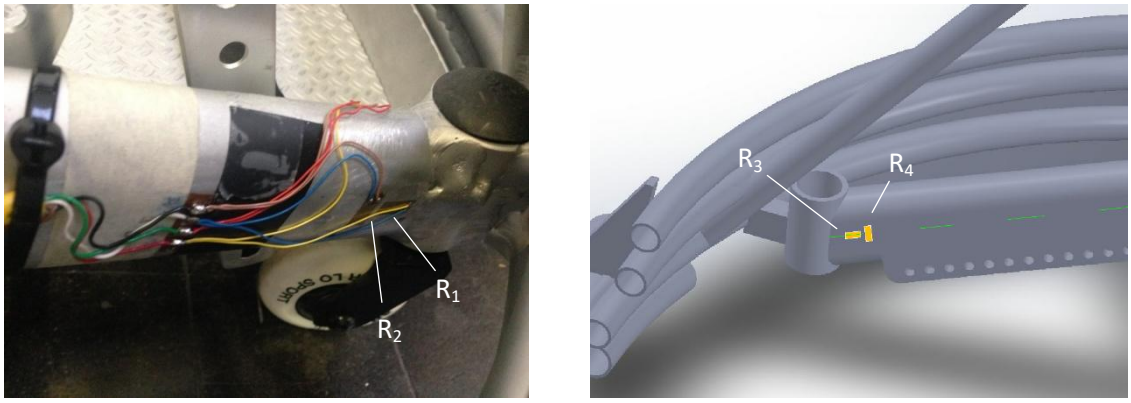

***Figure 3.14**: Position of the bridge RMT_AX*

The bridge 1 is supposed to measure the axial load, clearly the compression force that flows through the main tube during a hit. Two strain gauges, one for each main side of the tube, were positioned with their axles parallel to the axle of the tube, in the middle of the

height of it, 10 mm away from the soldering of the housing of the caster. The other two, one for side, were oriented perpendicularly to the other, 2 mm away from them.

This bridge was defined RMT_AX and it was set up in order to give a positive signal when it's under compression, as shown in the Figure 3.15. There are also indicated how the strain gauges were connected, so $\varepsilon_1=\varepsilon_3=\varepsilon$ and $\varepsilon_2=\varepsilon_4=-\nu\varepsilon$.

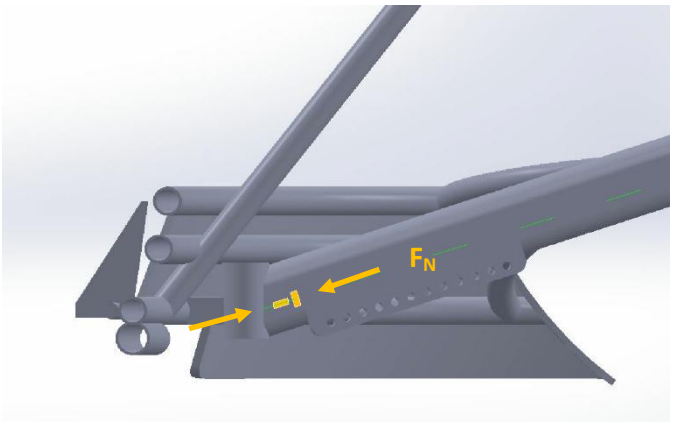

***Figure 3.15**: Definition of RMT_AX sign*

- Bridge 2 RMT_BE (Right Main Tube Bending) is a half Wheatstone bridge configuration: two strain gauges of the type HBM 1-LY43-6/350 were used. It's located on the main tube, near the axle of the main wheel, in the right side of the frame, as shown in Figure 3.16.

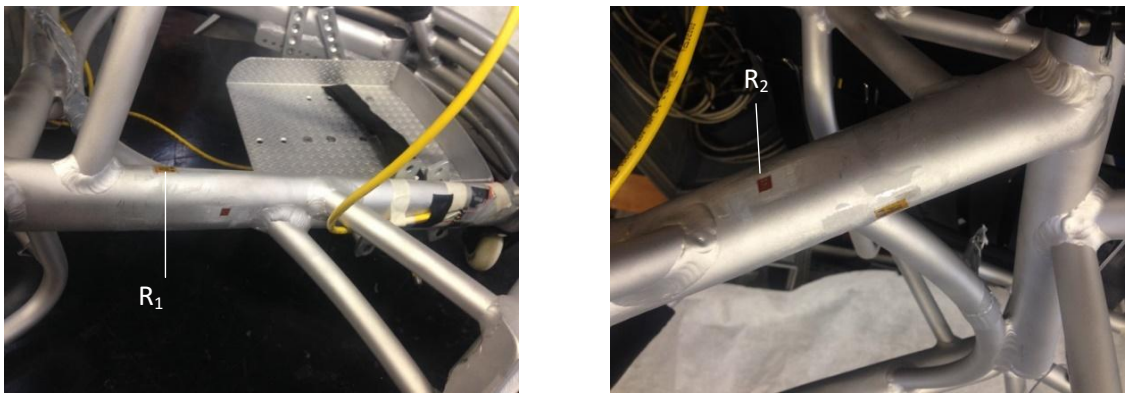

***Figure 3.16**: Position of the bridge RMT_BE*

The bridge 2 is sensitive to the bending moment acting on the main tube. The two strain gauges were positioned with their axes parallel to the axle of the tube, one on the top and one on the bottom of it. The upper one is 17 mm away from the welding of the first tube that supports the seat. The other one is on the lower side, in the same perpendicular cross section area of the tube.

This bridge is defined RMT_BE and it was set up in order to give a positive signal when it's under a bending shown in the Figure 3.17. There are also indicated how the strain gauges were connected, so $\varepsilon_1=\varepsilon$ and $\varepsilon_2=-\varepsilon$.

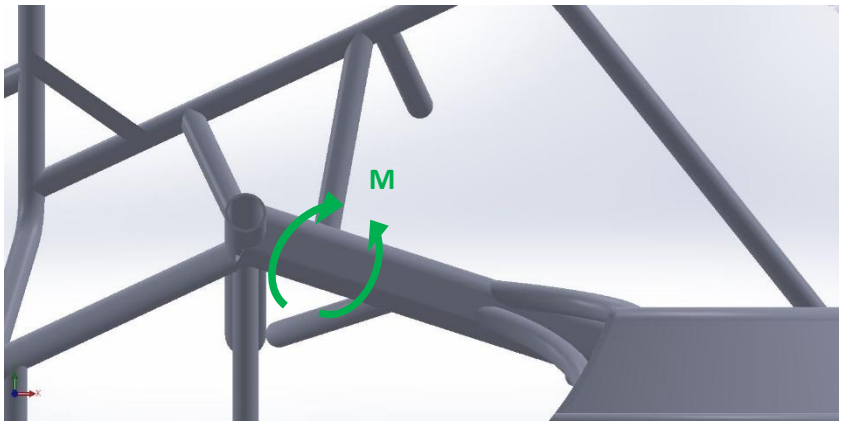

***Figure 3.17**: Definition of RMT_BE sign*

- Bridge 3 RFT_BE (Right Front Tube Bending) is a half Wheatstone bridge configuration. it is composed by two strain gauges of the type HBM 1-LY43-6/350. It's located on the front tube, near the curving of the tube, in the right side of the frame, as shown in Figure 3.18.

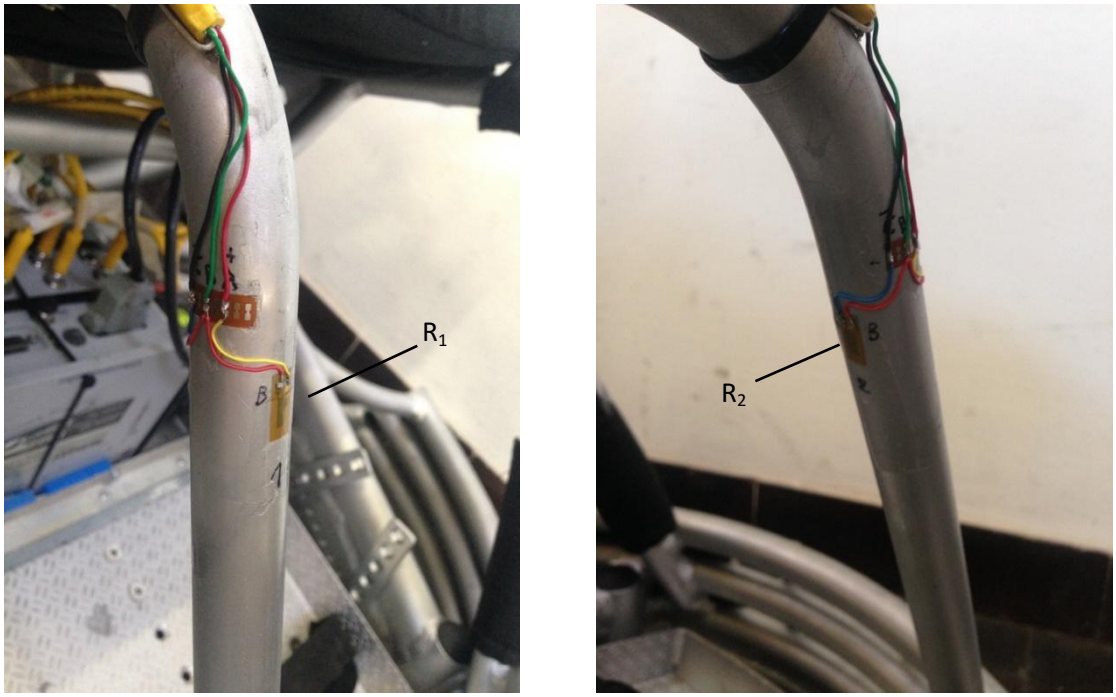

***Figure 3.18**: Position of the bridge RFT_BE*

The bridge 3 is sensitive to the bending moment acting on the front tube. The two strain gauges were positioned with their axles parallel to the axle of the tube, one on the top and one on the bottom of it. They are in the same perpendicular cross section area of the tube and they are about 30 mm away from the upper bending of the tube.

This bridge was defined RFT_BE and it was set up in order to give a positive signal when it's under a bending shown in the Figure 3.19. There are also indicated how the strain gauges were connected, so $\varepsilon_1=\varepsilon$ and $\varepsilon_2=-\varepsilon$.

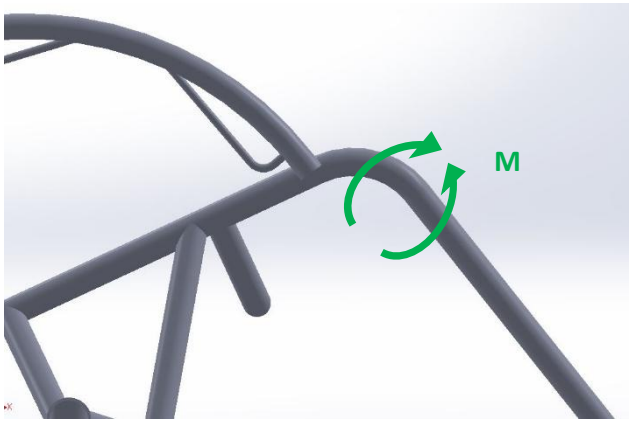

***Figure 3.19**: Definition of RFT_BE sign*

- Bridge 4 RST_BE (Right Side Tube Bending) is a half Wheatstone bridge configuration and it is composed by two strain gauges of the type HBM 1-LY43-3/120. It's located on the side tube, 20 mm away the rear connection with the back rest, in the right side of the frame, as shown in Figure 3.20.

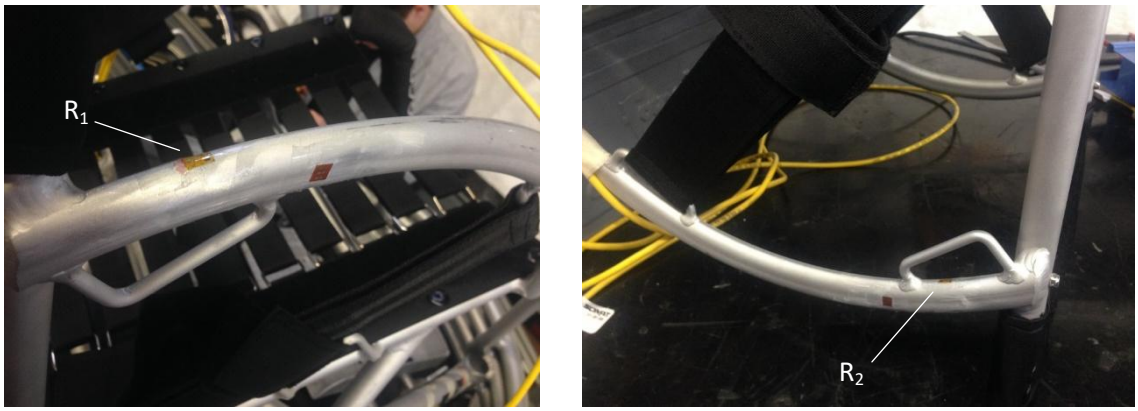

***Figure 3.20**: Position of the bridge RST_BE*

The bridge 4 is sensitive to the bending moment acting on the side tube. The two strain gauges were positioned with their axles parallel to the axle of the tube, one on the top and one on the bottom of it. They are in the same perpendicular cross section area of the tube.

This bridge was defined RST_BE and it was set up in order to give a positive signal when it's under a bending shown in the Figure 3.21. There are also indicated how the strain gauges were connected, so $\varepsilon_1=\varepsilon$ and $\varepsilon_2=-\varepsilon$.

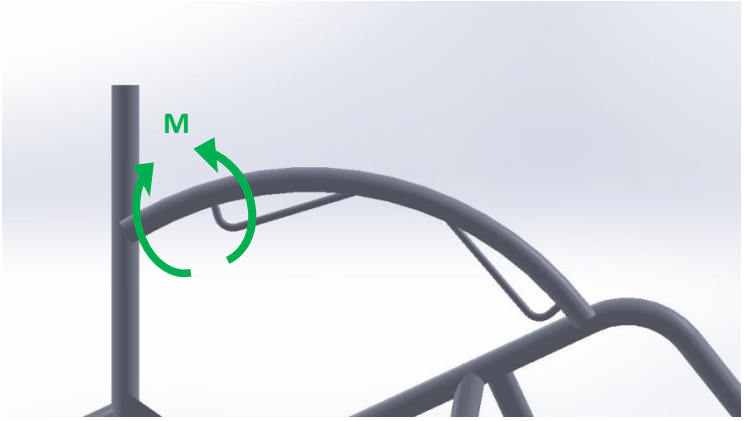

***Figure 3.21**: Definition of RST_BE sign*

3.5.2 Accelerometer

A triaxial accelerometer, of the type SAPE-HLS-3010 by HBM company was applied to the axle tubes' joint, below the seat. It was oriented with X in the front longitudinal, Y lateral left and Z vertical upright directions. The accelerometer was glued to a little aluminium plate and the plate was fixed to the frame with tape. The fixing was as strong as possible to avoid vibrations and relative movement between the accelerometer and the wheelchair. In Figure 3.22 it is possible to see the position of the accelerometer.

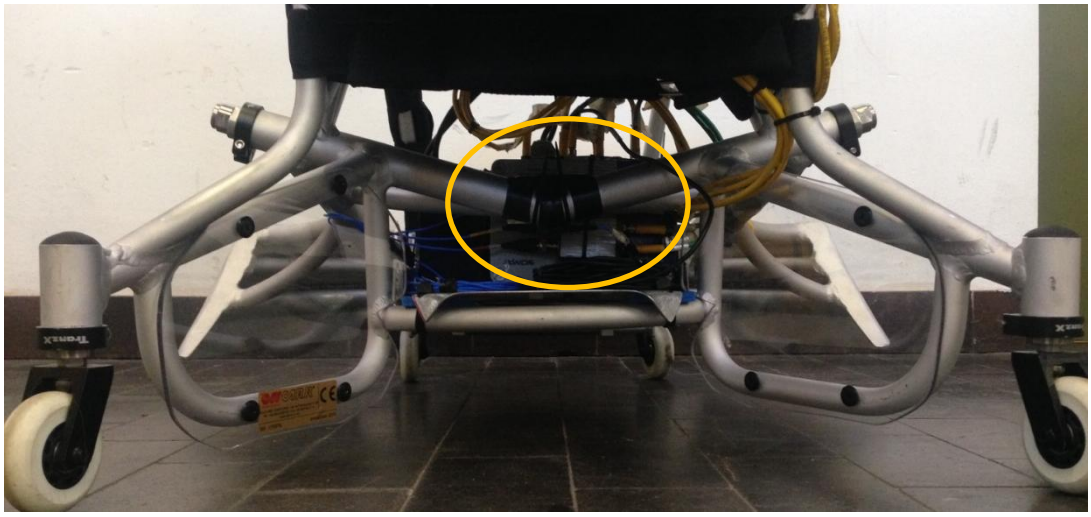

***Figure 3.22**: Position of the accelerometer*

3.5.3 Acquisition system allocation

It was necessary to find a safe allocation for the acquisition system and the battery power because the hit during the play are very strong in order to avoid that the system breaks off

the wheelchair. One alternative was to put the Somat and the battery in a bag and put it on the athlete's shoulder, but in this way it would influence his performance too much.

So a sturdy support was made and it was put in a position in which it would compromise the wheelchair manoeuvrability as little as possible.

A plate of aluminium was cut and bent and positioned between the foot rest and the rear part of the frame, as it is possible to see in Figure 3.23, and the Somat was screwed on it.

The clamping system of the foot rest was used for fixing the plate in the front and in the back it was fixed to the frame using hose clamps, passing through four holes made on it. The Somat was screwed on the plate using an aluminium L profile and the battery power was attached to the Somat with tape and a belt.
In this way, the plate guaranteed a solid place for the fixing of Somat and the battery and in the same time didn't contribute to increase the stiffness of the frame.

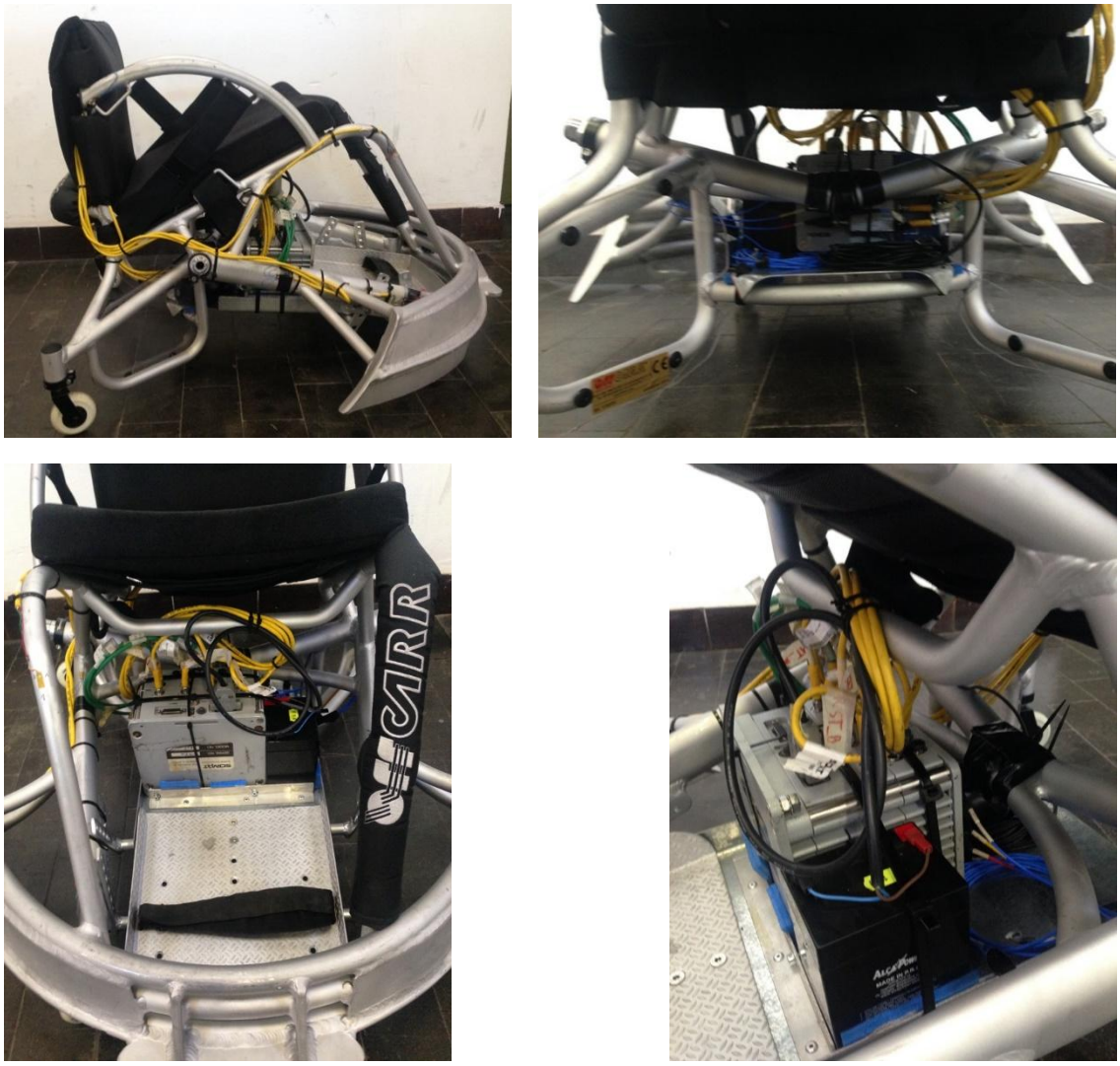

***Figure 3.23**: Details of aluminium plate fixation*

All the cables were attached to tubes using cable ties and they were gathered together under the seat. In total there was seven channels, one for each bridge and three for the accelerometer.

In the final and complete configuration the wheelchair weighed 25,95 kg.

CHAPTER 4: SYSTEM CALIBRATION

Three different calibrations of the system were made for searching the better configuration that mainly simulates the conditions to which the frame is submitted during an impact. The loads have many directions so it was necessary to make more than one configuration.
They were conducted in the Machine Design laboratory of the DII (Department of Industrial Engineering) of University of Padova.
The first one was a preliminary calibration, the second one was specified for horizontal loads and the third one for vertical loads.

4.1 Preliminary calibration

The first calibration, defined preliminary, attempts to simulate the horizontal component of the load applied on the frame.
The wheelchair was positioned vertically without the rear wheels, leaned against the rear casters and the tube behind the backrest and it was balanced, without any external supports.
The bridges were calibrated with the application of known axial loads applied to the front bumper by hydraulic cylinder controlled by a computer. The system is represented in Figure 4.1.

***Figure 4.1**: Setup of preliminary calibration*

The calibration consisted in the application of a ramp load steps, from 0 N to 1500 N, steps of 250 N every 10 seconds, increasing and decreasing. The system was turned on 20 minutes before the starting of the test and then the bridges signals were zeroed for avoiding the deviation caused by the Joule effect.

In Figure 4.2 there is represented the acquisition of the bridges' signals.

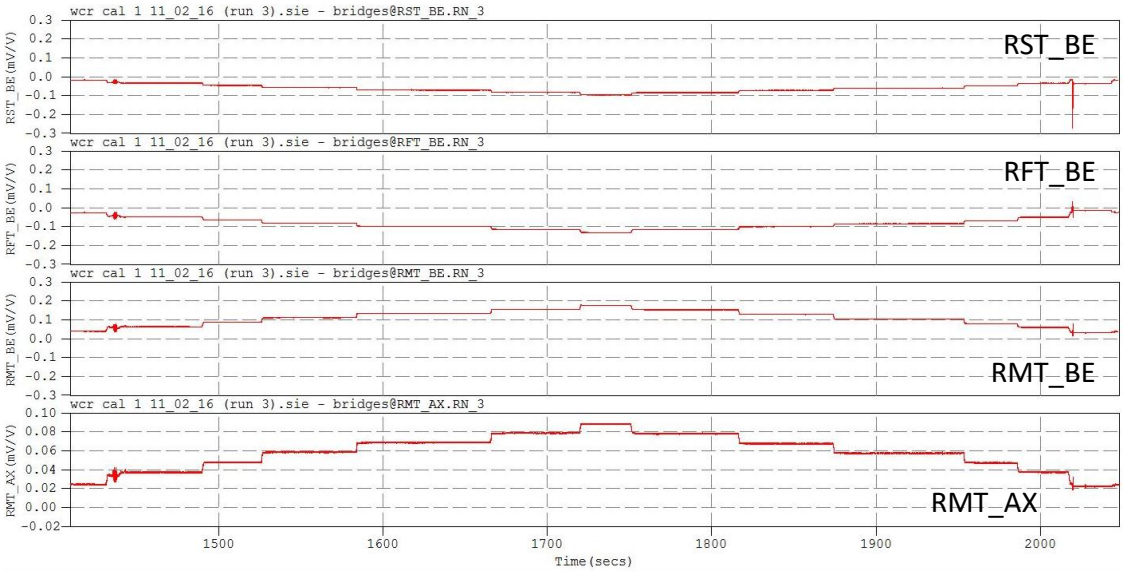

***Figure 4.2**: Preliminary calibration signals' acquisition*

The Somat InField software was used for the study of the signals.

For each step of load, the mean value of the signal in mV/V was extracted from each channel and from them the value of the 0 N level step was subtracted. The results obtained were drawn in the mV/V / N graph and then the regression lines for each channel was build, using Excel. The reciprocals of their slopes are the constants of calibration needed to transform the mV/V to Newton. In Table 4.1 there are reported the real values of bridge's signal, in Table 4.2 the correct ones and in Figure 4.3 there are represented the linear regression lines, with their equations and square of the coefficient of correlation.

Load	**RST_BE**	**RFT_BE**	**RMT_BE**	**RMT_AX**
[N]	[mV/V]	[mV/V]	[mV/V]	[mV/V]
0	-0,0192283	-0,0285941	0,0389284	0,0243523
250	-0,0334028	-0,0492144	0,0629577	0,0369977
500	-0,0459066	-0,0655737	0,0872469	0,0476809
750	-0,058334	-0,0817704	0,110537	0,058333
1000	-0,0711153	-0,0982992	0,132597	0,0685019
1250	-0,08387	-0,115258	0,154647	0,0785079
1500	-0,0965854	-0,132128	0,176703	0,0882143

***Table 4.1**: Real value of the mV/V signal*

Load	RST_BE	RFT_BE	RMT_BE	RMT_AX
[N]	[mV/V]	[mV/V]	[mV/V]	[mV/V]
0	0	0	0	0
250	-0,0141745	-0,0206203	0,0240293	0,0126454
500	-0,0266783	-0,0369796	0,0483185	0,0233286
750	-0,0391057	-0,0531763	0,0716086	0,0339807
1000	-0,051887	-0,0697051	0,0936686	0,0441496
1250	-0,0646417	-0,0866639	0,1157186	0,0541556
1500	-0,0773571	-0,1035339	0,1377746	0,063862

***Table 4.2**: Correct values of mV/V signal*

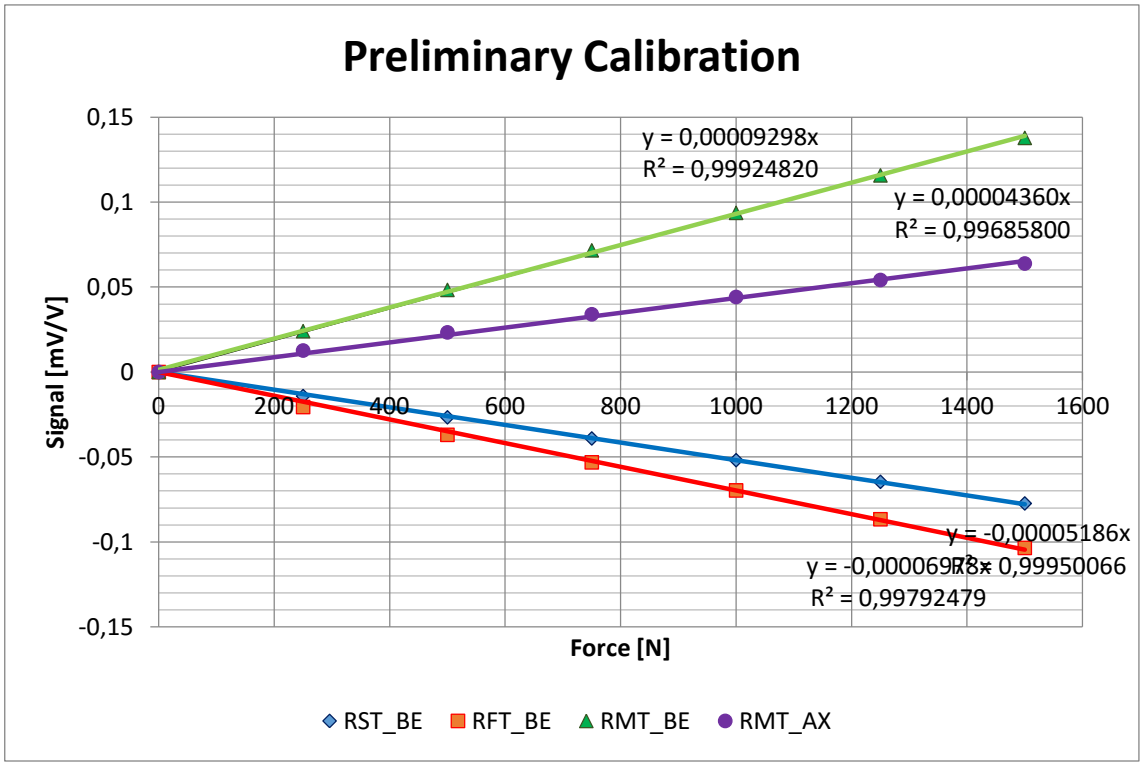

***Figure 4.3**: Regression lines of preliminary calibration*

The slopes of the four regression lines s and the constants of the calibration c_p are:

	RST_BE	RFT_BE	RMT_BE	RMT_AX
s [mV/V / N]	0,00005186	0,00006978	0,00009298	0,0000436
c_P [N / mV/V]	19282,7	14330,8	10755,0	22935,8

This calibration's configuration doesn't correspond with the real dynamics of a hit. In fact, in a real hit the rear casters are free and the constraints are represented only by the belt of the player, which is fixed around the backrest and on the knee. So this calibration was not taken in consideration in further data analysis.

4.2 Calibration for horizontal load

The second calibration has the aim of simulate the horizontal load applied on the frame. This is the most important calibration because the greatest forces in the instant of the collision are horizontal. It's useful to know the frame's behaviour and to find which points of it are more stressed.

For recreating the configuration of forces and constraints of a real hit, the wheelchair was put over a bench. An hydraulic cylinder was positioned horizontally acting on the frontal part of the bumper and the wheelchair was rested against a rigid element fixed to the bench. The wheelchair was rested only on the two tubes which support the backrest. This attempted to simulate the belt of the player. As already seen, the constraint on a real hit is represented by the inertia of the mass of the player locked by the belt fixed on the backrest. The configuration is visible in Figure 4.4.

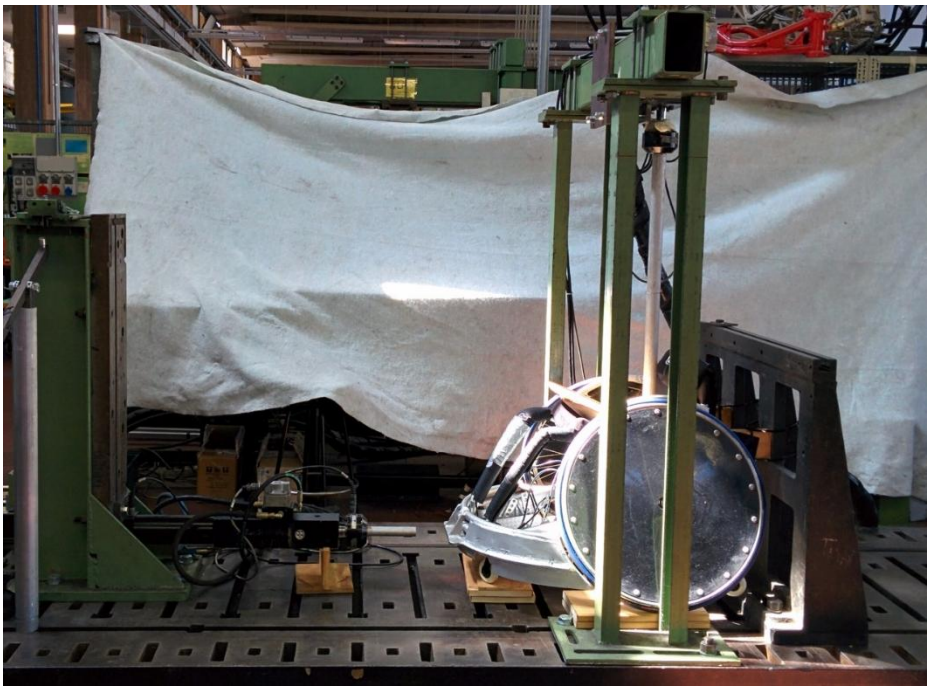

***Figure 4.4**: Setup of horizontal calibration*

Initially, two woodsy supports were used for restrain the wheelchair, but the mechanical characteristics of the wood didn't guarantee a rigid constraint. The resulting signals of the bridge wasn't linear because of the compression of the wood. So they were substituted by two heavy steel bars kept in position by two clamps. Two little pieces of rubber, 1 mm thin, were inserted between them and the tubes for avoid the relative slipping. They were positioned 50 mm above the transversal tube of the backrest and above, they were 5 cm wide. In Figure 4.5a there are reported the wood supports and in Figure 4.5b the final configuration, with the steel bars.

***Figure 4.5**: a) Woods supports b) steel bars*

The calibration consisted in the application of a ramp load steps, from 0 N to 1500 N by the hydraulic cylinder, with steps of 200 N and the last of 100 N every 20 seconds, increasing and decreasing. The system was turned on 20 minutes before the starting of the test and then the bridges signals were zeroing for avoiding the deviation caused by the Joule effect.

100 Hz sample rate was used and three sessions were made. The first was rejected for the adjustment of the system. In Figure 4.6, the signals of the third session are reported, filtered by a low pass filter with 1 Hz cut-off frequency.

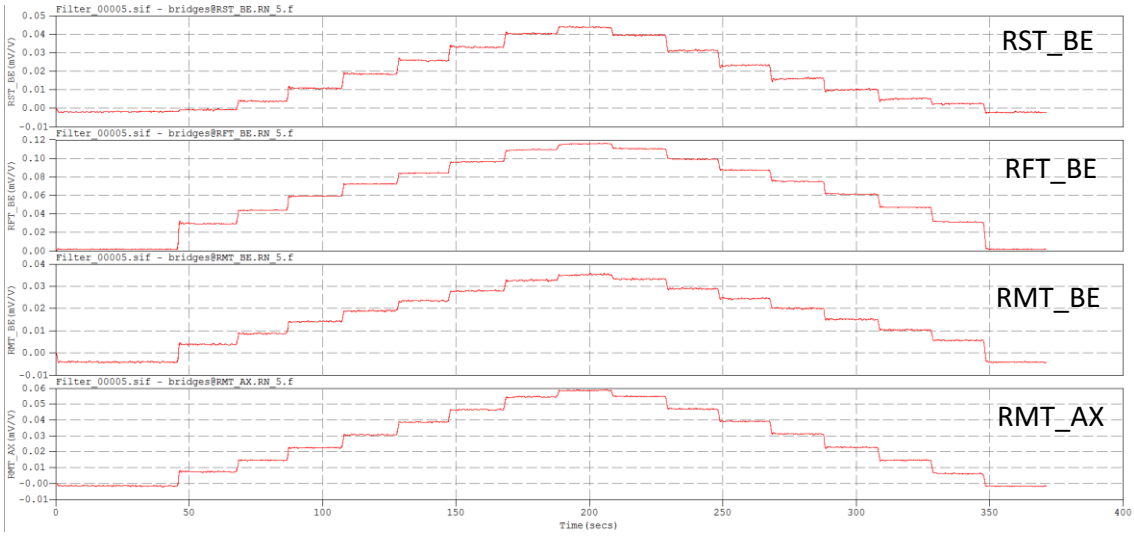

***Figure 4.6**: Horizontal calibration signals' acquisition*

The mean values of the signals of each load step of both sessions were extracted using inField software To obtain the calibration constants. The value recorded at 0 N level step was subtracted to each step value. Then the mean between the same step of the same channels of the two sessions was calculated. These values were inserted in mV/V / N graph and the regression lines for each channel were calculated, using Excel. The slopes were

obtained from their equations and their reciprocals are the constants of calibration. In Table 4.3 there are reported the mean values between the signals of the two sessions. In Figure 4.7 there are represented the linear regression lines, with their equations and square of the coefficient of correlation.

All the four channels are sensitive to the horizontal force. The most stressed is the bridge on the front tube, but it isn't taken as reference because it is sensitive also to the vertical load. The axial bridge on the main tube measures deformations caused practically only by horizontal load and it R^2 is almost 1, so it is used for the force estimation.

Load	**RST_BE**	**RFT_BE**	**RMT_BE**	**RMT_AX**
[N]	[mV/V]	[mV/V]	[mV/V]	[mV/V]
0	0	0	0	0
200	0,001147907	0,025484755	0,00736955	0,0082212
400	0,00521424	0,041032405	0,01239679	0,01561208
600	0,011896445	0,056691855	0,0178755	0,02353203
800	0,01933749	0,070509955	0,02283895	0,03176403
1000	0,02669039	0,082448605	0,0273938	0,03979653
1200	0,03422784	0,094545305	0,03178715	0,04762093
1400	0,04186099	0,107137405	0,0364627	0,05559708
1500	0,04542674	0,113411905	0,0390075	0,05967338
1400	0,04110089	0,108074905	0,03698565	0,05581488
1200	0,03274229	0,096606055	0,0327155	0,04795753
1000	0,02487509	0,084855855	0,0283227	0,04020713
800	0,01791134	0,072454955	0,0237925	0,03226688
600	0,01163092	0,058885805	0,0190169	0,02393788
400	0,006808675	0,044635855	0,0143013	0,01590458
200	0,004305075	0,028890505	0,009680265	0,007642735
0	-0,00024246	-1,4835E-05	0,000115395	-0,00006877

***Table 4.3**: Values of mV/V signal*

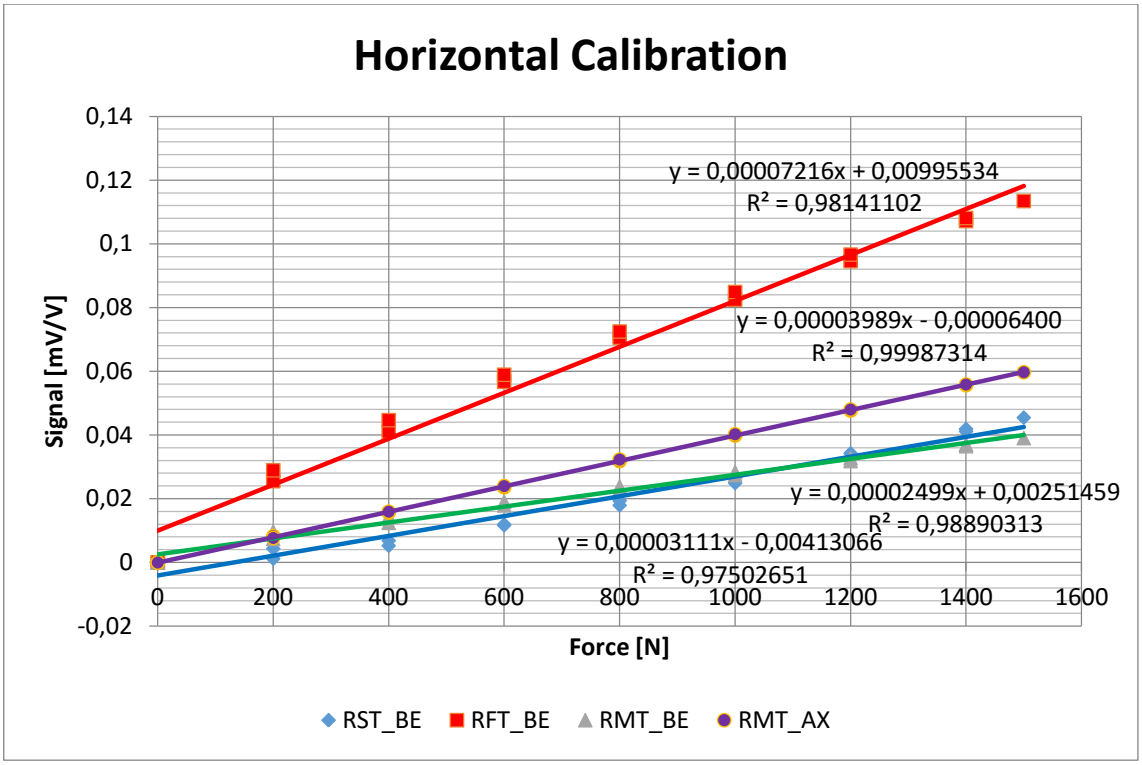

***Figure 4.7**: Regression lines of horizontal calibration*

The slopes of the four regression lines s and the constants of the calibration c_H are:

	RST_BE	RFT_BE	RMT_BE	RMT_AX
s [N / mV/V]	0,00003111	0,00007216	0,00002499	0,00003989
c_H [N / mV/V]	32144,0	13858,1	40016,0	25068,9

4.3 Calibration for vertical load

The third calibration had the aim to simulate the vertical load acting on the wheelchair, typically caused by the weight of the player in the moment of falling down after the collision.

A plate of wood were used for realize a horizontal support. They weight 3,33 kg and they were located over the cushion. The wheelchair had constraints only for avoiding it to go forward or backward. On this support, nine weights were loaded, each one weighs between 9,18 kg and 11,16 kg. They were put one by one, every 20 seconds, from 0 to 92,83 kg and returning to 0.

In Figure 4.8 it's possible to see the configuration.

***Figure 4.8**: Setup of vertical calibration*

100 Hz sample rate was used and three sessions were made. The first was rejected for the adjustment of the system. The system was turned on 20 minutes before the starting of the test and then the bridges signals were zeroed for avoiding the deviation caused by the Joule effect.

In Figure 4.9, the signals of the second session are reported, filtered by a low pass filter with 1 Hz cut-off frequency.

As it's possible to see from the values of the signals, only two bridges are sensitive to vertical loads. In fact, the signals of the bridge on the side tube and the one for axial load on the main tube are comparable with the noise and it's not possible to distinguish a clear ramp. The bridge for the bending of the main tube and that on the front tube measure positive deformations, so the frame behaves as expected and only these two channels were considered for the calibration.

For obtain the constant of calibration, the mean values of the signals were extracted of each load step of both sessions using inField software, then the mean between the same step of the same channels of the two sessions was calculated. These values were inserted in mV/V / N graph and the regression lines for each channel were build, using Excel. The slopes were obtained from their equations and their reciprocals are the constants of calibration. The first point isn't 0 N, but to 32,7 N, which corresponds at the weight of the wood, 3,33 kg. In Table 4.4 there are reported the mean values between the signals of the two sessions. In Figure 4.10 there are represented the linear regression lines, with their equations and square of the coefficient of correlation.

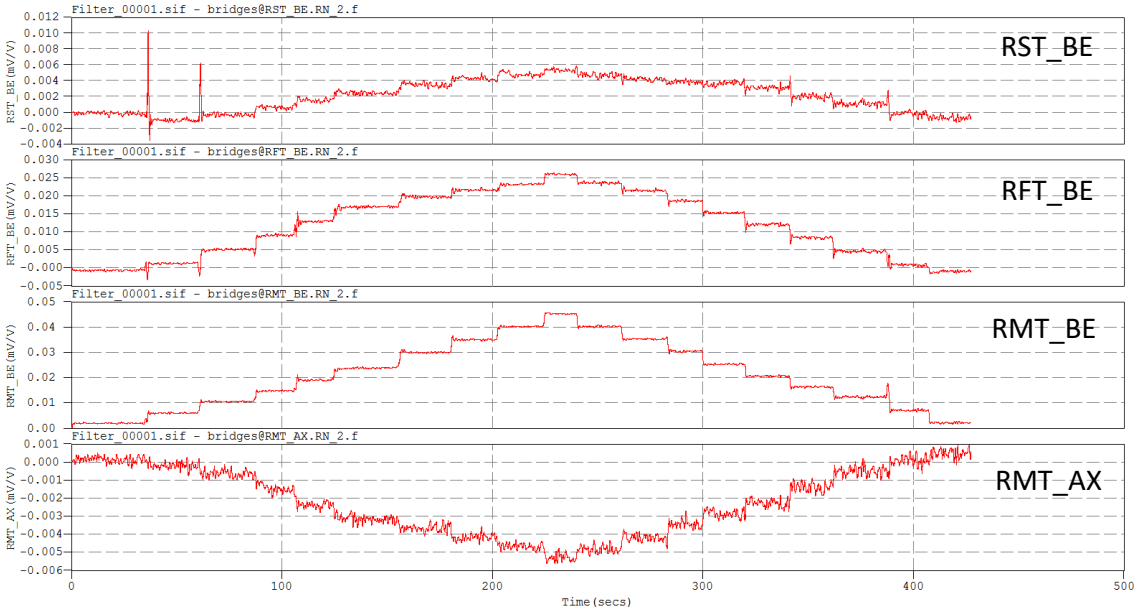

***Figure 4.9**: Vertical calibration signals' acquisition*

Weight	Load	RFT_BE	RMT_BE
[kg]	[N]	[mV/V]	[mV/V]
3,33	32,7	-0,000820527	0,00199292
13,1	128,5	0,00088551	0,0059899
24,26	238,0	0,00410701	0,0108944
34,52	338,6	0,00725717	0,015347
44,77	439,2	0,010676085	0,0198516
55,04	539,9	0,01344185	0,0248285
65,29	640,5	0,0154462	0,03049915
74,47	730,6	0,01698355	0,0353817
83,65	820,6	0,01805755	0,03993495
92,83	910,7	0,02029265	0,0441928
83,65	820,6	0,0182853	0,03966715
74,47	730,6	0,01647705	0,03508405
65,29	640,5	0,0149233	0,0306841
55,04	539,9	0,012123265	0,02582975
44,77	439,2	0,00947096	0,02143695
34,52	338,6	0,006645815	0,01715365
24,26	238,0	0,00362286	0,01273045
13,10	128,5	0,000420025	0,00703976
3,33	32,7	-0,001032696	0,002112215

***Table 4.4**: Values of mV/V signal*

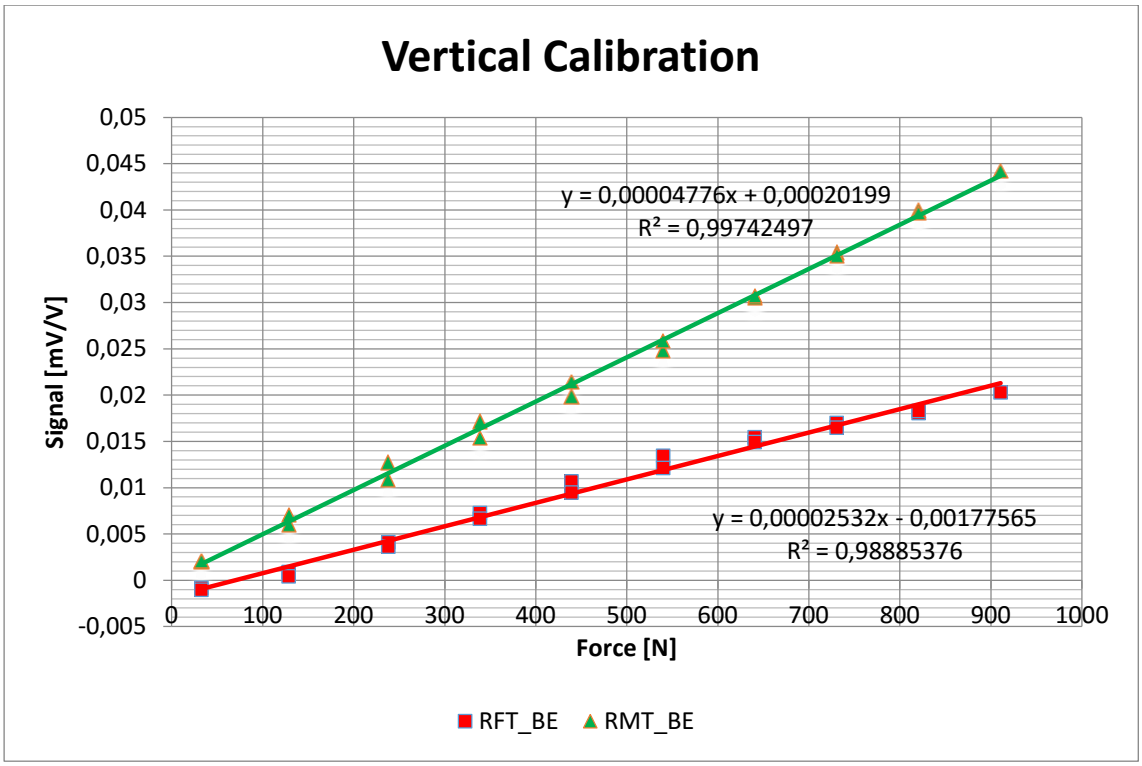

***Figure 4.10**: Regression lines of vertical calibration*

The ideal linearity has R^2=1, so the values of the two regression lines are acceptable. It's possible to notice that the bridge for the bending of the main tube is the most sensitive to vertical loads. This channel will be considered for the estimation of the vertical force acting on the seat.

The slopes of the four regression lines s, sensibility, and the constants of the calibration c_V are:

	RMT_BE	**RFT_BE**
s [N / mV/V]	0,00004776	0,00002532
c_V [N / mV/V]	20938,0	39494,5

In conclusion, the vertical calibration shows that there are only two channels which are sensitive to this load, the bridge on the front tube and the bending bridge on the main tube.

The horizontal calibration shows that the axial tube on the main tube is ideally for measure the horizontal impact forces. Also the bridge on the front tube is sensitive to this load, so it's useful for understand how the frame works.

CHAPTER 5: INFIELD TESTS

Many infield trials were made in order to find simple significant and replicable test. Frontal impact test were chosen and they had the purpose of studying the behaviour of the frame under impulsive forces acting on it during a hit that could occur in the game, because it is the most severe. Moreover, they give a measure of these loads and that will be used for some finite element method (FEM) simulations.

5.1 Mechanics of a frontal hit

First, many trainings and matches were observed and some videos were realized in order to understand which forces and which constraints are involved in every phase of the collision. This is necessary to put the instrumentation in the right location and to realize the correct procedure of calibration. Frontal impact between two players were taken as reference: they started in the same time then they crashed each other, Figure 5.1a and b.

During a frontal impact, the two wheelchairs get in touch only with the front of the bumpers. In this moment, a horizontal impulsive force is applied on the frame of the right wheelchair, as shown in Figure 5.1c. The inertia of the player, who is tied to the backrest by a belt, makes the rear wheels lift up from the floor (Figure 5.1d), depending on the player mass and the exact point of collision. The body of the player is thrown forward and it's important to use belts for fixing the feet, the knees, the pelvis and also the lower trunk to the wheelchair. The trunk belt is fixed around the backrest and represents the main type of load transmission in the system. The seat inclined by 30°, so also the thighs and the cushion transmit part of load. Then, after about 4 tenths of second, he touches down again. When the wheelchair starts to touch the ground, the return of the player's body mass causes a vertical force applied to the seat. In Figure 5.1e and f the last phases are represented.

a) start

b) run

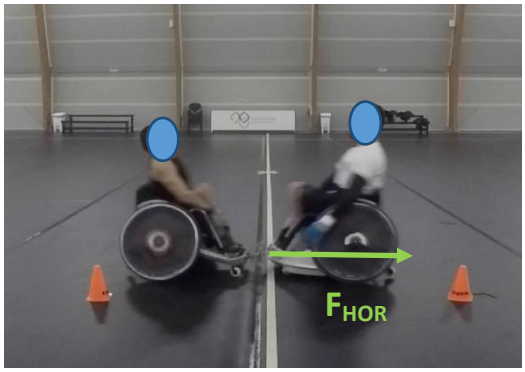

c) collision t=O

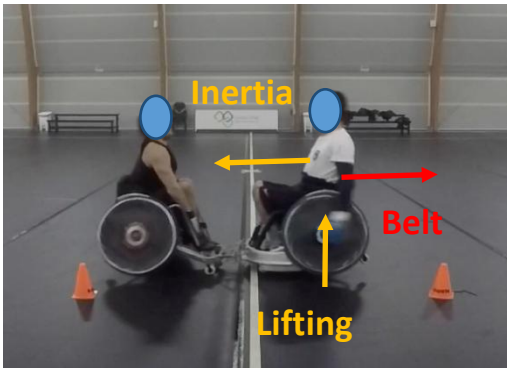

d) lifting

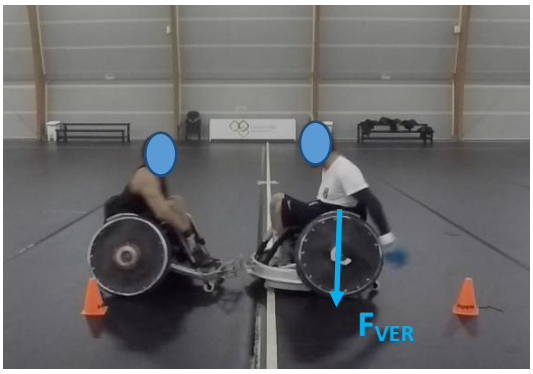

e) falling t=0,40 s

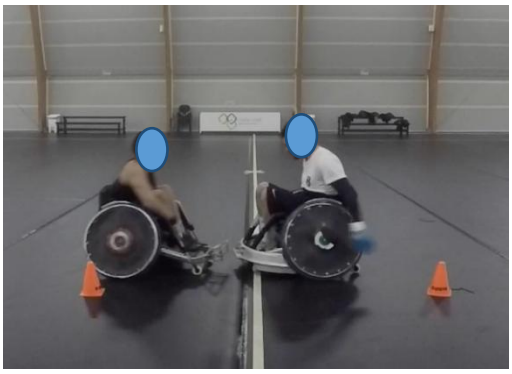

f) back

***Figure 5.1**: Phases of an impact filmed by GoPro camera*

5.2 Infield tests: impacts

These tests were conducted at the sports hall of the OIC (Opera Immacolata Concezione), in Padova, in February and March 2016 and involved four players of the Wheelchair Rugby Italian National Team.

They consisted in frontal hits between two players, with their wheelchairs, at three different defined run-in distances from each other, 2 m, 4 m and 6 m. They were made in two sessions, one for each two couples of players and for each distance three runs were conducted in the first session and four in the second one.

In the first session, N. T. with the instrumented wheelchair was opposed versus A. D. with a defensive model. In the second, V. Q. with instrumented wheelchair was opposed versus P. M. with offensive model. In Table 5.1, are reported the mass of the players.

Player	Player Mass [kg]	Player + Wheelchair Mass [kg]
A.D.	65	82
P.M.	74	94
V.Q.	80	106
N.T.	79	105

***Table 5.1**: Weights of players and wheelchairs*

The distance was signed by cones and in each runs the players started at the same time against each other from the established distance. All the tests were filmed with a GoPro camera in full HD definition at 59,94 fps.

For all the sessions, the signals of the four Wheatstone bridges and of the triaxial accelerometer were recorded by the Somat acquisition system at 5 kHz sample rate the first session and at 10 kHz the second.

5.3 Data analysis

The acquisition system records the displacements of the Wheatstone bridges caused by the strain gauges' deformations, so the output signal is milliVolt/Volt time history and it has to be converted. Each signal is converted in ε (microstrain) and in Newton, due to make comparisons between the deformations of the four channels and have an estimation of the size of the applied force.

This signal can be converted in ε (microstrain) using the general relation of the Wheatstone bridge:

$$\frac{\Delta V}{V} = \frac{K}{4}(\varepsilon_1 - \varepsilon_2 + \varepsilon_3 - \varepsilon_4)$$

where K is the gauge factor, V is the supply voltage and ΔV/V is the output signal.

In the three bending half bridges used on the wheelchair, the strain gauges were configured in order to have $\varepsilon_1=\varepsilon$ and $\varepsilon_2=-\varepsilon$, so it results

$$\frac{\Delta V}{V} = \frac{K}{4}(2\varepsilon)$$

Therefore, for obtaining the signal from milliVolt/Volt to ε

$$\varepsilon = \frac{\Delta V}{V} \cdot \frac{2}{K} \cdot \frac{1}{1000}$$

In the axial full bridge, $\varepsilon_1=\varepsilon_3=\varepsilon$ and $\varepsilon_2=\varepsilon_4=-\nu\varepsilon$ so

$$\varepsilon = \frac{\Delta V}{V} \cdot \frac{4}{2{,}66 \cdot K} \cdot \frac{1}{1000}$$

The output signals have to be divided by 1000 because they have to be expressed into Volt/Volt.

Using inField, all the acquired signals were scaled with the constant $k = \frac{2}{K} \cdot \frac{1}{1000}$ for the half bridges and with $k = \frac{4}{2{,}66 \cdot K} \cdot \frac{1}{1000}$ for the full bridge, calculated for each channel.

Moreover, the signals were also transformed in Newton, using inField scaling them with the constants found in the calibrations.

This is an example of the acquisition of one bridge of an impact test, Figure 5.2.

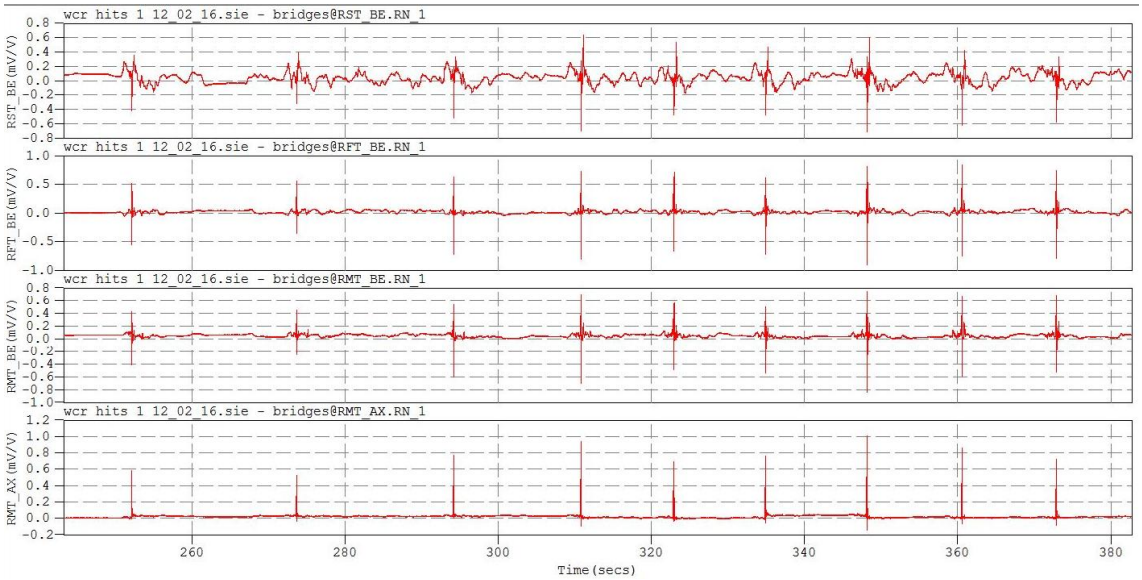

***Figure 5.2**: Impact test's acquisition in microstrain*

The maximum and the minimum values of the ε trend were extracted for each impact and the delta between them was calculated.

The velocities of the players at the instant of the collision were also estimated. These were extracted from the video, calculating the distance covered by the two players in the time of seven photograms of the video. A proportion was made using the distance between the midline and the first cone that was 1 m, known, extracted with AutoCAD, as shown in Figure 5.3, using the following equation. Then the sum of the players' velocities was made due to find the relative velocities. These data were inserted in max(ε)/velocity, delta(ε)/velocity and max Force/velocity graphs.

$$x = \frac{a \cdot 1}{b} \qquad t = \frac{1}{fps} \cdot 7 = \frac{1}{59{,}94} \cdot 7$$

$$v = \frac{x}{t}$$

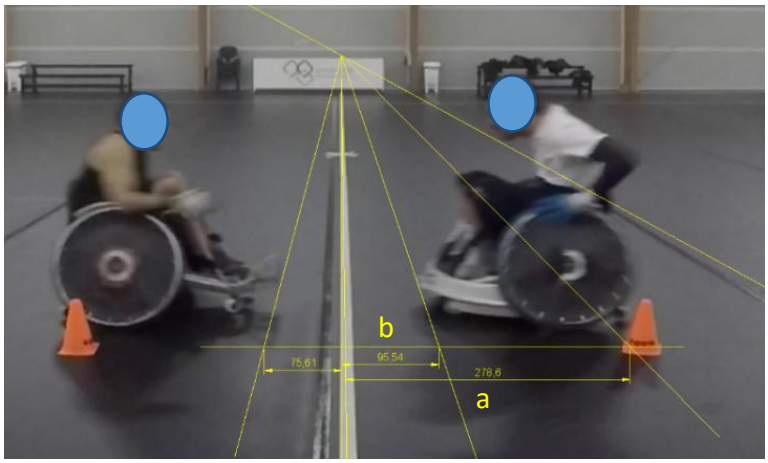

***Figure 5.3**: Example of velocity's calculation*

5.4 Results

5.4.1 Deformation analysis

After making the acquisition sessions, the signals of the four channels were converted in microstrain. The gauge factor K of RST_BE bridge is 2,05 and the gauge factors of RFT_BE, RMT_BE and RMT_AX bridges are 2,11.

Below there are the constants used for scaling the signal from mV/V to microstrain:

RST_BE: $k = \frac{2}{K} \cdot \frac{1}{1000} = 0{,}00097561$

RFT_BE: $k = \frac{2}{K} \cdot \frac{1}{1000} = 0{,}000947867$

RMT_BE: $k = \frac{2}{K} \cdot \frac{1}{1000} = 0{,}000947867$

RMT_AX: $k = \frac{2}{K} \cdot \frac{1}{1000} = 0{,}000712682$

In Figure 5.4 and Figure 5.5 there are reported the ε time history of the two impact test sessions.

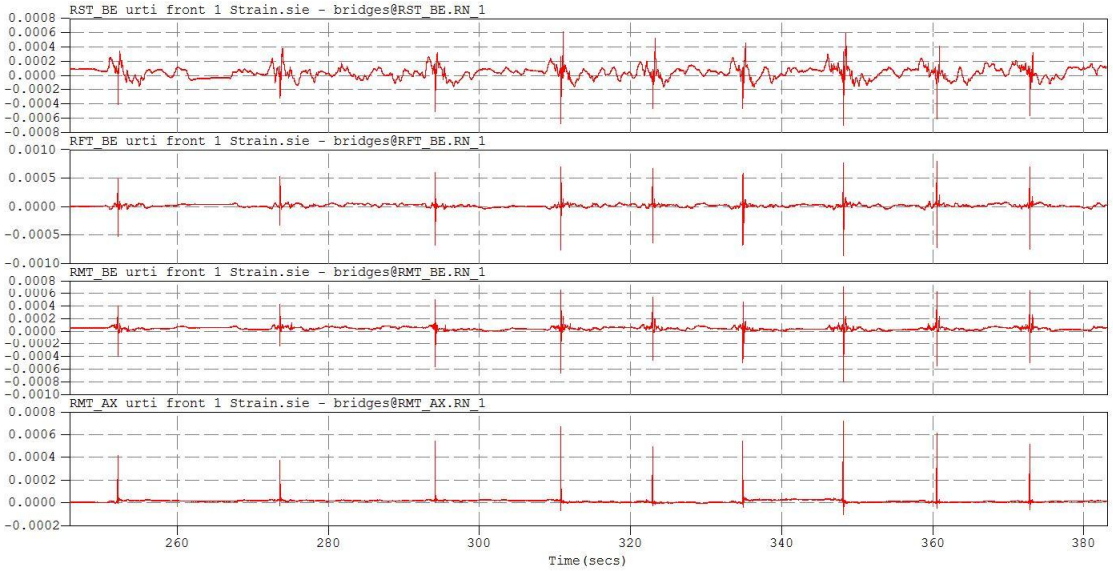

***Figure 5.4**: ε time history session 1 in microstrain*

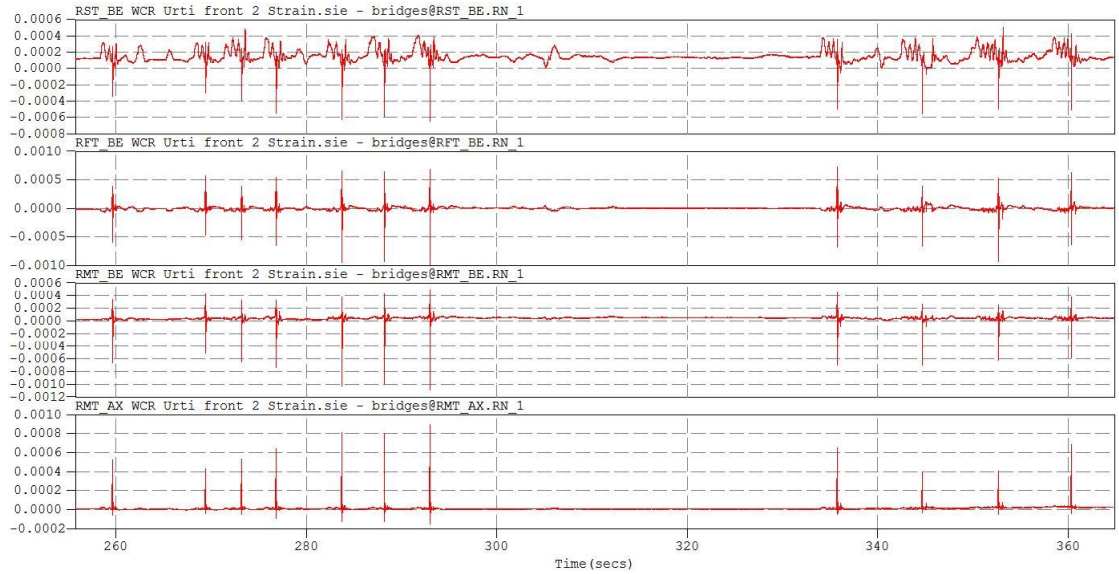

***Figure 5.5**: ε time history session 2 in microstrain*

It's important to notice that to each peak it corresponds a hit.

Zooming in a single hit, it's possible to analyse its phases, finding a correspondence by the signal and the video (Figure 5.6).

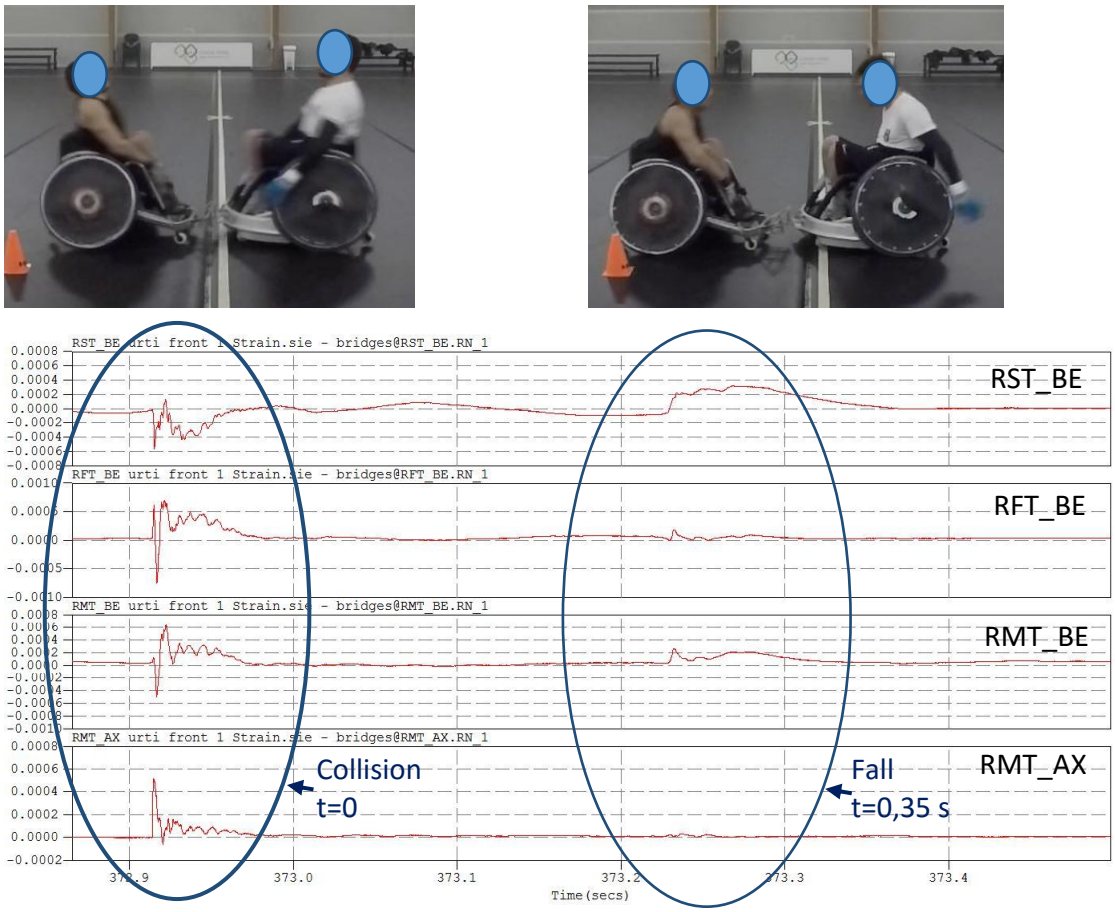

***Figure 5.6**: Correspondence between video and signal*

The first peak corresponds to the collision. The main tube receives an impulsive compression load, as it possible to see from the positive RMT_AX signal, according with the signs set up during the configuration. The front tube receives a positive bending first, then it goes negative. The negative peak has a modulus slightly greater than the value of the first peak. The same behaviour, with inverted signs, is noticed for the channel RMT_BE, the bending of the tube on the main tube near the wheel axle. The RST_BE has first a negative peak because the player was fixed to the backrest with a belt and his unbalancing forward causes the tube flexion. After 35 hundredths of second the player falls down and this is highlighted by the peak of the RMT_BE, which is the most sensitive bridge for vertical load, caused by the body mass return, and the positive increase of the RST_BE because the player leans against the backrest and this stretches the side tube.

Here there are reported the value of the measures of the two sessions.

5.4.1.1 Session 1: offensive vs defensive

The Session 1 of the impact tests was conducted on 12nd of February 2016 at the sports hall of the OIC (Opera Immacolata Concezione), in Padova. It got involved N. T., 2,5 points and 105 kg total mass, who used the instrumented wheelchair, and A. D., 1,5 points and 82 kg total mass, who used a defensive Go Try OffCarr wheelchair.

Three runs for each distance were made and 5 kHz sample rate was used. In Table 5.2 there are reported in microstrain the maximum value, the minimum value and delta between them of the deformation.

		RST_BE			RFT_BE		
Distance	**Run**	**Max(ε)**	**Min(ε)**	**Delta(ε)**	**Max(ε)**	**Min(ε)**	**Delta(ε)**
2 m	r1	0,000345	-0,000416	0,000761	0,000485	-0,000523	0,001007
	r2	0,000377	-0,000319	0,000696	0,000526	-0,000336	0,000863
	r3	0,000324	-0,000507	0,000832	0,000598	-0,000688	0,001286
4 m	r1	0,000616	-0,000685	0,001301	0,000692	-0,000764	0,001456
	r2	0,000524	-0,000468	0,000992	0,000670	-0,000640	0,001310
	r3	0,000458	-0,000470	0,000928	0,000579	-0,000689	0,001268
6 m	r1	0,000587	-0,000700	0,001286	0,000769	-0,000867	0,001637
	r2	0,000408	-0,000610	0,001018	0,000800	-0,000720	0,001520
	r3	0,000319	-0,000564	0,000883	0,000704	-0,000752	0,001455
		RMT_BE			**RMT_AX**		
Distance	**Run**	**Max(ε)**	**Min(ε)**	**Delta(ε)**	**Max(ε)**	**Min(ε)**	**Delta(ε)**
2 m	r1	0,000399	-0,000395	0,000794	0,000413	-0,000004	0,000417
	r2	0,000428	-0,000227	0,000656	0,000372	-0,000028	0,000400
	r3	0,000508	-0,000568	0,001076	0,000546	-0,000001	0,000547
4 m	r1	0,000652	-0,000666	0,001318	0,000668	-0,000067	0,000735
	r2	0,000536	-0,000463	0,000998	0,000495	-0,000028	0,000523
	r3	0,000470	-0,000505	0,000975	0,000540	-0,000043	0,000583
6 m	r1	0,000703	-0,000802	0,001505	0,000719	-0,000106	0,000825
	r2	0,000634	-0,000554	0,001188	0,000612	-0,000051	0,000663
	r3	0,000648	-0,000503	0,001150	0,000517	-0,000062	0,000579

***Table 5.2**: Strain analysis session 1*

In Table 5.3 there are reported the velocities of the two players calculated with the proportion between the distance obtained with AutoCAD from a photogram 7 photograms before the hit and their sums.

Distance	**Run**	**N.T. velocity** [m/s]	**A.D. velocity** [m /s]	**Relative velocity** [m/s]
2 m	r1	1,47	1,16	***2,63***
	r2	1,31	1,33	***2,64***
	r3	1,72	1,24	***2,97***
4 m	r1	1,87	1,69	***3,57***
	r2	2,11	1,64	***3,75***
	r3	1,73	1,68	***3,41***
6 m	r1	2,04	1,88	***3,92***
	r2	1,87	1,54	***3,41***
	r3	2,03	1,74	***3,77***

***Table 5.3**: Velocities session 1*

The graphs in Figure 5.7 and Figure 5.8 report respectively the values of the maximum deformations and the deltas between the minimum and maximum associated with the velocities.

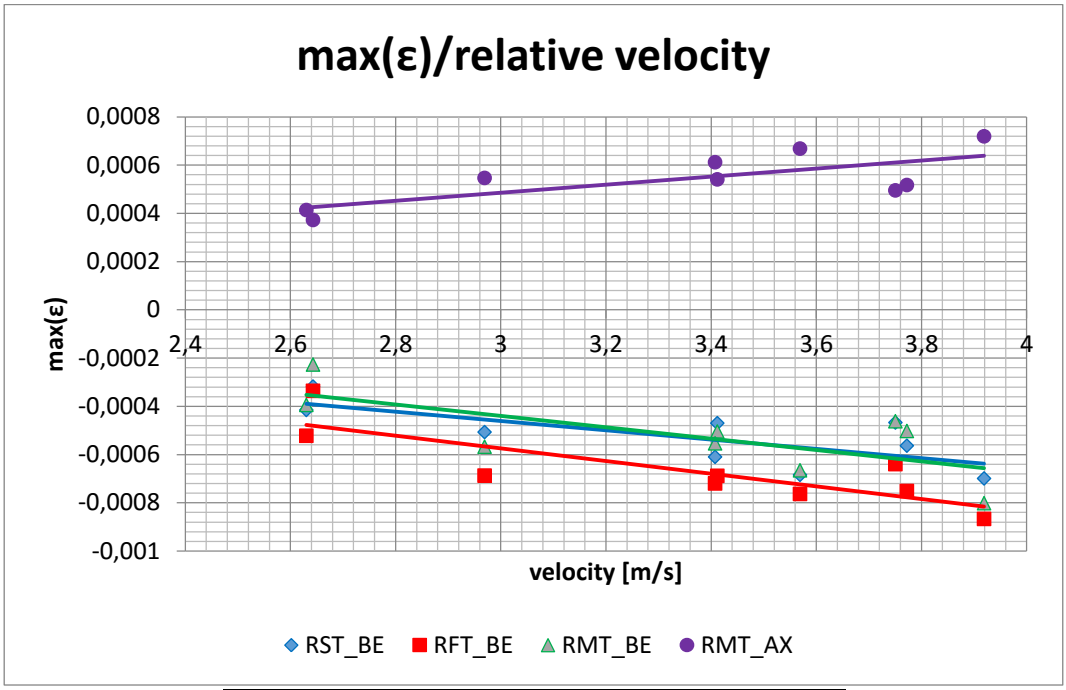

	RST_BE	RFT_BE	RMT_BE	RMT_AX
R^2	0,5502	0,6793	0,4963	0,5222

Figure 5.7: *Maximum strain over relative velocity session 1*

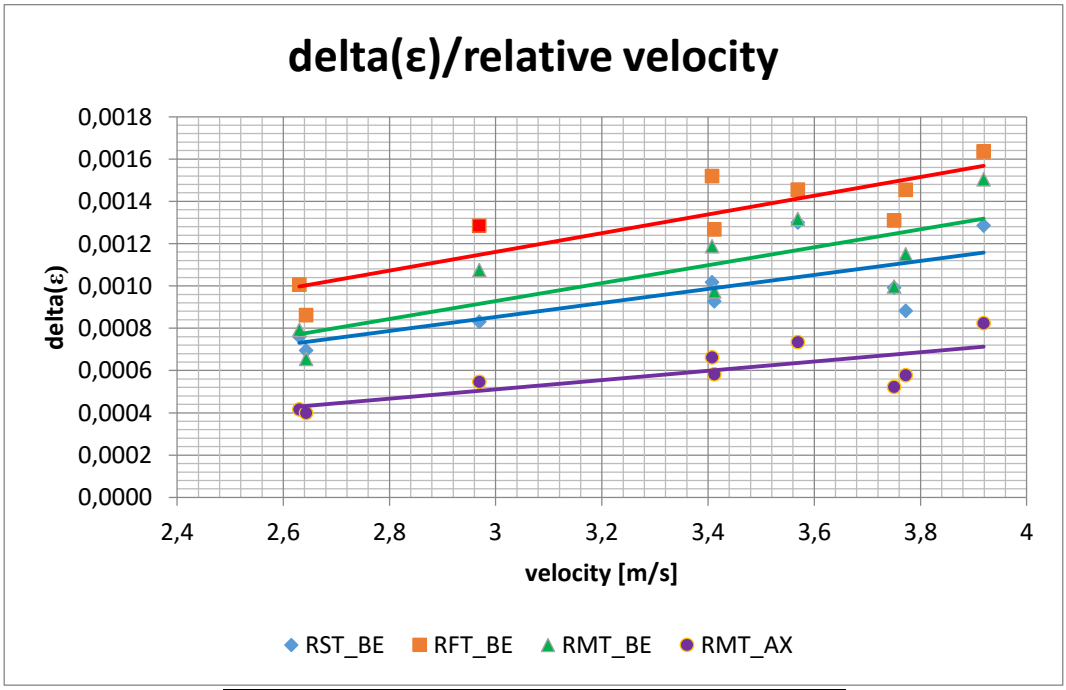

	RST_BE	RFT_BE	RMT_BE	RMT_AX
R^2	0,5715	0,7962	0,6350	0,5882

Figure 5.8: *Delta strain over relative velocity session 2*

5.4.1.2 Session 2: offensive vs offensive

The Session 2 of the impact tests was conducted on 12nd of March 2016 at the sports hall of the OIC (Opera Immacolata Concezione), in Padova. It got involved V. Q., 2,5 points and 106 kg total mass, who used the instrumented wheelchair, and P. M., 3,5 points and 94 kg total mass, who used an offensive Go Try OffCarr wheelchair.

Four runs for 2 m and 4 m distances were made and three for 6 m. 10 kHz sample rate was used. In Table 5.4 there are reported in microstrain the maximum value, the minimum value and delta between them of the deformation.

		RST_BE			**RFT_BE**		
Distance	Run	Max(ε)	Min(ε)	Delta(ε)	Max(ε)	Min(ε)	Delta(ε)
2 m	r1	0,000274	-0,000344	0,000617	0,000381	-0,000601	0,000982
	r2	0,000315	-0,000299	0,000614	0,000569	-0,000470	0,001040
	r3	0,000250	-0,000390	0,000640	0,000387	-0,000562	0,000949
	r4	0,000201	-0,000545	0,000745	0,000544	-0,000654	0,001198
4 m	r1	0,000233	-0,000624	0,000857	0,000660	-0,000956	0,001616
	r2	0,000217	-0,000601	0,000818	0,000648	-0,000938	0,001585
	r3	0,000227	-0,000651	0,000878	0,000685	-0,000998	0,001683
	r4	0,000356	-0,000503	0,000859	0,000725	-0,000689	0,001414
6 m	r1	0,000075	-0,000556	0,000631	0,000392	-0,000665	0,001057
	r2	0,000222	-0,000495	0,000718	0,000529	-0,000941	0,001469
	r3	0,000430	-0,000506	0,000936	0,000634	-0,000637	0,001271
		RMT_BE			**RMT_AX**		
Distance	Run	Max(ε)	Min(ε)	Delta(ε)	Max(ε)	Min(ε)	Delta(ε)
2 m	r1	0,000335	-0,000662	0,000998	0,000526	-0,000060	0,000587
	r2	0,000434	-0,000512	0,000946	0,000428	-0,000040	0,000468
	r3	0,000328	-0,000651	0,000978	0,000533	-0,000049	0,000582
	r4	0,000333	-0,000733	0,001066	0,000645	-0,000097	0,000742
4 m	r1	0,000375	-0,001029	0,001404	0,000807	-0,000129	0,000935
	r2	0,000426	-0,001004	0,001430	0,000799	-0,000131	0,000929
	r3	0,000495	-0,001097	0,001591	0,000898	-0,000150	0,001049
	r4	0,000455	-0,000695	0,001150	0,000650	-0,000048	0,000698
6 m	r1	0,000206	-0,000695	0,000901	0,000395	-0,000034	0,000429
	r2	0,000249	-0,000626	0,000875	0,000402	-0,000052	0,000454
	r3	0,000379	-0,000589	0,000968	0,000684	-0,000043	0,000726

***Table 5.4**: Strain analysis session 2*

In Table 5.5 there are reported the velocities of the two players obtained.

Distance	Run	V.Q. velocity [m/s]	P.M. velocity [m /s]	Total velocity [m/s]
2 m	r1	1,38	1,41	***2,79***
	r2	1,43	1,51	***2,94***
	r3	1,22	1,63	***2,85***
	r4	1,19	2,05	***3,24***
4 m	r1	1,80	1,98	***3,78***
	r2	1,88	2,03	***3,91***
	r3	1,81	2,22	***4,03***
	r4	2,13	2,39	***4,53***
6 m	r1	1,97	2,43	***4,41***
	r2	1,84	2,55	***4,39***
	r3	2,21	2,76	***4,97***

***Table 5.5**: Velocities session 2*

The graphs in Figure 5.9 and Figure 5.10 report the values of the maximum deformations and the deltas between the minimum and maximum associated with the velocities.

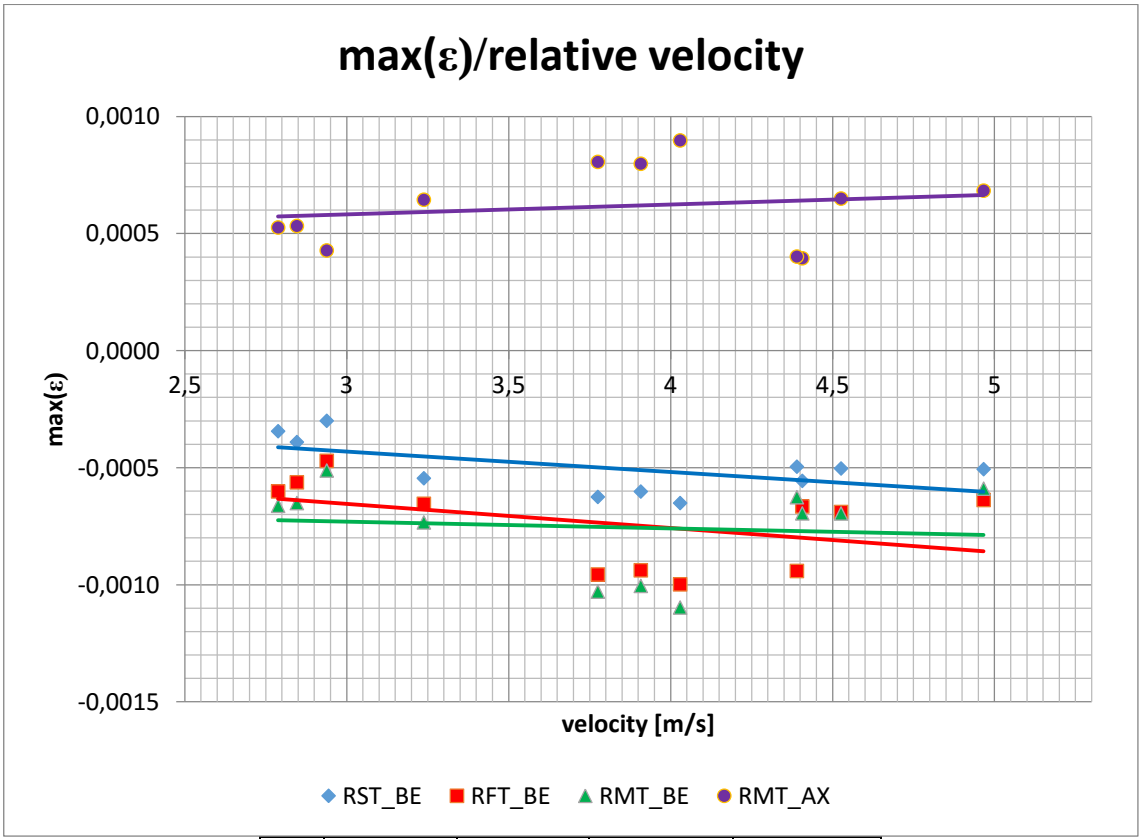

	RST_BE	RFT_BE	RMT_BE	RMT_AX
R^2	0,3295	0,1753	0,0123	0,0394

***Figure 5.9:** Maximum strain over relative velocity session 2*

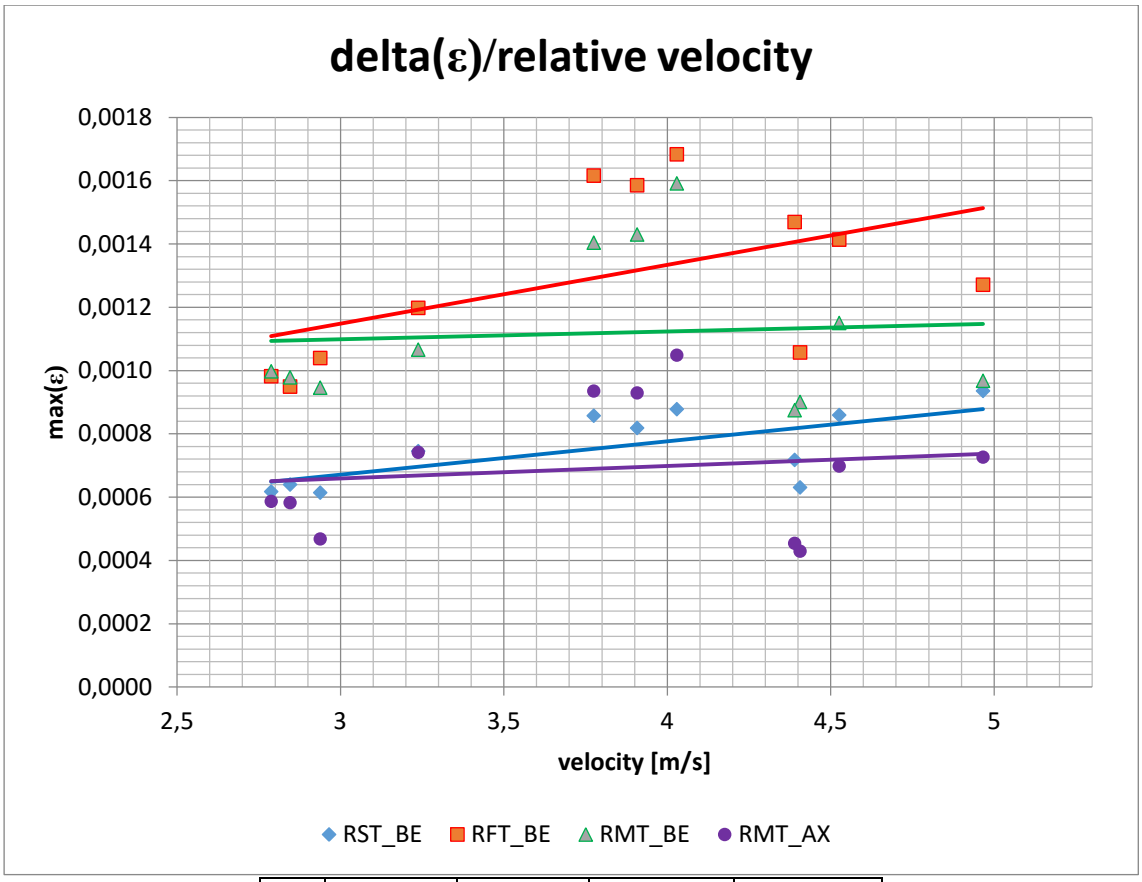

	RST_BE	RFT_BE	RMT_BE	RMT_AX
R^2	0,4437	0,2663	0,0058	0,0197

Figure 5.10: *Delta strain over relative velocity session 2*

5.4.2 Forces analysis

The first fundamental aspect of the strain gauge analysis is to obtain the value of the peaks of the impulsive force during the hit. With the constants calculated from the calibrations, it's possible to convert the signals from mV/V to Newton.

5.4.2.1 Horizontal Forces

For studying the horizontal component of the force, the axial bridge in the main tube is taken as reference. It's the bridge that better reacts to this type of force so only its acquisition is analysed.

For all the operations, the infield software was used.

Although the system was zeroed at the beginning of the session, the signal wasn't exactly 0 mV/V because of noise of the circuit. So first the mean value of the initial 10 second is extracted and all the signal is offset with this value. Then it is scaled with the found calibration constant:

C_H=25068,9 [N / mV/V]

In Figure 5.11 the typical trend during a hit is represented.

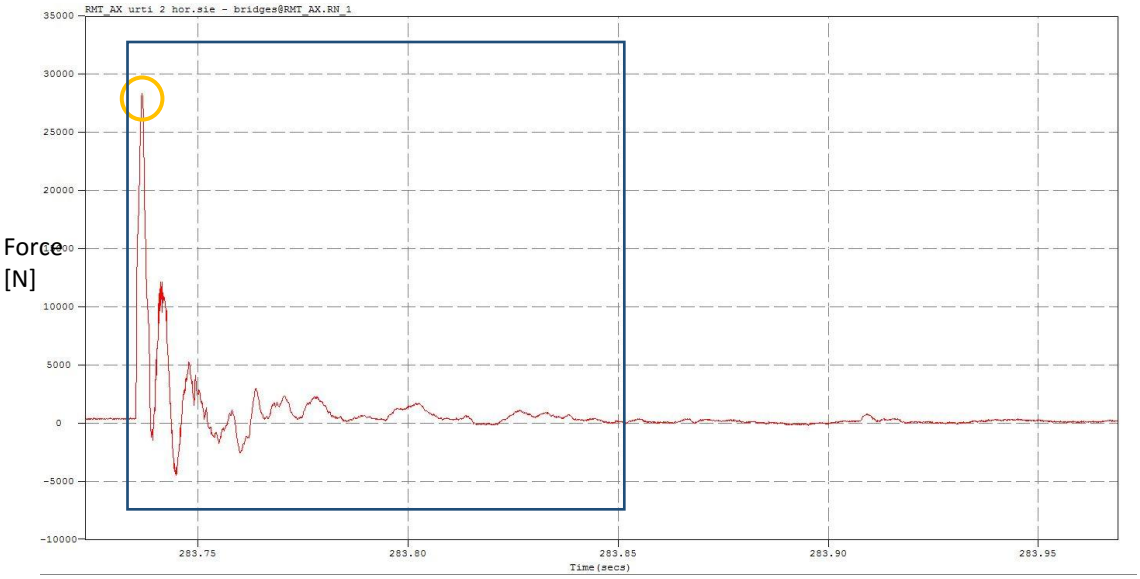

***Figure 5.11**: Force trend on RMT_AX during a hit*

It's possible to identify the first peak, that corresponds to the maximum value of the impulsive force and it is positive because it's a compressive load. For every single hit, this peak's value is extracted and all the measured forces are reported below in Table 5.6. After this positive peak, it's possible to notice a damped vibration which extinguishes in about 15 hundreds of seconds. In Figure 5.12 the peaks of the force are in relation with the relative velocities.

		SESSION 1		**SESSION 2**	
Distance	**Run**	**Horizontal Force** [N]	**Relative velocity** [m/s]	**Horizontal Force** [N]	**Relative velocity** [m/s]
2 m	r1	**14519,6**	*2,63*	**18517,7**	*2,79*
	r2	**13069,9**	*2,64*	**15064,8**	*2,94*
	r3	**19203,8**	*2,97*	**18748,7**	*2,85*
	r4	**-**	-	**22687,1**	*3,24*
4 m	r1	**23482,8**	*3,57*	**28375,5**	*3,78*
	r2	**17387,8**	*3,75*	**28093,6**	*3,91*
	r3	**18993,4**	*3,41*	**31597,5**	*4,03*
	r4	**-**	-	**22863,3**	*4,53*
6 m	r1	**25271,6**	*3,92*	**13890,3**	*4,41*
	r2	**21495,3**	*3,41*	**14148,7**	*4,39*
	r3	**18167,2**	*3,77*	**24053,4**	*4,97*

***Table 5.6**: Peak values of horizontal force measured by RMT_AX*

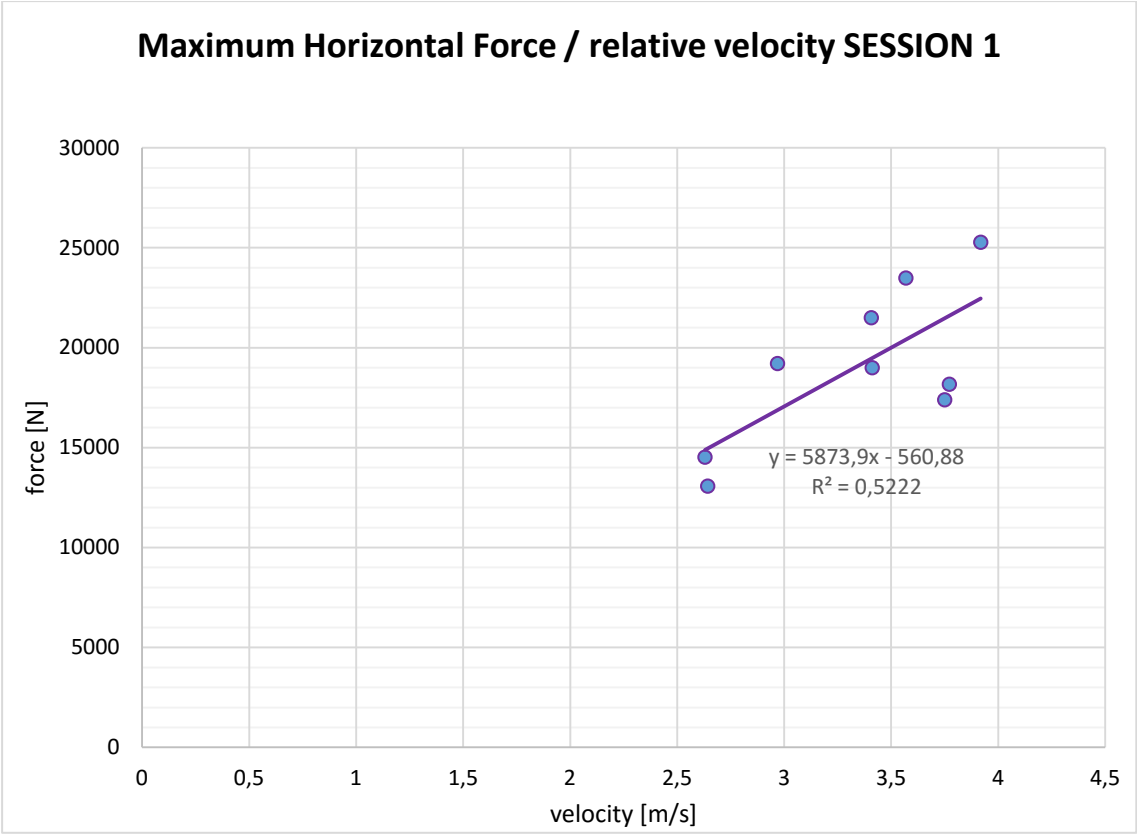

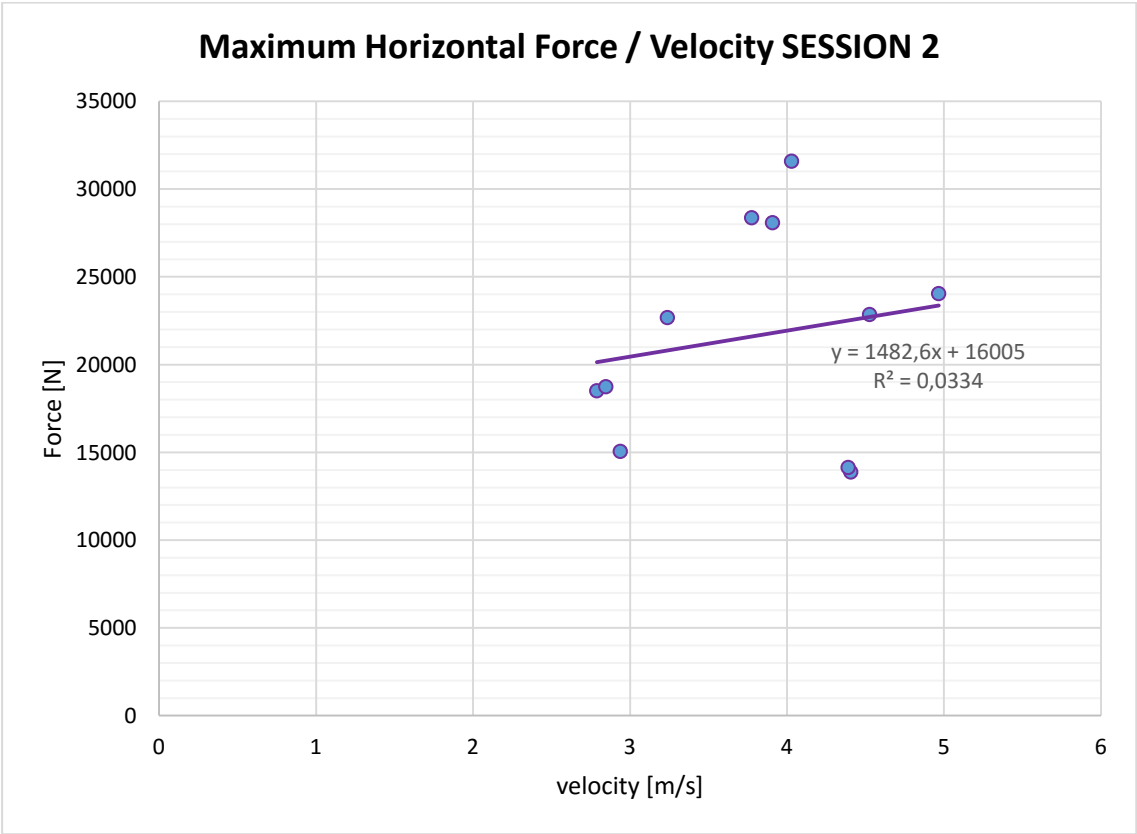

***Figure 5.12**: Maximum horizontal force over velocity*

The values of the force are very high, the highest estimated one is 31597,5 N, but they are impulsive loads, the impulse duration is few hundreds of second. From the graph of the first session, it's possible to see that the behaviour is quite linear and the intercept of the regression line is 560,88, it passes clear to the origin. In the second session the results are more scattered and their behaviour is different from the other session. This may depend on the shape of the wheelchair bumper. In the first session, the opponent used a defensive model and in the second an offensive one. The defensive configuration has a larger and lower bumper than the offensive configuration, as it's highlighted in Figure 5.13, so with defensive wheelchair, the collision occurs always on the little horizontal plate of the bumper. Instead, with offensive opponent, the impact may involve the two triangular supports of this plate. This occurs because all the wheelchairs can make some degrees of pitching and the thickness of this plate is only 10 mm. That causes a different transmission of the load to the frame and may explain the non-linear behaviour in the second session.

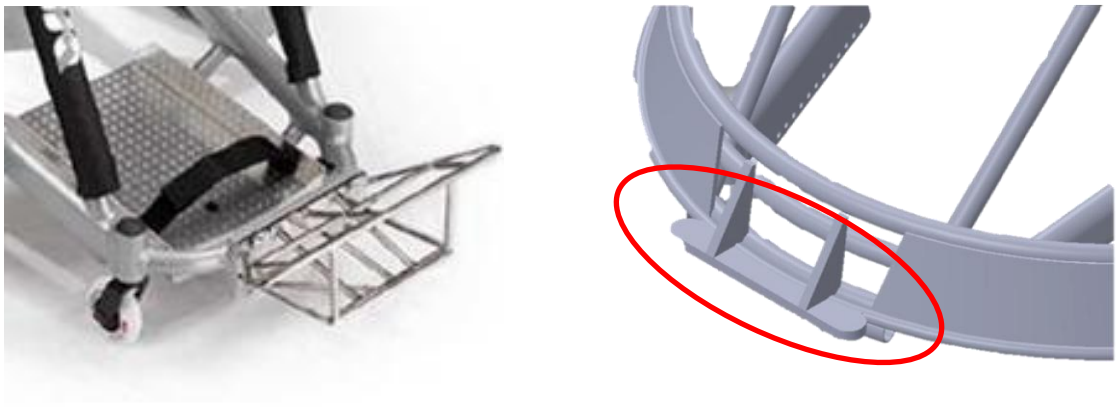

***Figure 5.13**: Particular of the defensive (left) and offensive (right) bumper*

5.4.2.2 Vertical Forces

Also vertical forces acting at the instant of the wheelchair landing from collision were analysed. As previously seen, this load is caused by the body weight and it depends on how much the wheelchair lifts.

For this vertical component, the bending bridge in the main tube is taken as reference. It's sensitive also to the horizontal load, but it responded very well to the application of weights on the seats during the calibration.

Using the infield software, first, the mean value of the initial 10 second is extracted and each signal is offset with this value. Then it is scaled with the found calibration constant:

C_{VER}=20938,0 [N / mV/V]

In Figure 5.14 an example of the behaviour of the signal at the moment of landing.

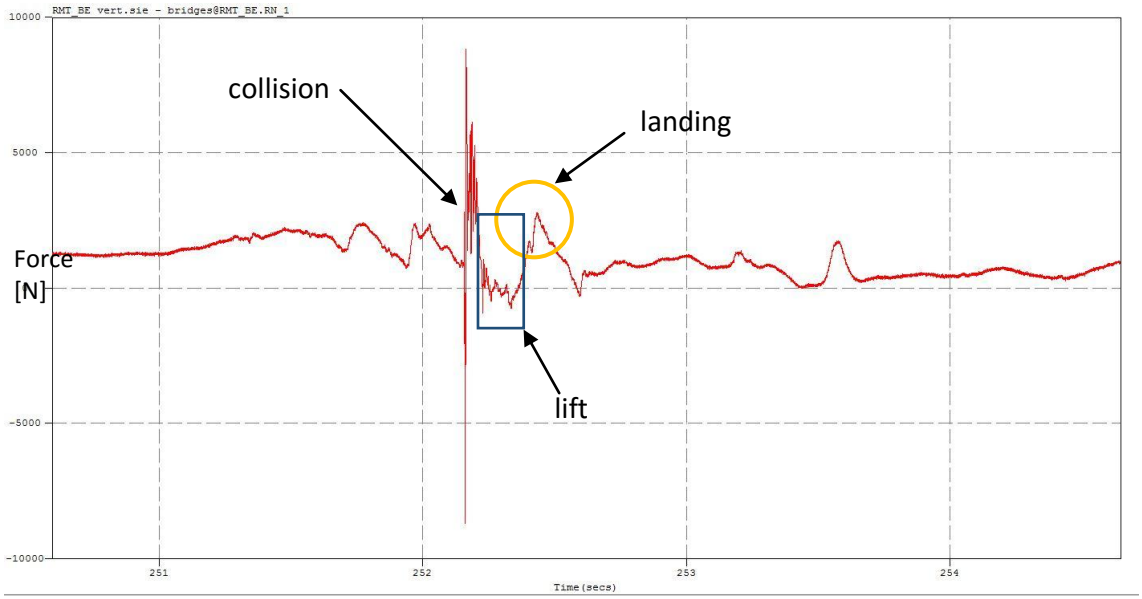

***Figure 5.14**: Behaviour of the RMT_BE in the instant of return*

From this extract, it's possible to notice that the return occurs three or four hundreds of second after the hit and it is represented by the peak indicated in the figure. The value and the shape of the peak depend on the lifting of the wheelchair. It can be pointy if the wheel leave the ground or it can be more gradual if the wheel remain on the floor and the inertia of the body mass makes the player jolt. The lifting height is obviously directly related to the relative velocity, but mostly it's related to the exact point of contact between the two wheelchairs. In both cases, the maximum value of the force in this phase is extracted and they are reported in Table 5.7. Moreover, the value before the hit isn't 0 because the system was zeroed before the player sat on the wheelchair and this offset corresponds to the weight force of his mass. Unfortunately, it was not possible to estimate the lift height of the wheelchair from the video.

Vertical Force [N]			
Distance	Run	**SESSION 1**	**SESSION 2**
2 m	r1	2782,85	1273,52
	r2	2473,66	1295,78
	r3	2092,87	2093,91
	r4	-	3314,94
4 m	r1	5324,69	2316,49
	r2	4498,02	2389,63
	r3	3603,01	3349,92
	r4	-	2167,04
6 m	r1	5158,71	1766,39
	r2	5340,97	3515,27
	r3	5725,01	2109,8

***Table 5.7**: Peak values of vertical force measured by RMT_BE*

5.4.3 Acceleration analysis

The aim of the use of the accelerometer was to find the value of the deceleration in longitudinal direction to which the wheelchair is subjected. With this sensor it could be possible to calculate a dynamic force multiplying it by the total mass and put it in relation with the impulsive force measured by the strain gauges.

Instead, the frame hit in the collision generates high vibrations, the highest value is over 500 g's, and it's impossible to recognize the first negative peak. The acceleration has a different behaviour in each hit and it can be notice in Figure 5.15a that shows some examples. In figure 5.15b it can be seen that also the vertical deceleration in the return phase isn't noticeable and seems to have the same problem. The first negative peak varies even 300 % and it isn't significant.

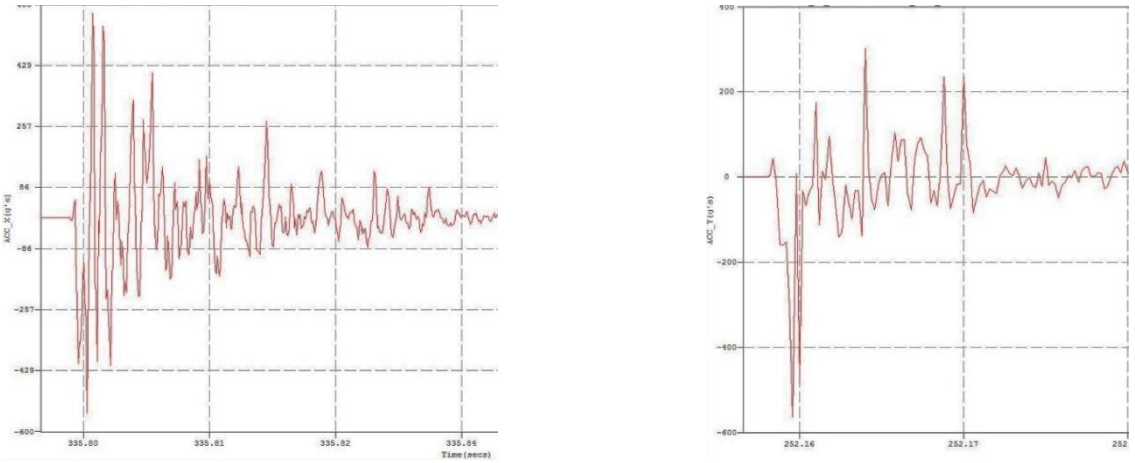

a) Trend of longitudinal acceleration in a hit

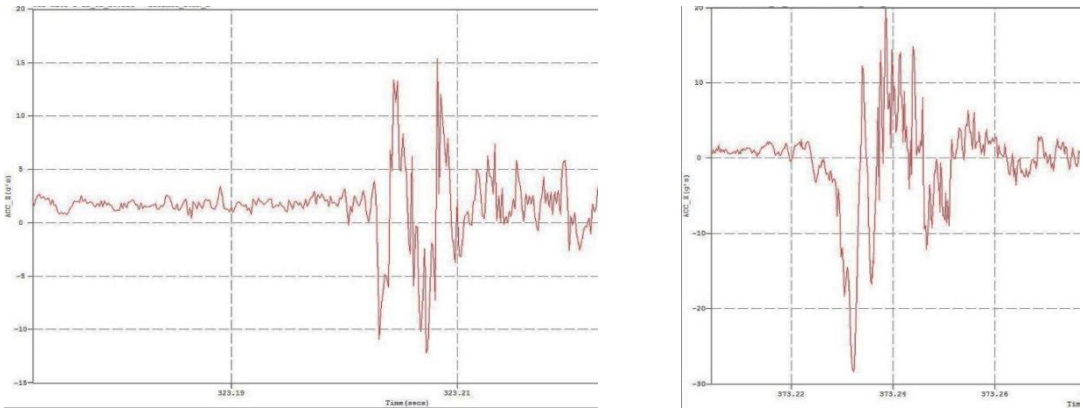

b) Trend of vertical acceleration in a hit

Figure 5.15

CHAPTER 6: PERFORMANCE TESTS

Inside the Wheelchair Rugby project, another work conducted by eng. Maria Laura Magrini was carried in collaboration with this study and many information were shared. The aim of her work was to measure the dynamic performances of athletes investigated by measuring their longitudinal acceleration and angular velocities in different situations, through MEMS inertial sensors. Moreover, she analysed the shoulder and elbow isometric force and the pressure distribution on the seat. There is an extract of her work regarding the performance tests conducted with this study.

In fact, Wheelchair Rugby is a very tactic game, based not only on mere athletes' muscular force, but much more on the way the athlete can use his force to express particular abilities and skills within the game. Impressing a good acceleration, velocity, and spinning, combined with a team play, are some of the most important features that a Wheelchair Rugby athlete has to learn and improve. Therefore, some situations present the necessity of impressing a big acceleration from a still position, for example to reach to the goal line or to receive the ball from a mate; another necessity is the ability of turning quickly, in situations as blocking an opponent or freeing from a blockage position.
This sport was born to give people with an incomplete upper limbs and trunk muscular control, the chance to compete using their residual capacities at best: in this way, athletes with low points and most severe impairments can have an essential role within the game.

6.1 Instrumentation

6.1.1 Xsens technology

The Xsens wireless Motion Tracker (MTw™) is a miniature wireless inertial measurement unit (IMU) realized with MEMS technology. It contains 3D accelerometers, 3D rate gyroscopes, 3D magnetometers and a barometer (pressure sensor). The embedded processor handles sampling, buffering, calibration and Strap Down Integration (SDI) of the inertial data, as well as the wireless network protocol for data transmission. SDI is a method to compute an orientation or position changing given an angular velocity or acceleration of a rigid body. The Xsens provides real time 3D orientation for wireless motion trackers in a network, returns 3D linear acceleration, angular velocity and (earth) magnetic field and atmospheric pressure data. The system used in this work consists in:

- **Motion Tracker wireless sensors (MTw's™):** portable sensors with their own battery (Figure 6.1). All wireless motion trackers send data wirelessly to the PC, via the Awinda Station™, placed on the desk next to the recording PC.

Figure 6.1: *MTw™ inertial sensor.*

- **Awinda Station™** that controls the reception of synchronised wireless data from all wirelessly connected MTw™ sensors, and charges up to 6 of them simultaneously (Figure 6.2); it is connected via USB with the PC for data acquisition;

Figure 6.2: *Awinda Station™.*

- **MT Manager™ Software** for visualising and recording data; it is possible to see the real time orientation of the connected sensor, together with their angles values, acceleration trend, magnetic field.

Sensors specifications are represented in the following Table 6.1*:*

	Angular Velocity	Acceleration	Magnetic Field	Pressure
Dimensions	3 axes	3 axes	3 axes	-
Full Scale	± 1200 deg/s	± 160 m/s2	± 1.5 Gauss	300 -1100 mBar[4]
Linearity	0.1% of FS	0.2% of FS	0.2% of FS	0.05% of FS
Bias stability[5]	20 deg/hr	-	-	100 Pa/year
Noise	0.05 deg/s/√Hz	0.003 m/s²/√Hz	0.15 mGauss/√Hz	0.85 Pa/√Hz
Alignment error	0.1 deg	0.1 deg	0.1 deg	-
Internal Sampling Rate	1800 Hz	1800 Hz	120 Hz (max.)	-
Bandwidth (analogue)	~120 Hz	~140 Hz	10-60 Hz[6]	-

Table 6.1: *Main sensing specifications.*

The patent-pending Awinda™ radio protocol is based on the IEEE 802.15.4 PHY. Using this basis, ensures that standard 2.4 GHz ISM chipsets can be used. The Awinda protocol provides time synchronisation of up to 32 MTw's across the wireless network to within 10 µs. With Awinda, the data are initially sampled at 1800Hz, down-sampled on the processor of the MTw to 600Hz, and using Strap Down Integration (SDI) the data are transmitted to the Awinda Station. Output sample rate of the MTw's™ can be chosen by the user and

changes with the number of connected sensors: with one MTw™ connected, the maximum frequency is 120 Hz; with two, the higher frequency automatically decreases to 100 Hz, and so on. The lower frequency is 20 Hz. Each MTw™ is powered with its own LiPo battery. At its current state of use, the battery lasts for almost 2 hours and can be recharged after one hour docked in the Awinda Station™ [35].

6.1.2 Sensor fixation

To perform dynamic measures, Xsens MTws™ were put in the same positions for each wheelchair: one on the frame, and one for each main wheel, as described in the following paragraphs.

6.1.2.1 Wheelchair frame sensor

The wheelchair frame sensor allows recording the forward acceleration and angular velocity of the system in movement. Considering the wheelchair-player system, its reference frame is considered with the origin in its Centre of Mass (COM), the X axis in the direction of movement (horizontal), the Z axis in the vertical plane and the Y axis obtained with the right hand rule. To measure the forward acceleration of the system and its angular velocity, the sensor must be ideally placed in the COM, but since its spatial coordinates are unknown, this is not possible: therefore, its position in the wheelchair frame is given by the centre of the beam connecting the wheels' axles. The Xsens is placed in a horizontal plane, with the X axis parallel to the wheelchair-user's X axis, as represented in Figure 6.3.

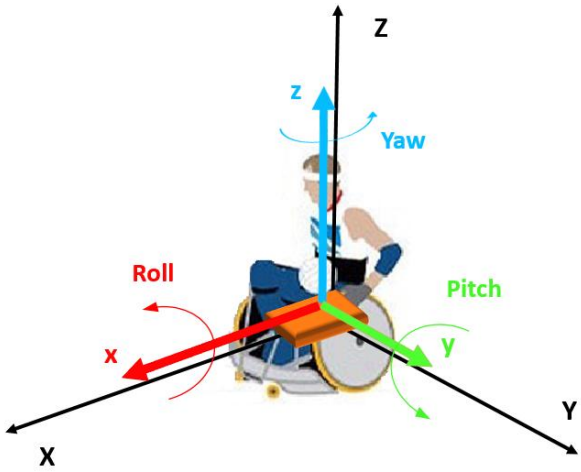

***Figure 6.3**: Player in its reference frame (black); Xsens reference frame with Roll, Pitch and Yaw angles.*

A support was attached to the wheelchair frame to fix the sensor. Since each frame had a slightly different structure, the support and its fixation were adaptable. The bends given from the Xsens set were used, which are provided with a click-mechanism that allows the sensor to be easily fixed.

***Figure 6.4**: Wheelchair with sensors (frame and wheels).*

6.1.2.2 Wheel sensors

An Xsens was placed on each wheel, to evaluate the velocity of rotation and the number of turns. After removing the wheels, a plastic support was fixed in the axle, and on it, an Xsense with the X axis in the direction of the axis of rotation of the wheel, oriented externally, to record wheel angular velocity (*Ang vel* X_w). The setting is shown in Figure 6.4.

***Figure 6.4:** Sensors in the wheels. Left: wheel system of reference; right: sensors fixation.*

6.3 Methods

In this work, the Xsens was used to measure the longitudinal acceleration and the angular velocity of wheelchair rugby players in different kinds of exercise, to obtain a quantitative evaluation of their performance on court.

6.3.1 Tests description

From the literature and the observation of the match, it was decided to evaluate the ability to push and finally brake during a 20 m linear sprint, the ability of turning left and right on spot, an 8 track which is more similar to a real game, combining linear sprint with turning. Finally, a match was analysed.

6.3.1.1 20 m sprint

The 20 m sprint is a time exercise assessing the ability of the player to push with his arms, as much and fast as possible. It corresponds to an explosive performance. In this path, the subject was asked to reach his maximum acceleration in 20 m and, once having passed the final point, brake instantaneously. In this way it was possible to measure the trend of the forward acceleration during the push phase, and the negative acceleration given by braking.

Players started from a fixed position (Figure 6.5), without moving, with the front castors aligned in a given line.

Figure 6.5: *An athlete at the starting position for 2the 20m sprint (yellow arrow).*

The Xsens started its acquisition when the subject was well positioned in the start line: in this way, the initial time of the longitudinal acceleration was visible on the recorded signal as an initial high positive value after a time of zero acceleration.

At the signal of "go" the player started pushing: time was counted with a hand chronometer. Once he passed the final cones, time was stopped and the Xsens acquisition was stopped few seconds after the final braking. This exercise was repeated three times, with a brief recovery (almost one minute) after each trial.

6.3.1.2 Rotation

In this exercise, the subject was asked to rotate on place (Figure 6.6) to evaluate his ability to turn left and right and the eventual difference on the performance between the left and the right side, measuring the Z angular velocity of the frame sensor.

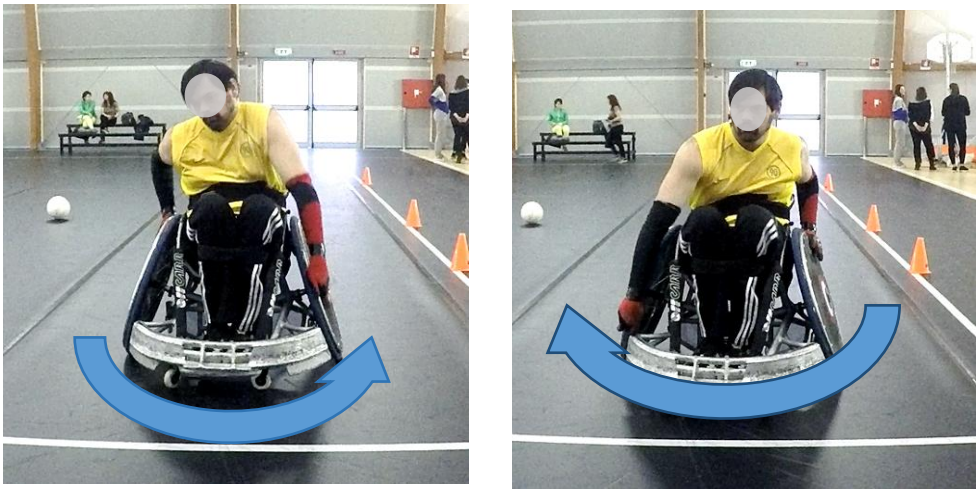

***Figure 6.6**: Left rotation; right rotation.*

The player started from a given position, and at the signal of start, he executed as fast as he could, a 360° turn on place, in the right direction, trying to turn around the vertical axis that ideally passes through the point of intersection of the wheel axis (the Z axis of wheelchair-player reference frame). Three seconds after the first rotation, he turned on the other direction. This left-and-right session was repeated three times, with a brief recovery (10 s) between each trial. Xsens registered each trial.

6.3.1.3 Eight track

The eight track is a time exercise, described by cones, in which linear acceleration and rotation are combined: this is more similar to a real game situation. During this exercise we measured the linear acceleration and the Z angular velocity of the player.

The path is shown on Figure 6.7.

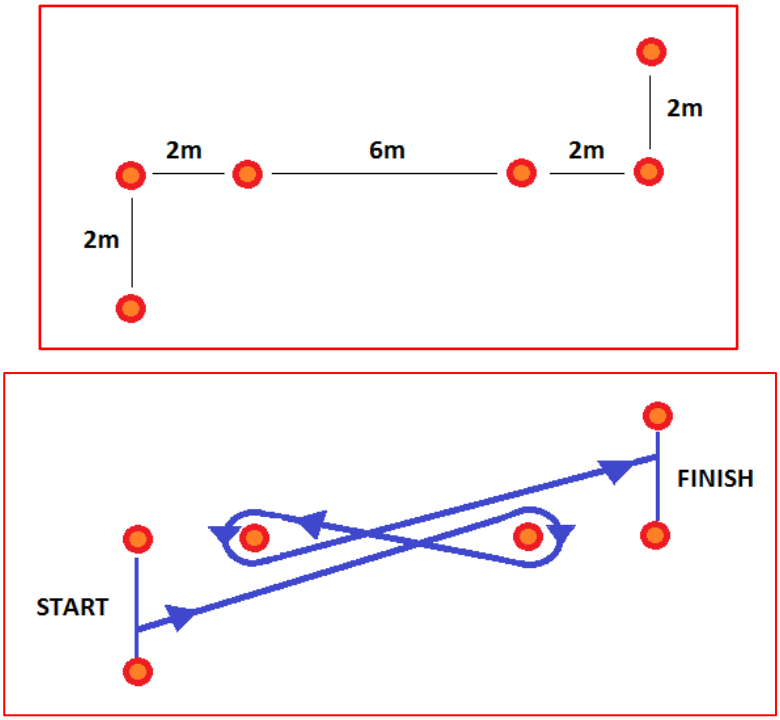

Figure 6.7: *The red points represents the cones. Up: distances between cones; Down: 8 track (blue lines) from start to final point.*

The subject started from a given position (Figure 6.8) and after the signal of "go", he started pushing. Time was stopped when he passed the last two cones. This exercise was repeated three times, with a brief recovery (almost one minute) between each trial.

Figure 6.8*: Eight track from starting position.*

6.3.2 Signal analysis

The MT manager software saves the Xsens file as MT binary log file (*.mtb*). The aim of the signal analysis was the extraction of:

- max and mean values of forward acceleration for the 20 m sprint;
- maximum value of left and right angular velocity in rotation tests;
- maximum value of forward acceleration and of left and right angular velocity in eight track tests;
- maximum forward acceleration and distribution of acceleration values within a match.

6.4 Results

This paragraph describes the results about the dynamic test: push shape and frequency, and the data coming from the Matlab analysis.

6.4.1 Push shape

Data analysis of forward acceleration trend revealed that each player has his personal pushing style. One push is defined from the lower negative point of the previous push to the lower negative point after the final descending trend. With a first approximation, a push of acceleration can be described as an initial growing trend and a consecutive decreasing trend. Nevertheless, this description is not complete, since in this work, the forward acceleration signal of the majority of players present a more complex trend. *Figure 64* represents the pushing trends found in the present analysis, during the middle part of a 20 m sprint (without considering initial and last pushes).

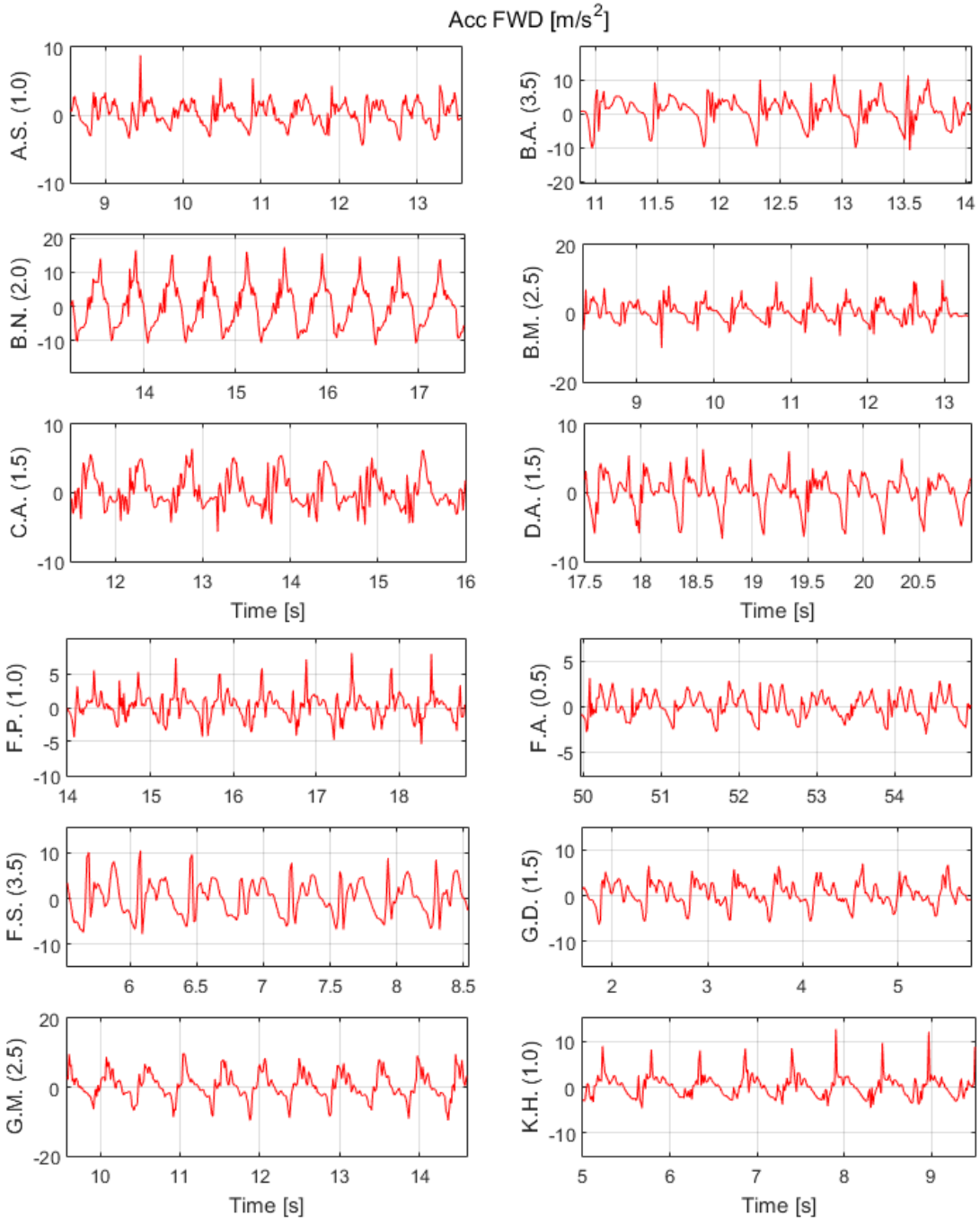
Acc FWD [m/s^2]
A.S. (1.0)
B.A. (3.5)
B.N. (2.0)
B.M. (2.5)
C.A. (1.5)
D.A. (1.5)
Time [s]
Time [s]
F.P. (1.0)
F.A. (0.5)
F.S. (3.5)
G.D. (1.5)
G.M. (2.5)
K.H. (1.0)
Time [s]
Time [s]

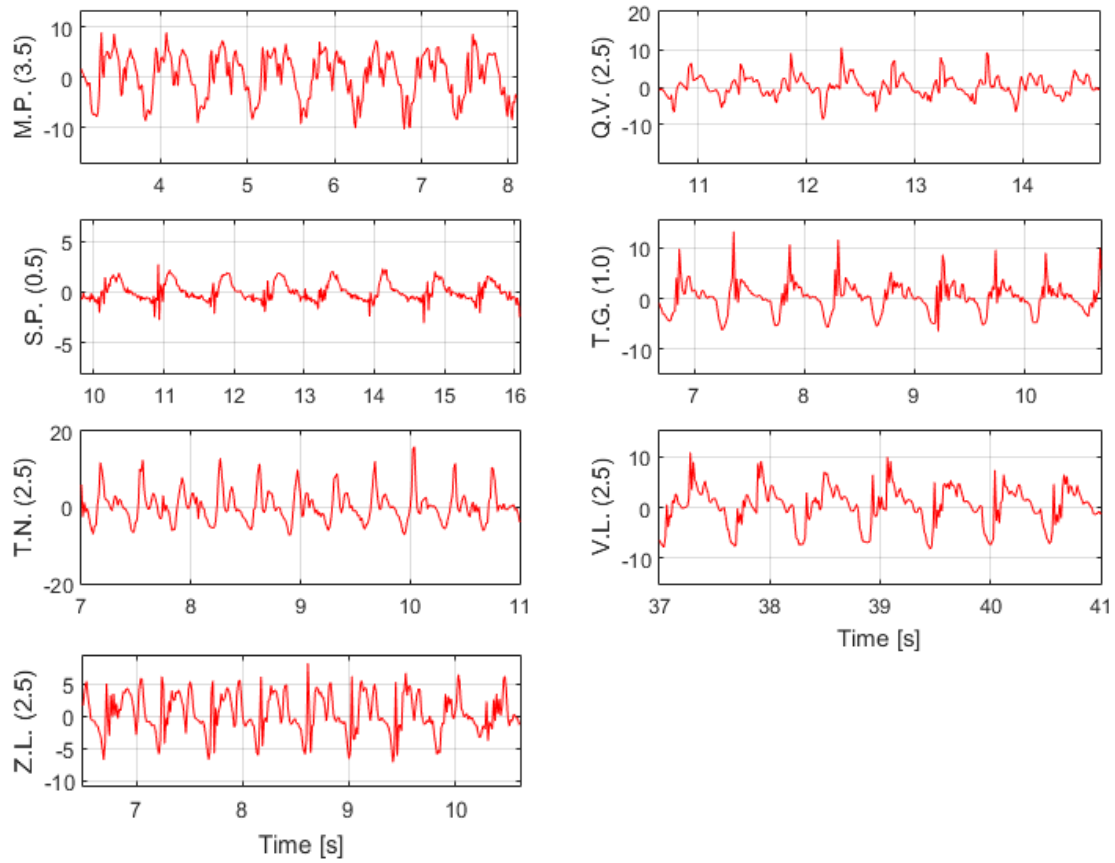

***Figure 6.9**: Comparison between forward acceleration trends in a 20 m sprint. For each player is represented the point of classification.*

6.4.2 Push frequency

In data analysis of 20 m sprints, the calculation of the power spectrum of forward acceleration allowed extracting the push frequency. The push frequency of each single player was extracted as an average between the push frequencies of the three trials. The push frequency locates between 1.18 and 2.67 Hz; with an average of 2.079 Hz (SD ±0.360). There is no correlation between the push frequency and the point of classification.

6.4.3 Performance tests

Dynamic performanc tests with inertial sensors are described by parameters of forward acceleration and angular velocity. In particular, 20 m sprint and eight track give values of max and mean acceleration: these values, multiplied by the body weight of the athlete, give the expression of a force. In the data analysis and the comparison between different

athlete's performance, it is important to rely to this value of force instead of the acceleration values. In fact in a dynamic test the acceleration trend depends, besides that, on the mass of the athlete-wheelchair system.

There are many parameters influencing the acceleration trends: mass of the system, inertial forces, friction (wheels-floor, with the air, in the wheels' bearing), wheelchair structure, physical parameters and properties of the person and many others. Each value of force gives an expression of the force that an athlete has to use to overcome the resistance given by all these factors.

For each test, force values were put in a descending order, giving for each athlete in the specific exercise, the rank. In the following graphs (*figures 6.10, 6.11, 6.12, 6.13*) the results for the force values in 20 m sprint and eight track are represented.

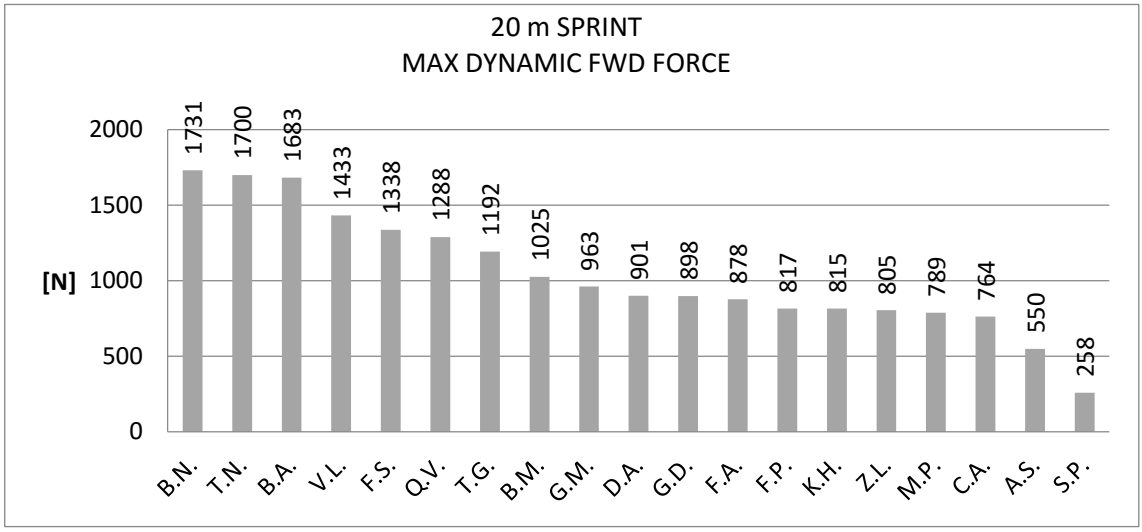

Figure 6.10: *Max dynamic forward force in 20 m sprint.*

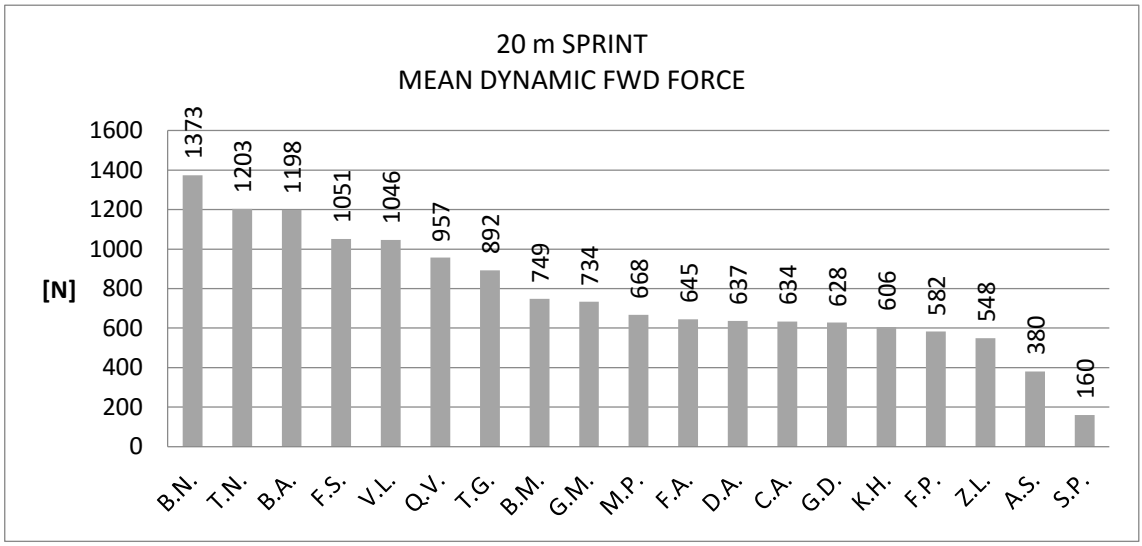

Figure 6.11*: Mean dynamic forward force in 20 m sprint.*

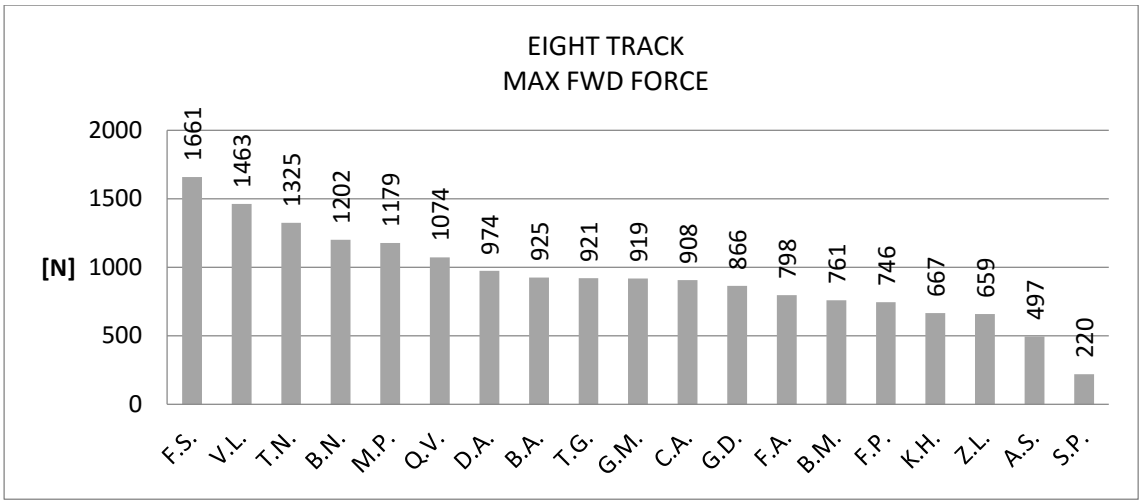

Figure 6.12: *Max forward force in eight track.*

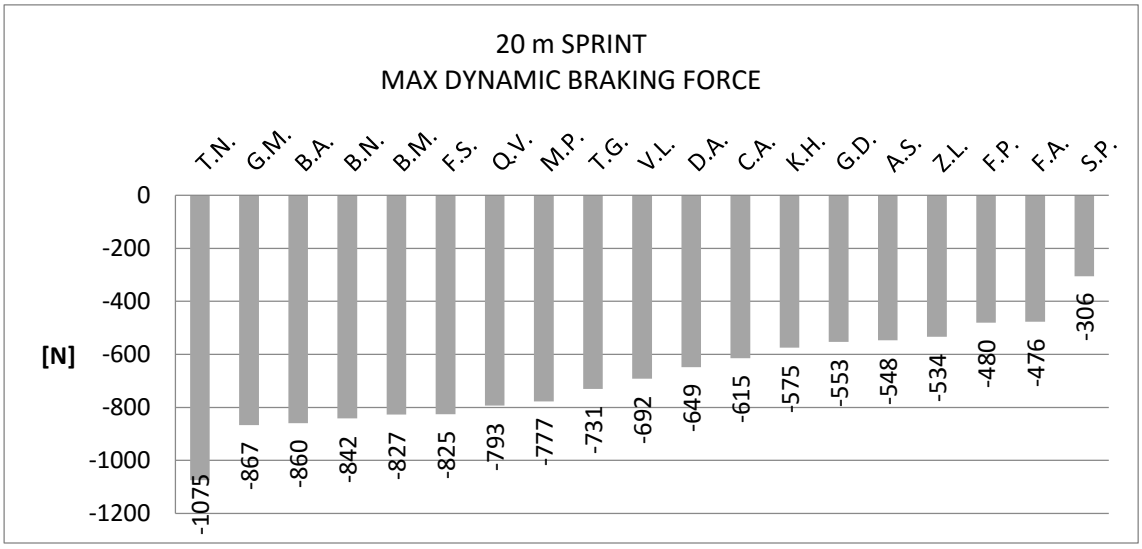

Figure 6.13: *Max braking forward force in 20 m sprint.*

The maximum and mean dynamic forward force rankings generally agree. Two of the 3.5 points (B.A., F.S.) are in both cases among the first five places; the exception is M.P. that situates at the 16th place in the max force, and in the 10th place in the mean force. The reason can be found in the comparison between the isometric force, in the next paragraph. The braking force ranking agrees with the forward force ones.

The results for the rotation and eight track are represented in the following graphs (Figures 6.14, 6.15).

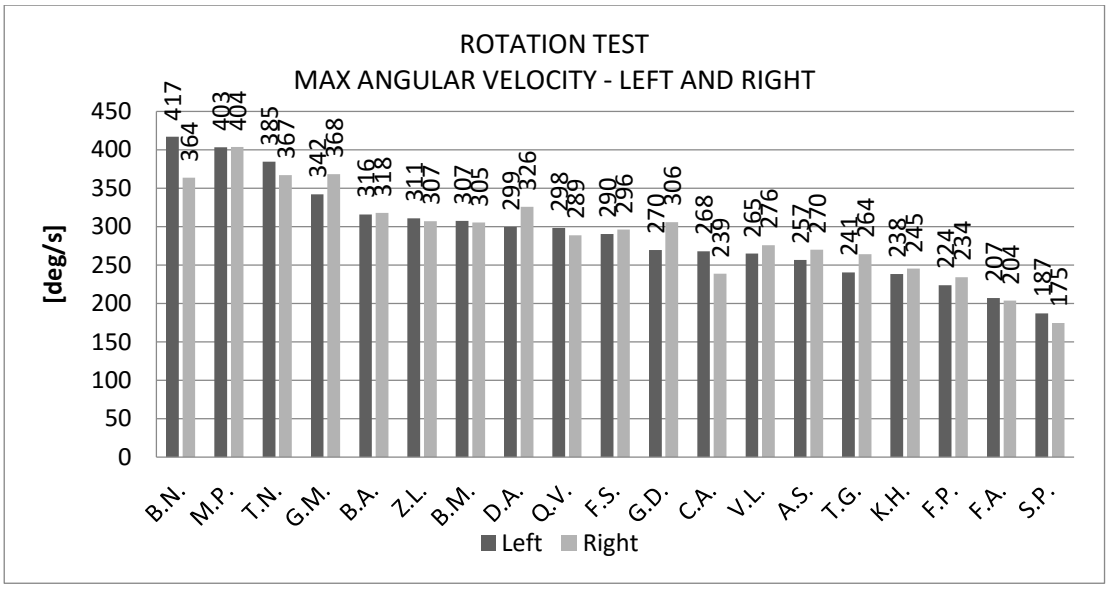

Figure 6.14: *Angular velocity values in the rotation test, sorted by the left side.*

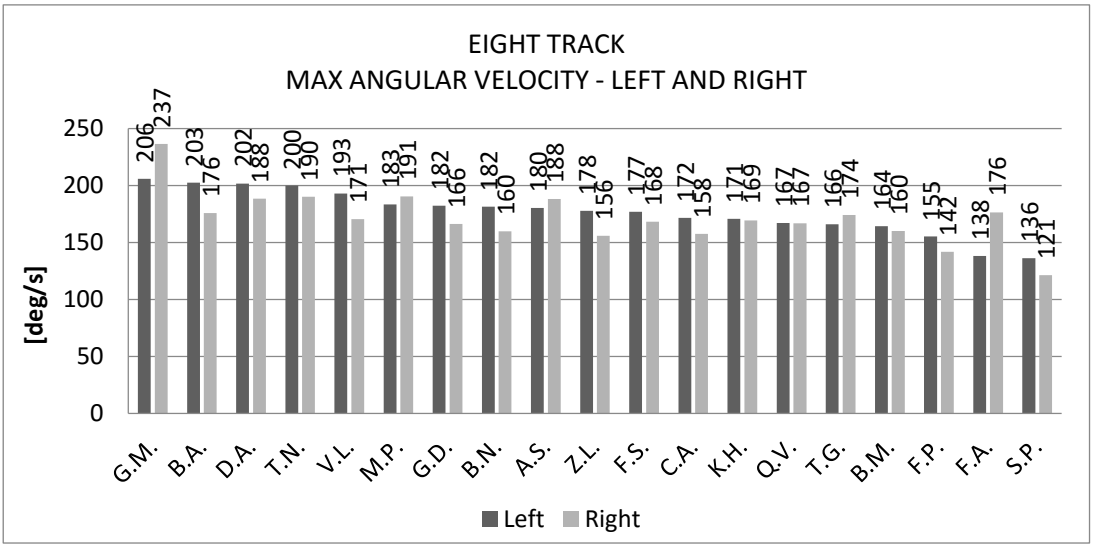

Figure 6.15: *Angular velocity values in eight track, sorted by the left side.*

The angular velocity force values for the rotation are, in average, 80% higher than eight track values: this was expected, since the rotation took place around the Z axis of the wheelchair-player system on place, while in the eight track the player had to turn around a fixed point, external to his system and coming from a forward acceleration phase. The situation was different also because, in the rotation test, the subject had to equally use his arms, in different directions, to execute the movement while in the eight track, turning around a cone, while an arm is pushing the opposite is braking. In general, players do not present high differences between the left and right side performance.

The following graphs (Figures 6.16, 6.17, 6.18) show the push frequency ranking in a 20 m sprint and time rankings in 20 m and eight track.

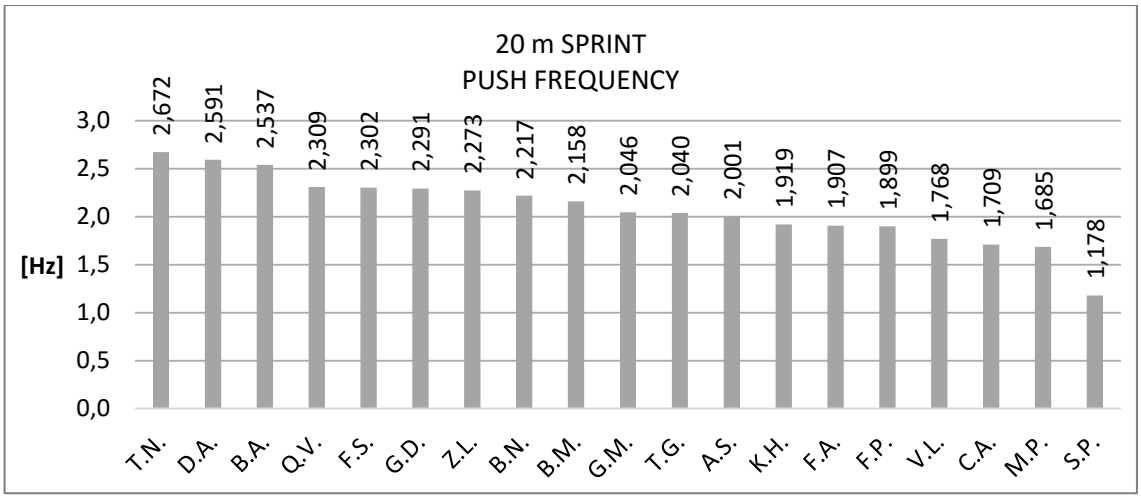

***Figure 6.16**: Push frequency in 20 m sprint.*

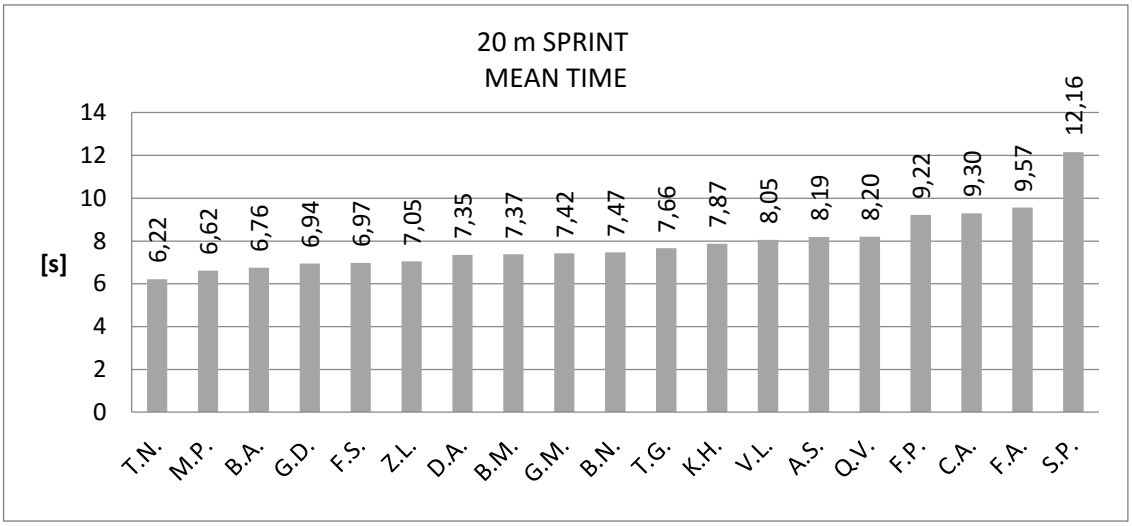

***Figure 6.17:** Mean time in 20 m sprint.*

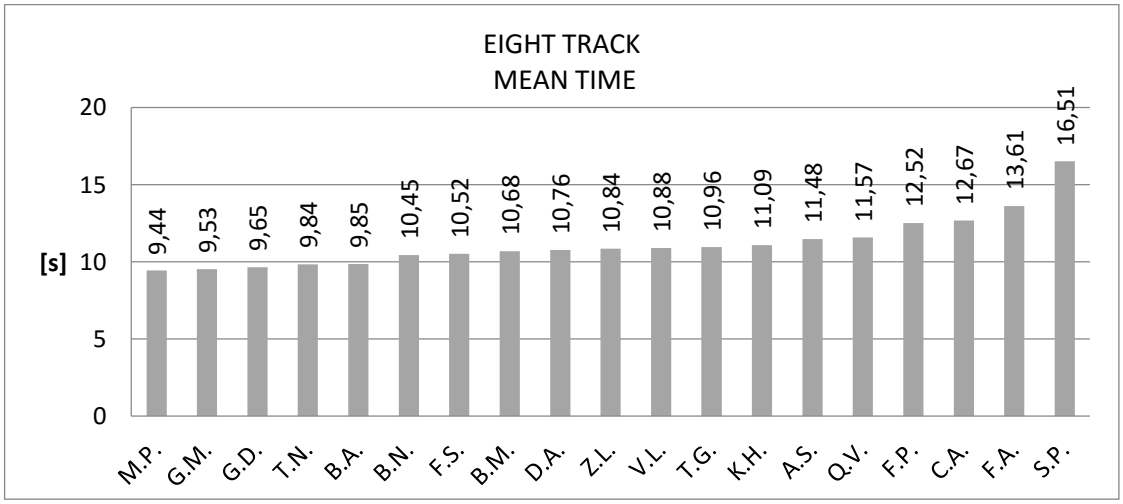

***Figure 6.18**: Mean time in eight track.*

The following graph (Figure 6.19) shows the relation between the point of classification of each player and his mean FWD force in the 20 m sprint. The tendency line, obtained with a three order polynomial fit, reveals that there is a correlation between the point and the

explicated force: the 3.5 points express double force respect to the 0.5 points. Nevertheless, some situations must be noticed: the 3.5 points express, on average, the same force of the 2 and 2.5 points (a linear regression, as done for the isometric push forward force, was avoided since it could not show this fact). Assuming that the increment between points should be linear, this means that the aim is to increase the pendency of the last part of the curve, by improving the performance of the higher points.

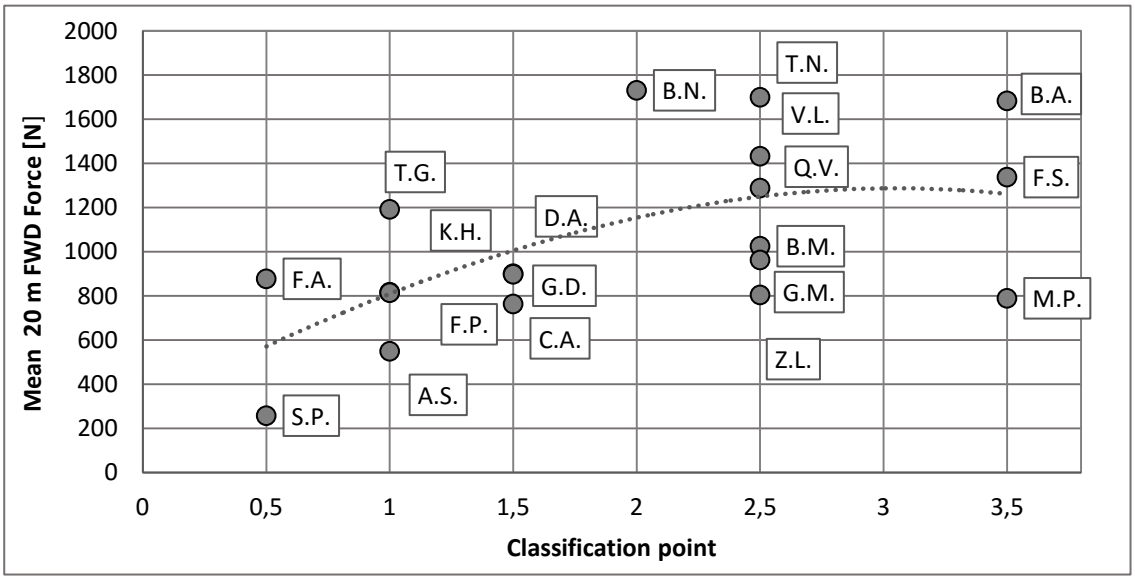

Figure 6.19: *Point of classification vs mean FWD force in a 20 m sprint. Dashed line: tendency line.*

6.5 Wheelchair propulsion references

Wheelchair propulsion technique, in daily use as in sport, is determined by three basic features:

i. the user (the motor) who produces energy and power for propulsion;

ii. the wheelchair, which determines power requirements;

iii. the wheelchair-user interaction, which determines the efficiency of power transfer from the motor to the wheelchair.

The wheelchair-user connection is a system producing an amount of work, to win some resistance forces: some studies demonstrated that the mechanical efficiency of this system in the propulsion movement, is low. The contribution of biomechanics and physiology to the understanding of these elements in improving the performance in wheelchair sports and daily use is fundamental [3]. In the present chapter, a literature research of biomechanical studies about wheelchair propulsion is reported.

6.5.1 Basis of wheelchair propulsion

Some studies investigated the propulsion kinematic technique of a wheelchair, in ordinary activities and for different kind of sports. Wheelchair propulsion is studied as a cyclic movement: a given propelling motion is repeated over the time at a given frequency (*f*), to generate a certain linear velocity (*v*). With a first approximation, a cycle of propulsion can be divided into two phases, as shown on Figure 6.20:

- push phase: hand in contact with the rim, effective force production;
- recovery phase: non propulsive phase, hand is not in contact with the rim since the arm is preparing to restart the next push.

In each push of the wheel, the user produces an amount of work (*W)*. The product of push frequency (*f*) and work (*W)* gives the average external power output (P_{out}), according to:

$$P_{out} = f \cdot W$$

The work produced in each push constitutes the integral of the momentary torque (*M*) applied by the hands to the handrim over a more or less fixed angular displacement (*Q*). The above equation can be rewritten into:

$$P_{out} = f \cdot \sum M \cdot dQ$$

where torque is the product of the bi-manual tangential force, which is applied on the handrim, and the radius of the hand rim.

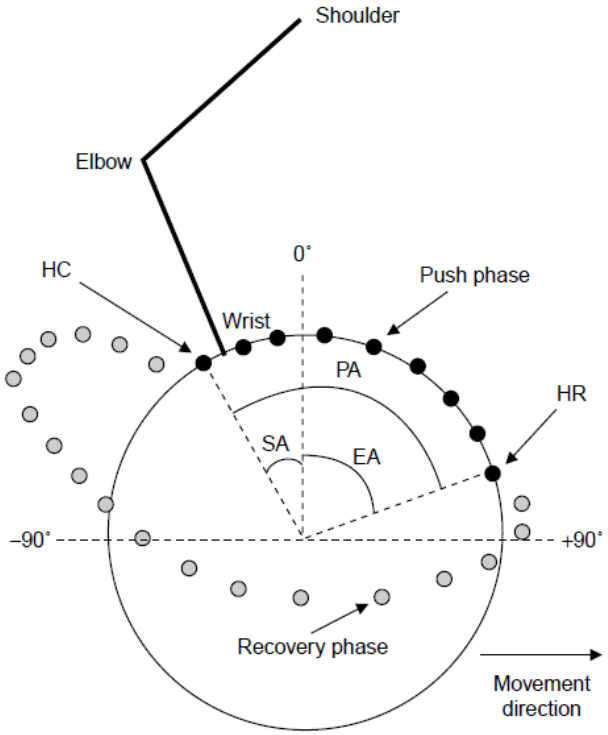

Figure 6.20*: Representation of a wheelchair propulsion technique: HC=hand contact; HR=hand release; PA=propulsion angle; SA=start angle; EA=end angle. [4]*

Physiological measures (i.e. energy cost, physical strain) can be linked with biomechanical measures (i.e. power output, work, force and torque production) to obtain a general view of the force acting on the system. Considering wheelchair sports, the wheelchair-user combination is approached as a free body that moves at a given speed (v) and encounters the following resistance forces (F_{drag}): rolling friction (F_{roll}), air resistance (F_{air}), internal friction (F_{int}) and the metabolic consumption of the user (F_{met}). Power production during wheelchair propulsion is achieved by upper body work, primarily the arms. The forces (F_{prop}) acting to propel the system and winning the resistance are: inertial force of the system in movement (F_{inert}), the action produced by arms (F_{arm}) and the push force produced by the movement of the trunk (F_{trunk}). In conclusion, the acting forces are:

$$F_{drag} = F_{roll} + F_{air} + F_{int} + F_{met}$$

$$F_{prop} = F_{inert} + F_{arm} + F_{trunk}$$

The output force is given by:

$$F_{out} = F_{prop} - F_{drag}$$

The power output that must be produced by the system to maintain the velocity v is:

$$P_{out} = F_{out} \cdot v$$

Starting from this statements, it is possible to perform tests in order to obtain a quantitative evaluation of the mechanical efficiency of the movement [5,8].

6.5.2 Moments and forces at the handrim

In wheelchair pushing, any force that has a tangential component respect to the wheels, contributes to the propulsion. Forces in other directions do not directly give a contribute to the forward movement. The studies reporting only tangential forces or moments about the hub, do not take into account the components of the handrim forces. For this reason, a three dimensional analysis of the force generation pattern at the handrim, is a prerequisite to relate force application strategies to risk for injuries, and to understand how the propulsion technique can be improved in order to obtain a better sportive performance [4].

6.5.2.1 Moments and forces measuring

The recording of force acting on the handrim during wheelchair propulsion needs the use of an instrumented wheel; a new instrument that allows this measures is the Smartwheel®: a modified wheel, instrumented with a 3-beam system that allows the

determination of three dimensional forces and moments [5]. As the Smartwheel® can be mounted on the individual's own wheelchair, wheelchair-user interface and external conditions can be simulated. The output of the Smartwheel® consists of forces and moments in three dimensions, determined by a world coordinate frame. The force components *Fx , Fy* and *Fz* are defined as directed horizontally forwards, horizontally outwards and vertically downwards, respectively, in a right-hand coordinate system (Figure 6.21); they are combined to give the resultant force F_{tot} .

To relate the forces to the wheel, the coordinate frame can be rotated such that the force components *Fx* and *Fz* represent, respectively, the tangential (*Ft*) and radial (*Fr*) force components of the hand rim.

The tangential force component *Ft* is the only force component that contributes to the forward motion of the wheel. The radial force component *Fr*, and the axial force component *Fy*, create the friction necessary to allow *Ft* to be applied. The resultant force F_{tot}, which is the total force applied to the hand rim, is mathematically calculated by taking the vector sum of the 3 force components *Fx, Fy* and *Fz* [4].

Veeger et al. [6] also introduced a parameter called Fraction of the Effective Force (FEF), as a measure for the effectiveness of force application. FEF is the ratio of the effective propulsion moment measured at the wheel hub (M_{hub}) to the resultant force:

$$FEF = (M_{hub}/r) /F_{tot} \cdot 100\ (\%)$$

where *r* is the radius of the rear wheel.

Some studies analysed the wheelchair propulsion to find a reason why users statistically choose a mechanically disadvantageous movement. An explanation can be found in biomechanics [4].

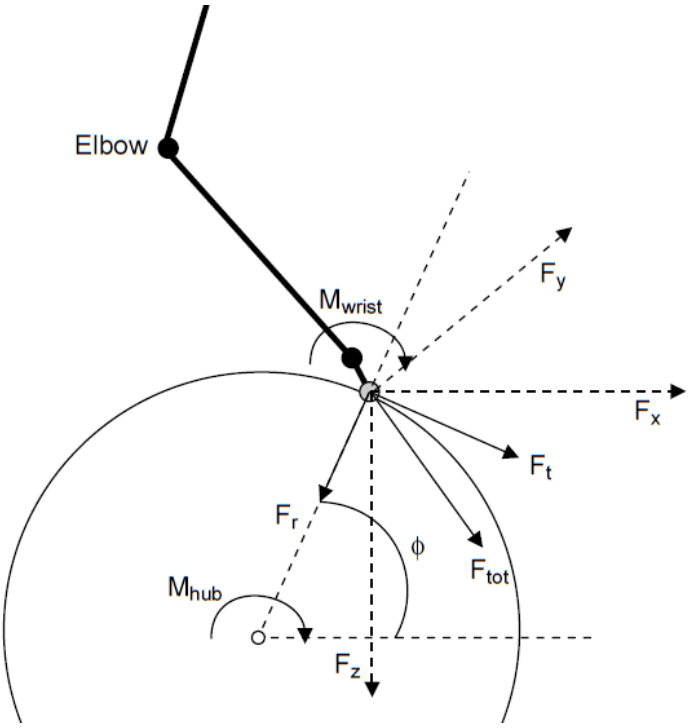

Figure 6.20: *Coordinate frames on the instrumented wheel [4].*

6.5.2.2 Effective vs actual force at the handrim

Since, during the push phase, the hands hold the rims, the movement of hands and arms is considered as a guided circular movement. In guided movements, forces applied by the hands do not directly influence the trajectory of the hands. As a consequence, it is possible to apply a force that is not tangential to the hand rims.

Experimental results in which propulsion forces were measured with instrumented wheels, showed that propulsion forces are indeed not tangentially directed. The direction of the forces applied on the handrim does not agree with the most optimal direction in terms of mechanical power production, i.e. the direction tangential to the handrims. Surprisingly, this apparently, in mechanical terms, suboptimal direction of actual force application was found for athletes as well as untrained subjects [6, 7, 8, 9]. It appears that this particular manner of force application is the most efficient force application technique. In other words, subjects appear to adopt the technique that demands them the least energy, given the mechanical constraints of the wheelchair-user combination [10]. The reason why the users choose this force pattern can be found in the muscle contraction during propulsion.

Veeger and van der Woude [11] studied this concept, represented in Figure 6.21.

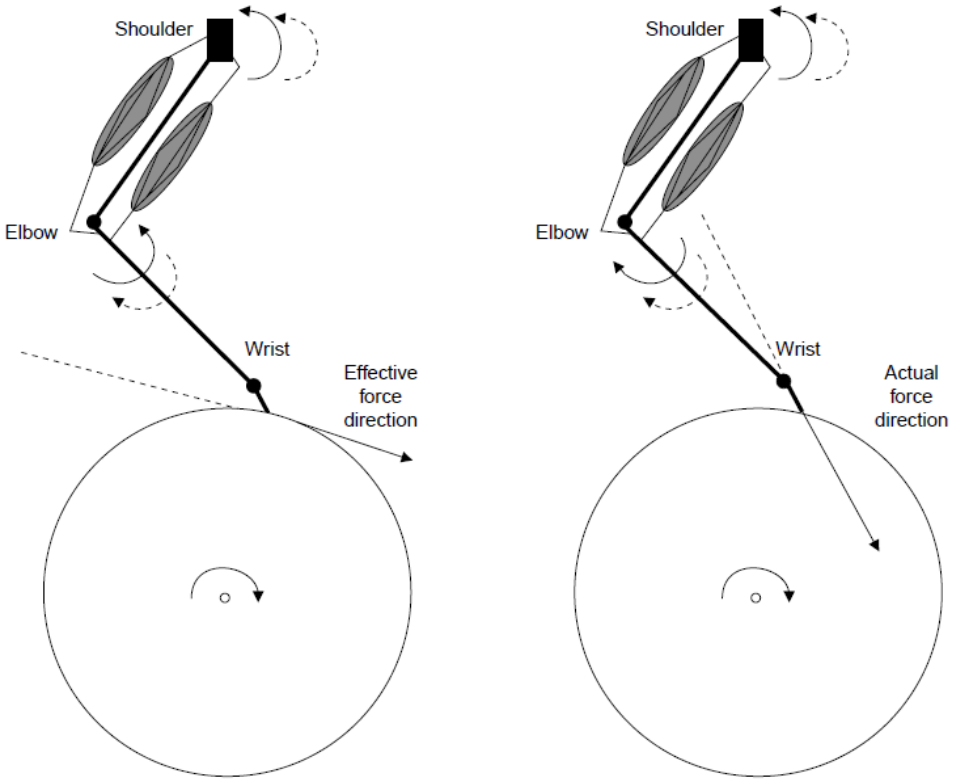

a) *b)*

Figure 6.21: *Difference between effective a) and actual b) force: relationship between force direction and calculated net joint torques around shoulder and elbow. Solid lines: moment around the joint; dashed lines: rotation direction of movement [4].*

Figure 6.21a shows that the application of the tangential force (effective force) might lead to a contradictory situation in which the elbow joint is extending while at the same time a flexor moment ought to be generated for a mechanically optimal results. In this case, the elbow has to be extended (dashed lines) to follow the hand rims in order to be able to apply force on those rims. As a consequence, to direct the force only tangentially, the elbow flexors have to apply force against stretch, which is highly inefficient. In this case, the contribution of elbow flexors would increase the effectiveness of the propulsion force, but the total force would be smaller. A second aspect of this force direction is that the strong elbow extensors cannot be used. The condition in Figure 6.21b depicts the force direction in which no conflict between torque direction and movement direction occurs. This is the situation that is generally found in the studies. The reason of this mechanical inefficient form of propulsion, is based on fact that this is the most efficient solution for muscle biomechanics: the production of negative power is prevented and the strong elbow extensors can be used [4].

6.5.2.3 Moments at the handrim in static propulsion: a study

Some studies measured, with an instrumented wheel, the moments at the rim in wheelchair propulsion. A work by Lan-Yuen Go et al. [12] examined 5 male healthy subjects (non wheelchair-users) during a maximal isometric wheelchair propulsion. The study wanted to demonstrate that, given a subject specific profile of the strengths of each of the upper extremity joints as a function of joint angle, there is an optimal direction of force application in the handrim to maximize the propulsion moment about the wheel axle at each instant of the propulsion cycle. In the experimental setting, the instrumented wheel had a handrim radius of 25.4 cm, and was locked to prevent the forward movement as the subjects pushed with maximum isometric effort. Five hand positions, corresponding to wheel angles θ of 120, 105, 90, 75 ,60° (Figure 6.22) were assigned in a random order.

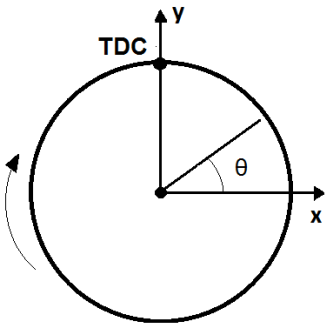

Figure 6.22: *Definition of angle θ and Top Dead Centre (TDC)*

The subjects performed four trials of maximal wheelchair propulsion effort for each hand position.

Applied hand forces in the laboratory reference frame and progression moments about the wheel axle were averaged for the four repetitions to represent each subject's performance at each hand position. The force direction and magnitude of force applied to the handrim were determined.

To estimate the joint strength in an isolated loading condition, the isometric shoulder flexion and extension muscle strength were measured at different angles, using a dynamometer. Muscle strength at each position were determined as the peak force generated during a 3s contraction; three trials of muscle strength were collected.

The optimal force direction was determined at each instant with a linear optimization problem which aims to maximize the moment about the wheel axis, M_0, considering the constraints of the subject's shoulder and elbow joint moment-generation capabilities for the specified joint angles. The results are represented in the following figures (6.23, 6.24, 6.25).

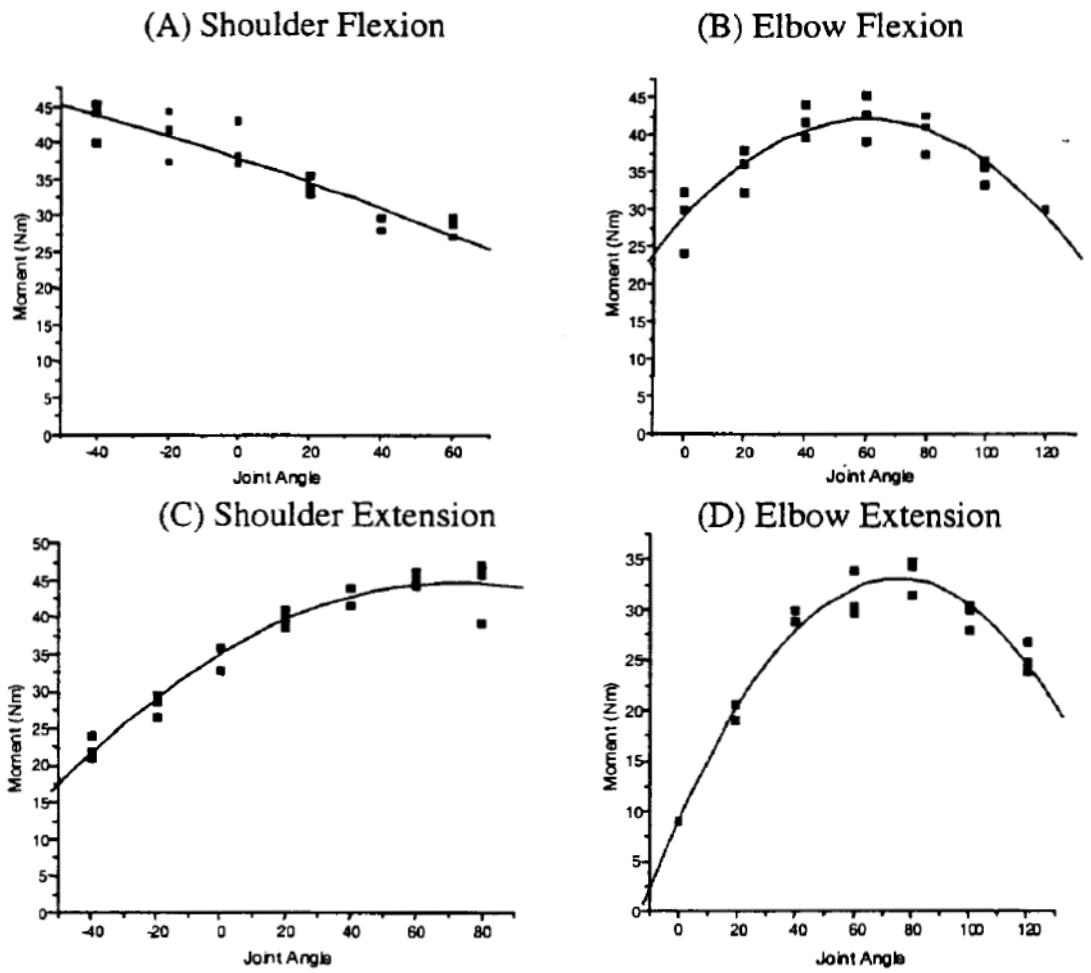

***Figure 6.23**: Moment of elbow and shoulder flexion/extension during isometric contractions [12].*

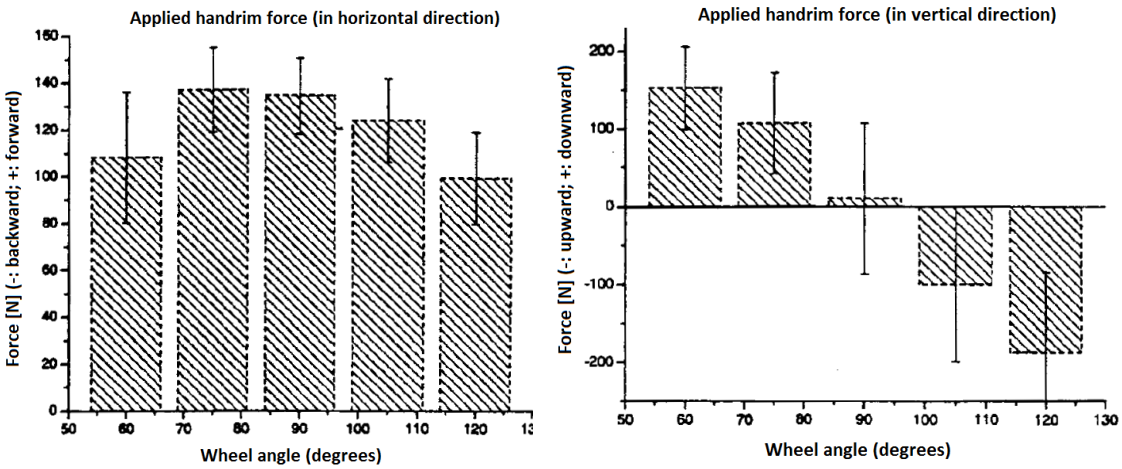

***Figure 6.24:** Mean and standard deviation of handrim force in the horizontal (left) and vertical (right) directions [12].*

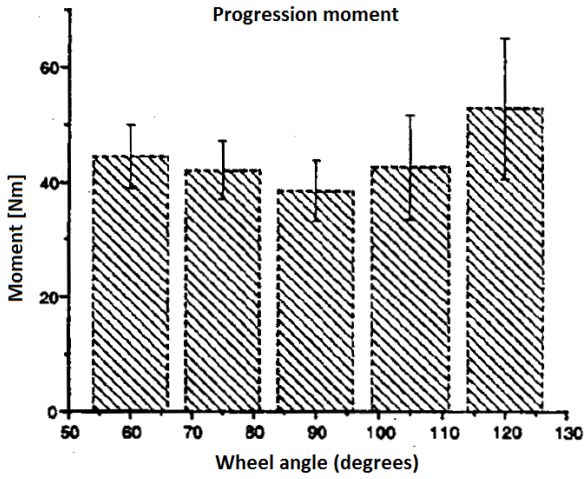

***Figure 6.25**: Mean and standart deviation of progression moment ath the hand rim, at five hand positions [12].*

The results revealed that the progression moment was greater at both initial and terminal propulsion positions (wheel angles of 120° and 60° respectively) and smaller in the mid propulsion position (wheel angle of 90°). The applied handrim force in the horizontal direction, however, was smaller in the initial and terminal propulsion positions and larger during mid-propulsion while the applied handrim force in the vertical direction showed a bimodal pattern, negative prior to top dead centre (TDC) position. These vertical and horizontal force directions correspond to a force which is radially away from the wheel axle posterior to the TDC and radially toward the wheel axle anterior to TDC.

6.5.2.4 Moments in dynamic and static propulsion

The results described in the previous paragraph are an example of the data collected in different studies of static propulsion. Nevertheless, they are in contrats with those documented for dynamic tests: for example, the wheelchair user does not have to initiate acceleration of the wheel at all hand positions as in the static equivalent.

During dynamic wheelchair propulsion, the progression moment reaches its maximum value in mid-propulsion while in experimental models and static studies, the peak in the progression moment is recorded at the beginning and terminal phases of the propulsion cycle. The static analysis reveals that the hand position at TDC may not be optimal to for the upper extremities to generate large forces in the handrim: since the applied handrim force is sperimentally nearly perpendicular to the line from the hand to the shoulder, a large shoulder moment will result. For example, in wheelchair racing, users always flex their trunk anteriorly to propel the handrim with their hand anterior to TDC: this hand position allows larger progression moments to be generated because their lever arms enable the upper extremities to tolerate greater external loading.

Moreover, the force direction posterior to TDC found in static propulsion, differs greatly from the results of dynamic wheelchair propulsion. The direction of handrim force during dynamic wheelchair propulsion is toward the wheel axle during the whole propulsion phase, including the period when the hand position is behind the TDC (Figure 6.26).

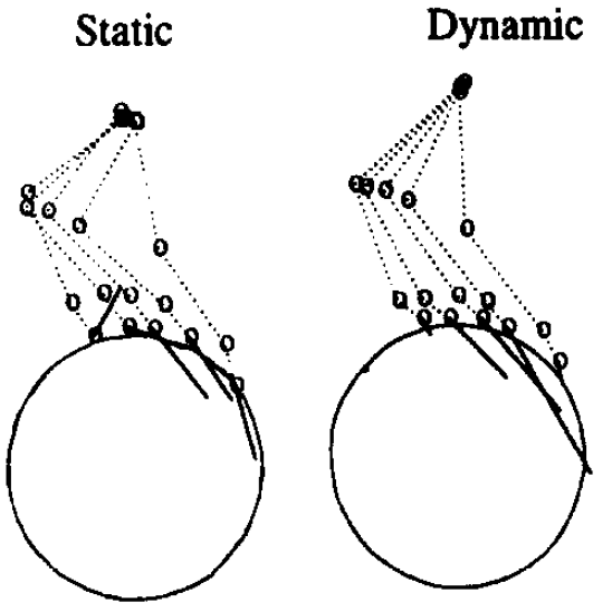

Figure 6.26*: Stick diagrams showing the position of the upper extremity during static and dynamic wheelchair propulsion. The force vector at the rim is shown [23].*

To generate a push force directed away from the wheel axle, the elbow flexor must be activated, and this would indeed be beneficial for propulsion as the elbow must flex during this phase of the cycle (behind TDC). However, halfway through the propulsion phase, the applied force must change to progress the wheel and so the elbow extensor needs to be immediately activated at that point in the cycle. During static propulsion, switching from elbow flexion to extension is not difficult, however, the change in muscle activation from elbow flexor to elbow extensor dynamically may result in a more complex and inefficient movement.

It could then be hypothesized that users could be trained through biofeedback to activate their muscles more like that seeing during static analysis, to increase mechanical efficency [12]. Nevertheless, care should be taken when using increasing FEF as a rehabilitation goal, as higher FEF values shift handrim force contributions from muscles crossing the elbow to those crossing the shoulder, which are already susceptible to overuse injuries [13].

Considerable differences in force application during steady-state wheelchair propulsion [14] and sprinting [15] have been demonstrated between people with quadriplegia and those with paraplegia. The FEF in quadriplegics is the consequence of a significantly larger inwards directed lateromedial force component (*Fy*). Friction at the hand rim is necessary

to produce the tangential component and can be generated through hand grasping, wrist moment generation and/or directing the resultant force away from the tangential direction. In quadriplegics without hand function, only the latter option is available. If triceps function is limited, the generation of friction in a downward or outward direction is hampered. Therefore, the inwards-directed lateromedial force component can serve as an effective alternative for friction generation [4].

CHAPTER 7: FEM SIMULATION

In this work, a finite element analysis was conducted in order to validate the results of the strain gauges' measurement and to simulate different load types to find possible structural critical zones.

The two different calibrations' load conditions tested in field were simulated using the Ansys Workbench 15.0 software.

The aims of this part of work are the following three:

- measuring the numerical strain from the simulations in the strain gauges' location in calibrations' load configuration and finding a correspondence calculating the percentage error between the numerical and experimental values
- finding the most stressed points of the frame and calculating a set of prediction factors in relation with the stress measured at the strain gauges positions

7.1 Introduction to finite element method (FEM)

The finite element method (FEM) is a computer numerical simulation technique for the resolution in discrete and approximate form of general systems of partial differential equations. The finite element method is one of the most versatile, effective and reliable for the approximate solution of one or of a system of partial differential equations. In fact, when the geometry is not so simple, the analytical resolution is very difficult or even impossible. With the FE method instead it is realized a discretization of the domain in order to limit the resolution of complex equations that describe the system within each finite element. EFs are connected together at particular points, called nodes, which can be found in the vertices of the elements, in internal points or sides. FEM can be used for structural, thermal and fluid analysis.

Depending on its characteristics, the object of the study can be divided with different element. There are linear, surface and solid elements and for each one specific parameters can be set up. With the chosen element, it is possible to generate the mesh that divides the model in parts, depending on the element size. Then setting the boundary conditions, the solution can be obtained.

7.2 Method

7.2.1 Wheelchair model

The manufacturing company, OffCarr s.r.l., provided the 3D model of the GoTry Offensive wheelchair realized with SolidWorks software. To facilitate and lighten the analysis, the frame of the wheelchair was a unique solid component and all other parts, wheels, casters and bearings were removed.

Also at this stage it is useful to define the frame's elements with names in order to facilitate the comprehension. In Figure 7. the name of all elements1 are reported.

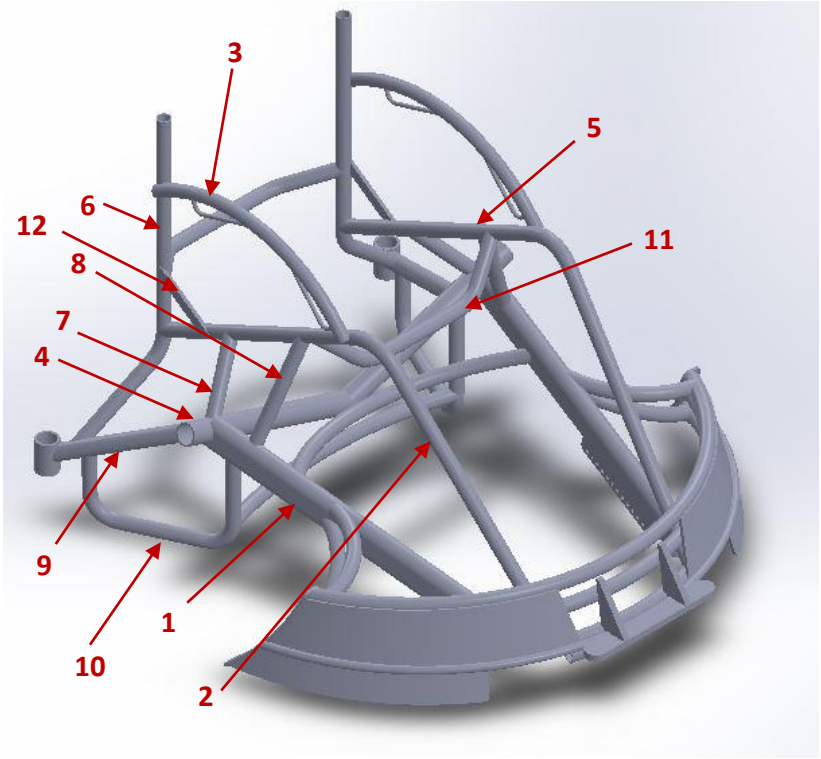

1: Main Tube *2: Front tube* *3: Side Tube* *4: Axle Tube* *5: Seat Tube* *6: Back Tube*
7: Rear Strut *8: Front Strut* *9: Rear Stay Tube10: Rear U Tube* *11: Seat U Tube* *12: Seat stiffener*

***Figure 7.1**: Definition of frame's element*

The geometry corresponds to the real model, except for three differences. The section of the side tube is circular and in the reality it is oval; the length of the seat tubes is slightly shorter than the real one; the weld beads weren't modelled and the tubes are simply joined each other as a unique solid body.

7.2.2 Ansys Workbench 15.0 Software

Ansys is one of the most used FEA (Finite Method Analysis) software and it is divided in many parts. In the preprocessor phase, it is possible to define the geometry of the model and the engineering data, such as the materials. It is possible to apply the boundary conditions, the constraints and the forces or pressures acting in the configuration. Then the mesh can be generated selecting the better way depending on the model, with the possibility to refine it in some specific points. When all these parameters are set, it's possible to start the solver and view the solutions. Ansys offers all types of solutions, stress, strain, deformations and others and they can be displayed for all the geometry or for a single part.

7.3 Ansys Workbench setup

7.3.1 General Settings

In this paragraph all the general parameters set up are described for all the three simulations with Ansys Workbench.

Geometry

The 3D model of the wheelchair was imported from the ParaSolid file, .x_t extension, provided by OffCarr company as an unique solid part. To original geometry, six other pieces were added, described in singular configuration.

Engineering Data

In the Engineering Data field, the mechanical characteristics of the two materials were inserted. For 7020 Aluminium Alloy 73000 MPa for Young modulus and 0,33 for Poisson's Ratio, for 5754 Aluminium Alloy 70000 GPa for Young modulus and 0,33 for Poisson's Ratio. The tubes of the frame were associated to 7020 Aluminium and the plates of the bumper were associated to 5754 Aluminium.

Mesh

For the mesh, tetrahedron solid elements were used on the tube thickness with a global imposed size of 3 mm. it's a mesh adequately thick and it generated a large number of nodes, but unfortunately it wasn't possible to create a coarser mesh with refinements only in few parts.

7.3.2 Boundary conditions

In this paragraph it's explained how the boundary conditions of constraints and forces were modelled due to reply the real configurations.

5.3.2.1 Calibration for horizontal load

In horizontal calibration, the constraints were represented vertically by the four wheels and horizontally by the two steel supports acting on the back tubes. In Ansys, the aim is to realize a carriage on the front wheels. Since the model was without wheels, two cones were added to the frame. They, with height of 55 mm, were positioned in the housing of the front casters in order to simulate the front forks (Figure 7.2a). The vertical displacement of the points of the two cones was suppressed, keeping the longitudinal and lateral displacements free. In order to recreate the constraints on the backrest, other two cones, with height of 5 mm, were modelled in correspondence of the contact points between the supports and the back tubes (Figure 7.2b). In this case, a fixed hinge was reproduced because in the field test the wheelchair didn't lie perfectly on all the support's surface, but only in one point, around that small rotations were possible, so the points of the cones on the backrest were fixed. The force was applied in the front of the bumper I longitudinal direction (Figure 7.2c). The sketch is visible in Figure 7.3.

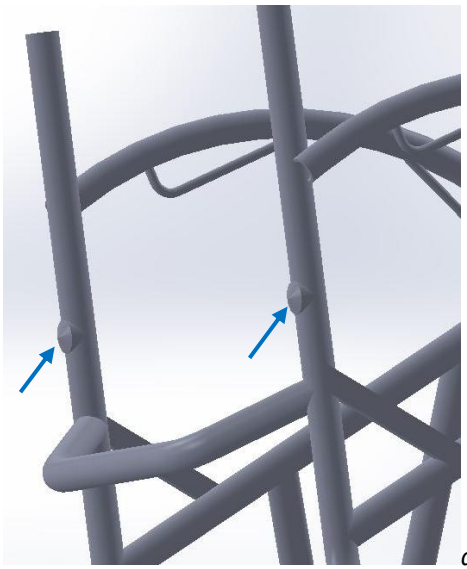

a)

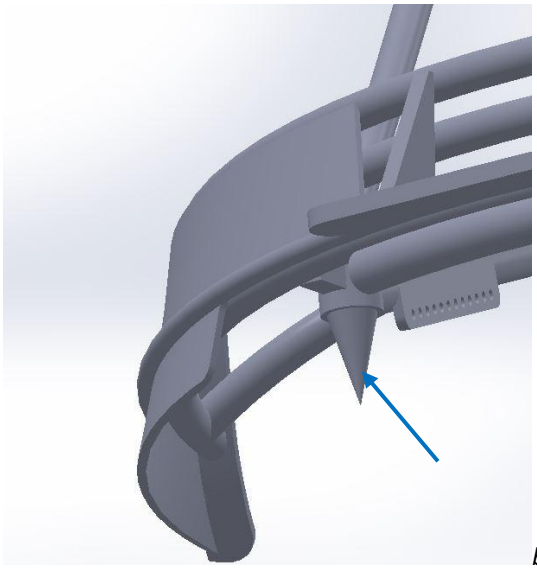

b)

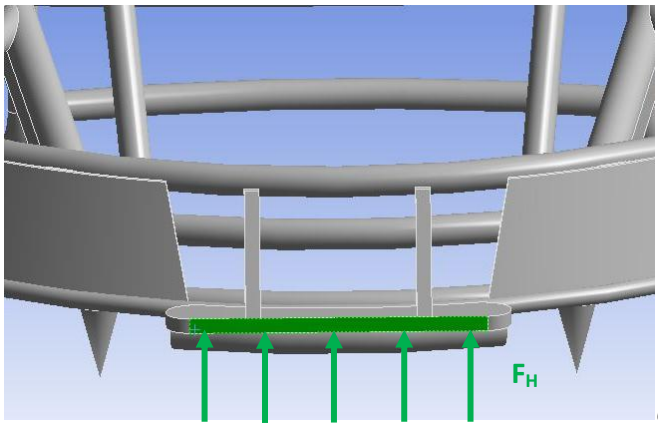

c)

***Figure 7.2**: Boundary conditions of horizontal calibration: a) back tubes cones b) front cones c) force horizontally applied on the bumper*

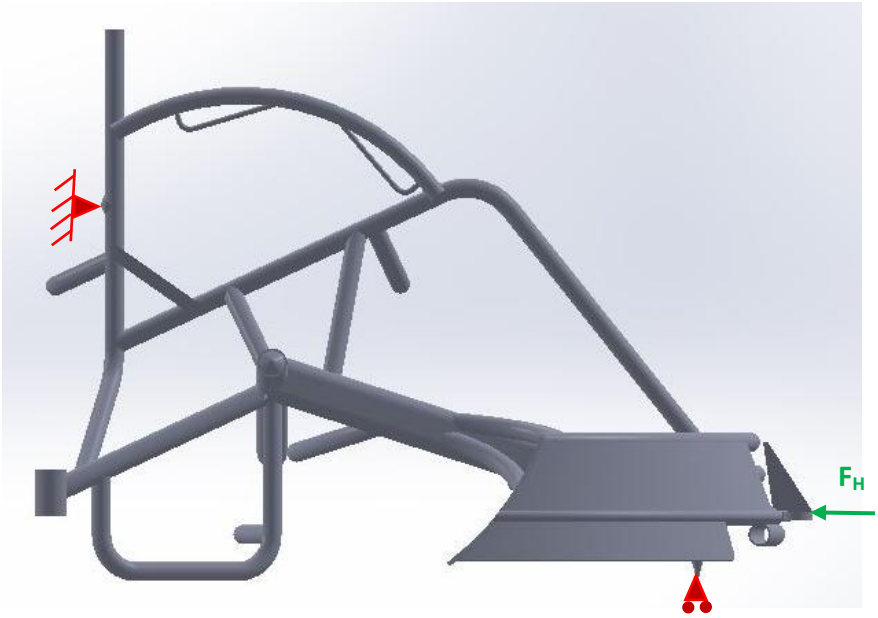

***Figure 7.3**: Sketch of the horizontal simulation*

5.3.2.2 Calibration for vertical load

In this calibration, the constraints were represented by the contact of the four wheels on the floor and the vertical force was applied on the seat with weights. As previous, in correspondence on the front casters two carriages were recreate, suppressing the vertical displacements of the front cones' points. Other two cones, with height of 5 mm, were built in correspondence of the rear main wheels' hubs (Figure 7.4a) and the vertical and longitudinal displacements of their points were suppressed. The force was distributed in vertical direction over the two seat tubes (Figure 7.4b), which support the seat. This configuration is shown in Figure 7.5.

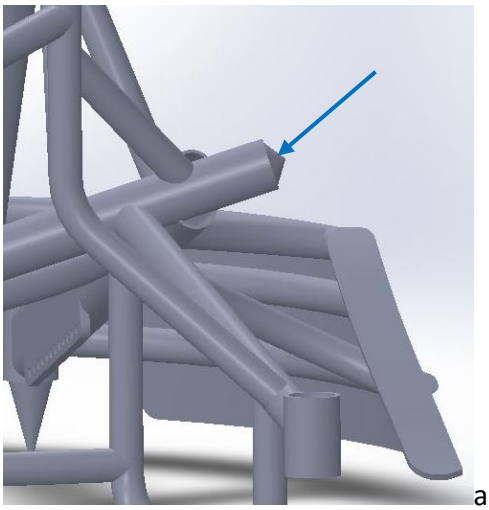
a)

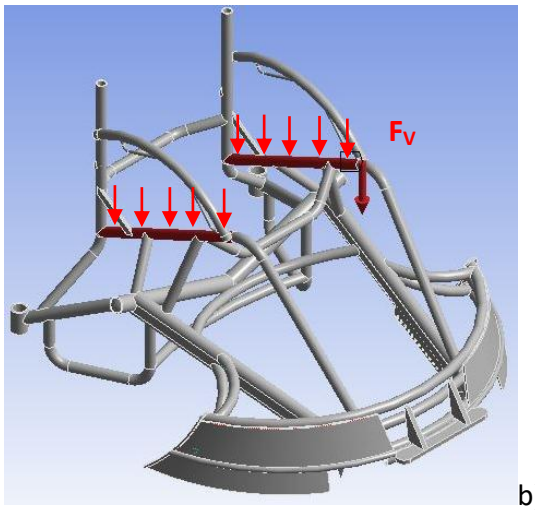

b)

Figure 7.4: Boundary conditions of vertical calibration: a) cones on rear axle b) force vertically applied on the seat tube

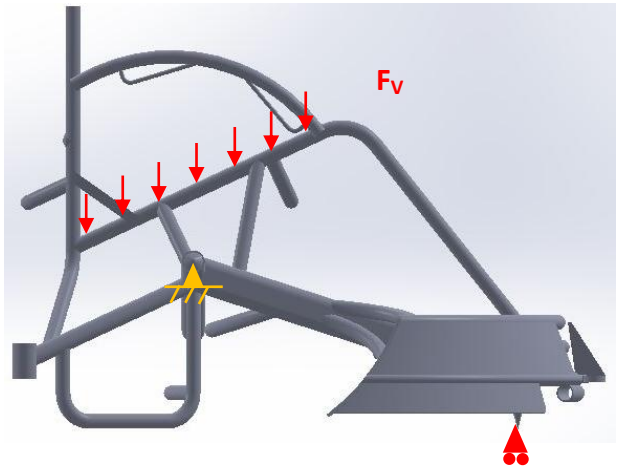

***Figure 7.5**: Sketch of the vertical simulation*

7.4 Data analysis

7.4.1 Local strain analysis

The aim of this part was to find the strain in strain gauges positions.

For the two different types of test, the strain of the frame was extracted in the exact points where the strain gauges were located. It wasn't possible to create paths on the model so the strain was analysed locally.

In correspondence of the three bending half bridges, the shape of the deformation was observed and superior and inferior fibres were defined with this connection: the stretched fibres were the superior and the compressed ones were inferior depending on the load condition. For the inferior fibres the maximum principal strain ε_1 was considered and for

the superior ones the minimum principal ε_3, extracted from the simulations' solution. This is an approximation, but it wasn't possible to extract the strain in the element's reference system. The total numerical strain ε_N was calculated as:

$$\varepsilon_N = \varepsilon_t - \varepsilon_c$$

with ε_t traction strain and ε_c compressive strain respectively for inferior and superior fibres.

Then the normal component ε_{nor} and the flexion component ε_{flex} of the strain were calculated with the following equations:

$$\varepsilon_{nor} = \frac{\varepsilon_t + \varepsilon_c}{2} \qquad \varepsilon_{flex} = \frac{\varepsilon_t - \varepsilon_c}{2}$$

The experimental strain was calculated from the calibrations data acquisition with the Wheatstone bridge's equation:

$$\varepsilon_{sghb} = \frac{\Delta V}{V} \cdot \frac{2}{K} \cdot \frac{1}{1000}$$

with K gauge factor and ΔV/V is the output signal in mV/V.

The total half bridge's experimental strain ε_{EXPhb} was found as.

$$\varepsilon_{EXPhb} = 2 \cdot \varepsilon_{sghb}$$

Instead, for the axial full bridge, the minimum principal strain ε_1 was extracted for both tube's side, internal and external, because this was subjected principally to a compressive load. The total bridge's numerical strain ε_{EXP} was found as.

$$\varepsilon_N = (1 + 0{,}33) \cdot \varepsilon_{int} + (1 + 0{,}33) \cdot \varepsilon_{ext}$$

The experimental strain was calculated with the Wheatstone bridge's equation:

$$\varepsilon_{sgfb} = \frac{\Delta V}{V} \cdot \frac{4}{2{,}66 \cdot K} \cdot \frac{1}{1000}$$

The total full bridge's experimental strain ε_{EXPfb} was calculated as.

$$\varepsilon_{EXPfb} = 2{,}66 \cdot \varepsilon_{sgfb}$$

Then the percentage error was defined as.

$$e_{\%} = \left| \frac{\varepsilon_N - \varepsilon_{EXP}}{\varepsilon_{EXP}} \right|$$

7.4.2 Stress analysis and prediction factor's definition

7.4.2.1 Horizontal load configuration

For this configuration, the axial full bridge on the main tube was considered because it is the best that reacts to horizontal frontal force. In its position, the minimum principal stress σ_3 was extracted in the internal and external tube's faces because it is subjected to a compressive load. The numerical normal stress acting on this part of the main tube was calculated as:

$$\sigma_N = \frac{\sigma_{1int} + \sigma_{1ext}}{2}$$

This stress is taken as reference for defining a prediction factor for horizontal load K_H. It puts in relation the equivalent Von Mises stress of other investigated points of the frame with this compressive stress acting on the main tube. It's definition is:

$$K_{Hi} = \frac{\sigma_{VMi}}{\sigma_N}$$

7.4.2.2 Vertical load configuration

For the vertical configuration, the flexion stress on the main tube was calculated. From the solution, the minimum principal stress σ_3 value was extracted for the superior fibres and the maximum principal stress σ_1 value was extracted for the inferior fibres. In correspondence of the main tube's bending bridge, the flexion stress was:

$$\sigma_f = \frac{\sigma_{1low} - \sigma_{3sup}}{2}$$

With the analogue definition of the previous, also an prediction factor for vertical load K_V was defined. Its expression is:

$$K_{Vi} = \frac{\sigma_{VMi}}{\sigma_f}$$

Each point can have its prediction factor at the instant of the peak force, one for the vertical load and one for horizontal load. The purpose is to find the more stressed zones in the two configurations and for these calculating these factors. The K_H and K_v factors, obtained from the numerical simulations, allow to estimate the stress's values on the most critical frame's points from the measures made by the strain gauges, without the need to put other strain gauges in all these points.

7.5 Results

7.5.1 Local bridge strain comparison

7.5.1.1 Horizontal calibration

The second FEM analysis simulates the horizontal calibration. The compressive horizontal force applied has a value of 1500 N, as the maximum force acted in the calibration. The Figure 7.6 shows the deformed shape of the frame.

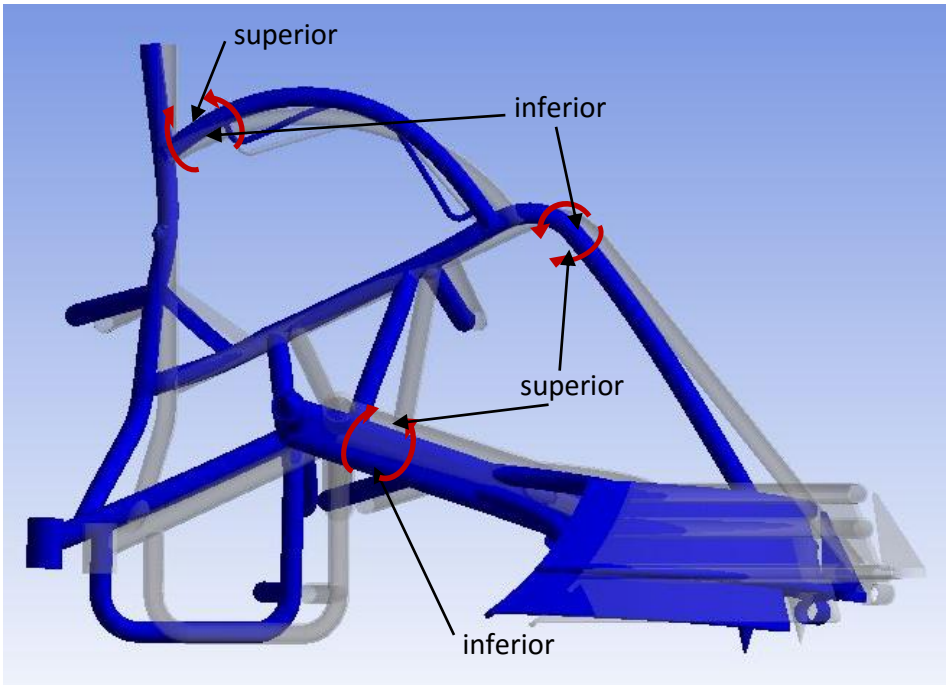

***Figure 7.6**: Deformed frame in horizontal simulation*

With the procedure described in the previous paragraph, it's possible to make the comparison between experimental and numerical strain and find the percentage errors. In Table 7.1 there are the results of this simulation.

EXPERIMENTAL STRAIN				
Bridge	Signal [mV/v]	mV/V -> me factor	ε_{sg} [me]	$\boldsymbol{\varepsilon_{EXP}}$ [me]
RST_BE	0,04543	0,0009756	4,432 e-05	**8,864 e-05**
RFT_BE	0,11341	0,0009479	1,075 e-04	**2,150 e-04**
RMT_BE	0,03901	0,0009479	3,697 e-05	**7,395 e-05**
RMT_AX	0,05967	0,0007127	4,253 e-05	**1,131 e-04**

NUMERICAL STRAIN						***% ERROR***
Bridge	ε_c [me]	ε_t [me]	$\boldsymbol{\varepsilon_N}$ [me]	ε_{nor} [me]	ε_{flex} [me]	$\boldsymbol{e_{\%}}$
RST_BE	-4,684 e-05	2,110 e-05	**6,794 e-05**	-1,287 e-05	3,397 e-05	***23,35****
RFT_BE	-1,424 e-04	7,324 e-05	**2,157 e-04**	-3,460 e-05	-1,078 e-04	***0,32***
RMT_BE	-4,197 e-05	3,503 e-05	**7,700 e-05**	-3,474 e-06	3,850 e-05	***4,12***
Bridge	ε_{int} [me]	ε_{est} [me]	$\boldsymbol{\varepsilon_N}$ [me]			***e%***
RMT_AX	-3,792 e-05	-3,994 e-05	**-1,036 e-04**			***8,46***

***Table 7.1**: Local bridge strain analysis*

7.5.1.2 Vertical calibration

The first FEM analysis simulates the vertical calibration, as previous described. The vertical force applied has a value of 910 N direct to the ground, as the maximum force acted in the calibration. The figure 7.7 shows the deformed shape of the frame.

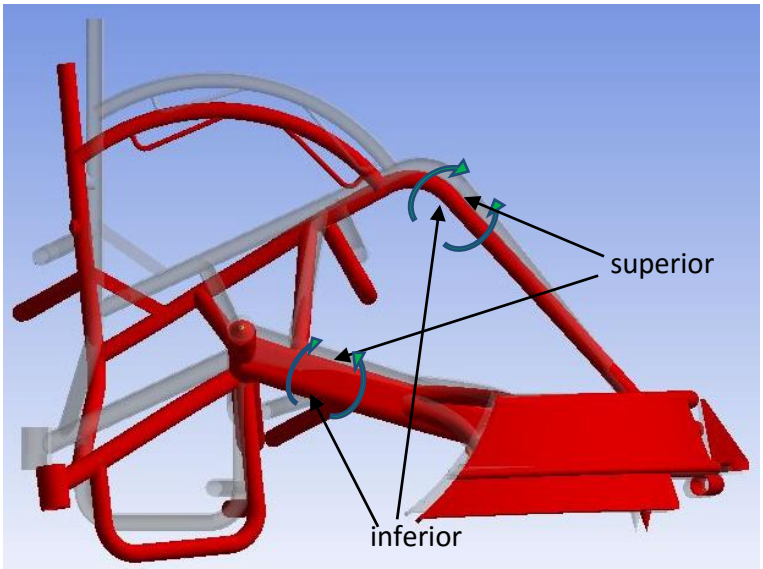

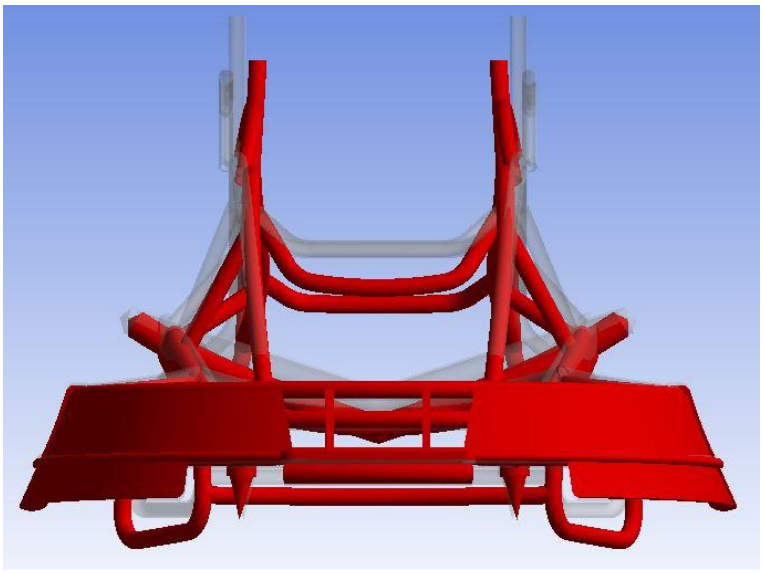

***Figure 7.7**: Deformed frame in horizontal simulation*

In Table 7.2 there are reported the results of the comparison.

EXPERIMENTAL STRAIN				
Bridge	Signal [mV/v]	mV/V -> me factor	ε_{sg} [me]	$\boldsymbol{\varepsilon_{EXP}}$ [me]
RFT_BE	0,02029	0,0009479	1,923 e-05	**3,847 e-05**
RMT_BE	0,04419	0,0009479	4,189 e-05	**8,378 e-05**

NUMERICAL STRAIN						***% ERROR***
Bridge	ε_c [me]	ε_t [me]	$\boldsymbol{\varepsilon_N}$ [me]	ε_{nor} [me]	ε_{flex} [me]	$\boldsymbol{e_{\%}}$
RFT_BE	-1,957 e-05	1,994 e-05	**3,950 e-05**	1,860 e-07	1,975 e-05	***2,68***
RMT_BE	-4,166 e-05	4,921 e-05	**9,087 e-05**	3,778 e-06	4,544 e-05	***8,47***

***Table 7.2**: Local bridge strain analysis*

It is possible to notice that each comparison between numerical and experimental values gives an error less than 10%, only the RST_BE has an upper error and this can be explained with the different section of the side tube between the real wheelchair and the 3D model. All the results are commented in the next chapter.

7.5.2 Global frame stress analysis

7.5.2.1 K_H horizontal prediction factor

The frame was subjected to 1500 N horizontal compressive force and the normal stress in the main tube in correspondence of the full axial bridge was calculated:

$$\sigma_N = \frac{\sigma_{1int} + \sigma_{1ext}}{2} = \frac{-3{,}45 - 3{,}05}{2} = -3{,}25\ MPa$$

Three most critical points were detected and their K_H prediction factor was calculated. In Figure 7.8 there are reported the positions of A, B, C.

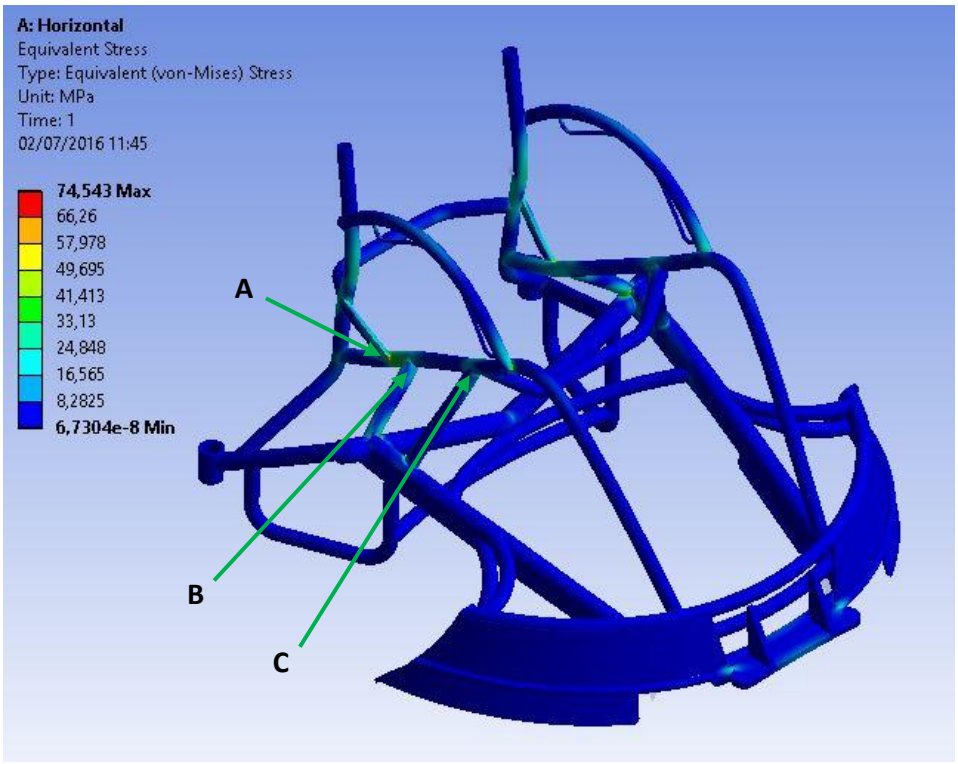

***Figure 7.8**: Positions of A, B, C points*

These are the points:

- Point A: it is on the connection between the seat tube and the seat stiffener (Figure 7.9)

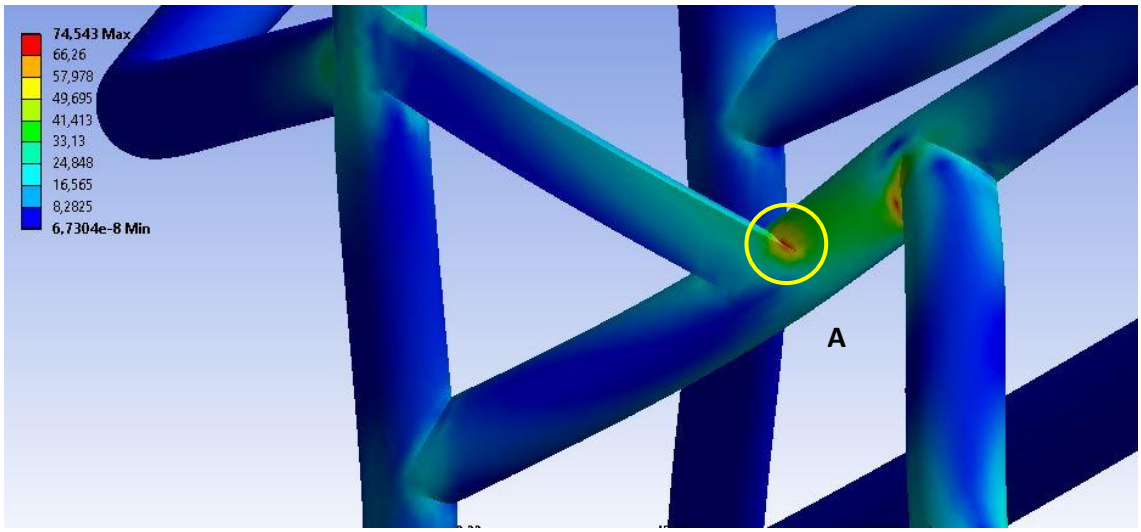

***Figure 7.9**: A position*

- Point B: it is near the connection between the seat tube and the rear strut (Figure 7.10)

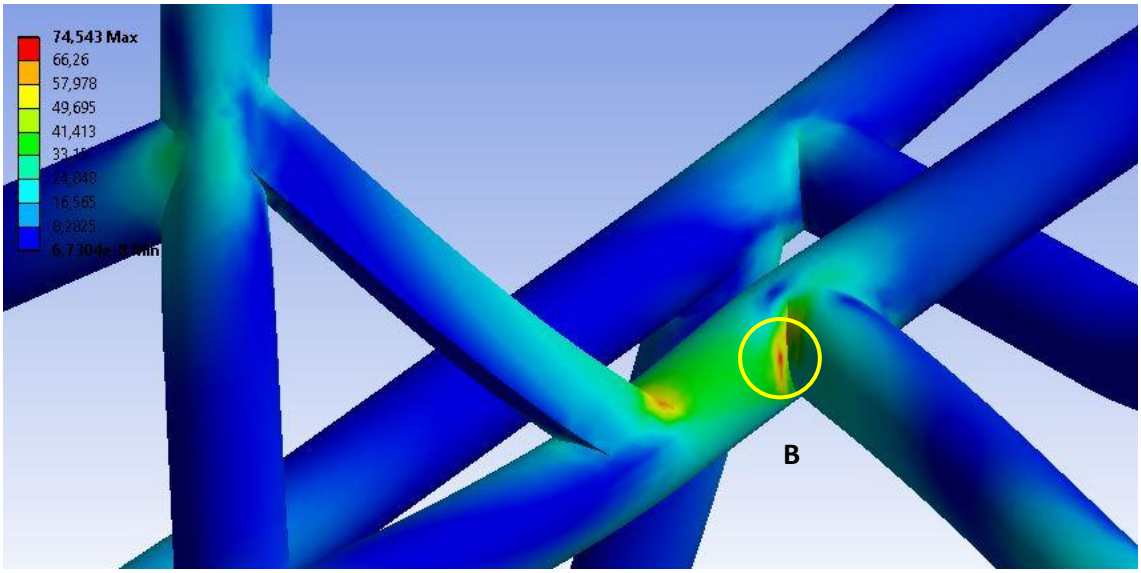

***Figure 7.10**: B position*

- Point C: it is on the connection between the seat tube and the front strut (Figure 7.11)

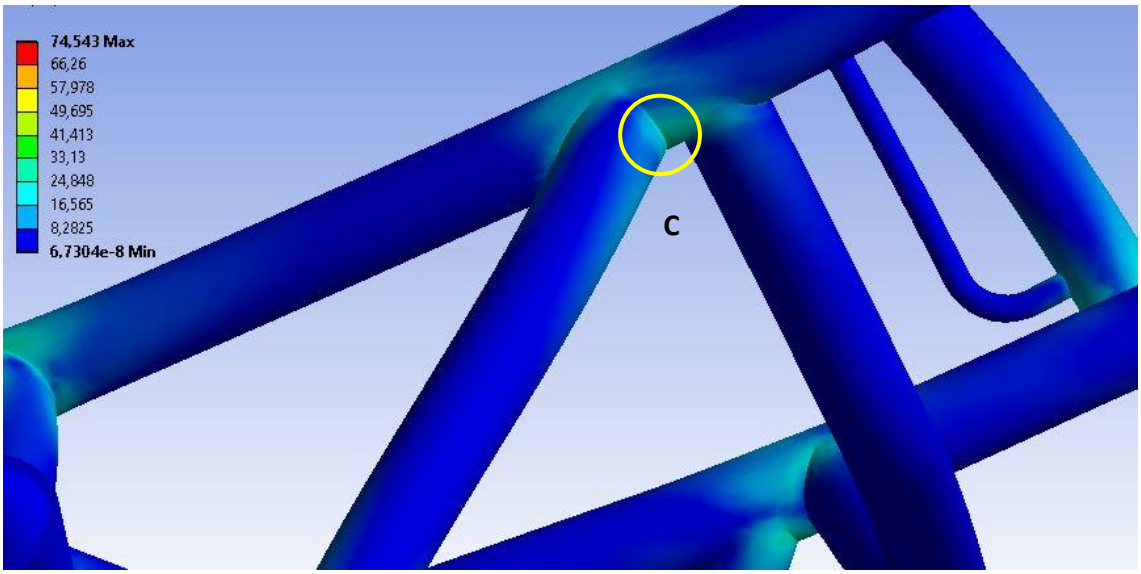

***Figure 7.11**: C position*

In Table 7.3 there are reported the value of the K_{Hi} horizontal prediction factors calculated as previously described.

Point	σ_{VM} [MPa]	K_V
A	71,02	***21,9***
B	70,13	***21,6***
C	27,21	***8,4***

***Table 7.3**: K_{Hi} horizontal prediction factors*

7.5.2.2 K_V vertical prediction factor

First, the flexion stress in correspondence of the bending half bridge on the main tube was calculated with 910 N vertically applied on the seat tubes.

$$\sigma_{fMT} = \frac{\sigma_{1low} - \sigma_{3sup}}{2} = \frac{3{,}32 - (-3{,}89)}{2} = 3{,}60\ MPa$$

Then the equivalent Von Mises stress was analysed for all he frame due to find the most stressed points. Six critical points were identified and in these the Von Mises stress maximum value was extracted. Below there is the description of the six critical zones. In Figure 7.12 there are reported the positions of M, N, P, Q, R, S.

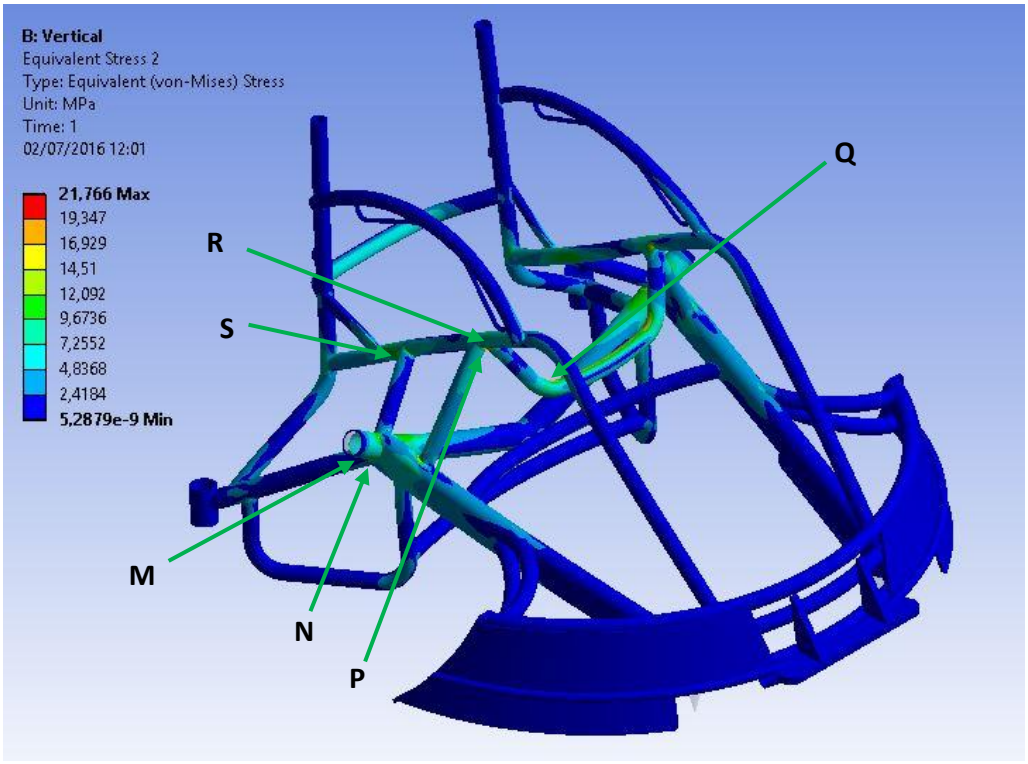

***Figure 7.12**: Positions of M, N, P, Q, R, S points*

These are the six points:

- Point M: it is in the connection zone between the main tube and the axle tube (Figure 7.13)

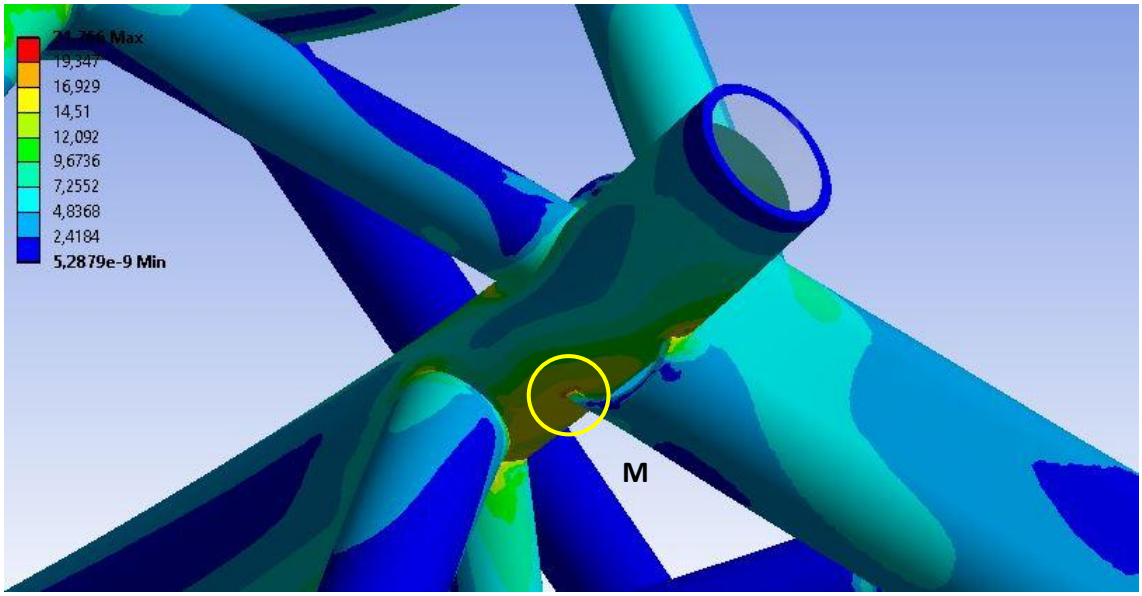

***Figure 7.13**: M position*

- Point N: it is in the connection zone between the axle tube and the rear U tube (Figure 7.14)

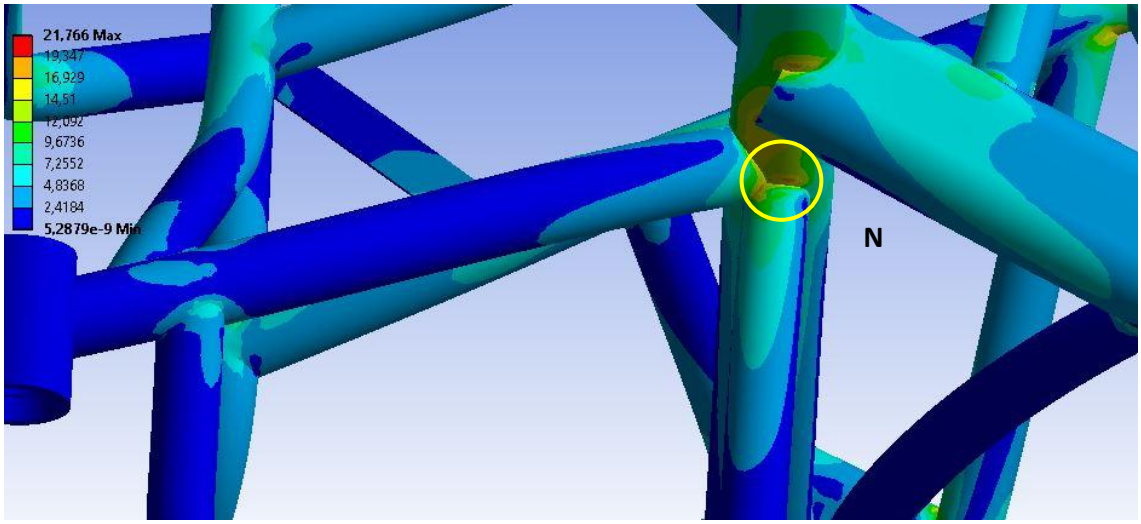

***Figure 7.14**: N position*

- Point P: it is located in the zone of the connection between the seat tube, front strut and seat U tube (Figure 7.15)

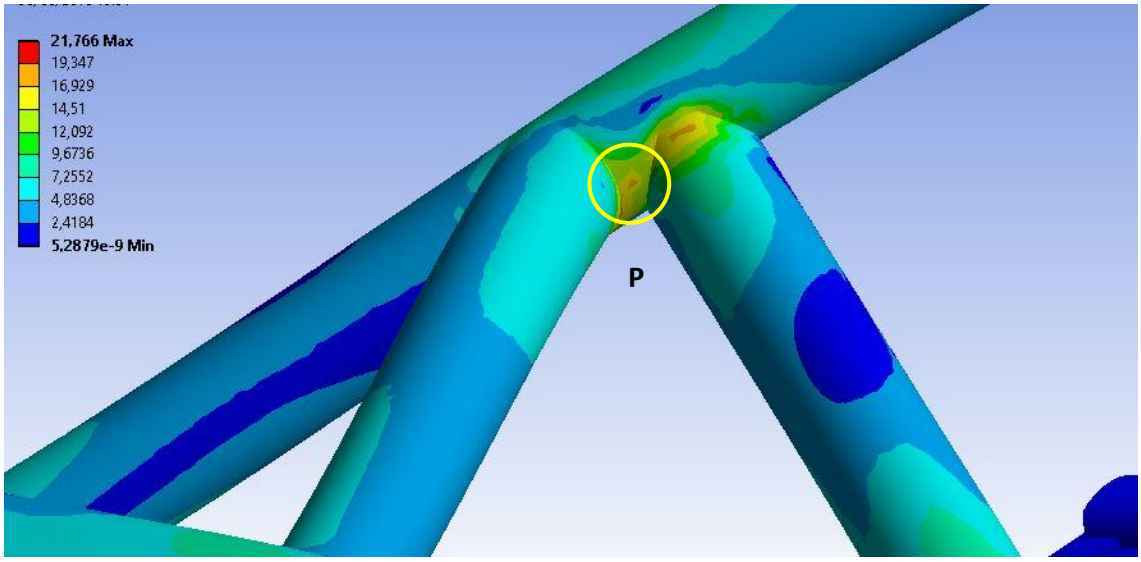

***Figure 7.15**: P position*

- Point Q: it is located on the internal faces of the bending of the seat U tube (Figure 7.16)

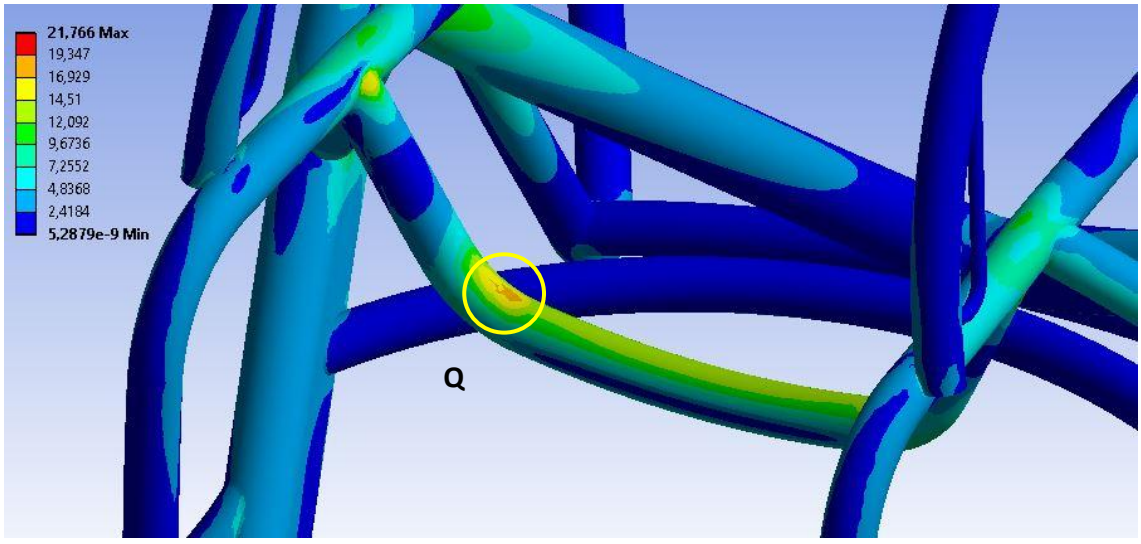

***Figure 7.16**: Q position*

- Point R: it is in correspondence of the connection between the seat tube and the seat U tube (Figure 7.17)

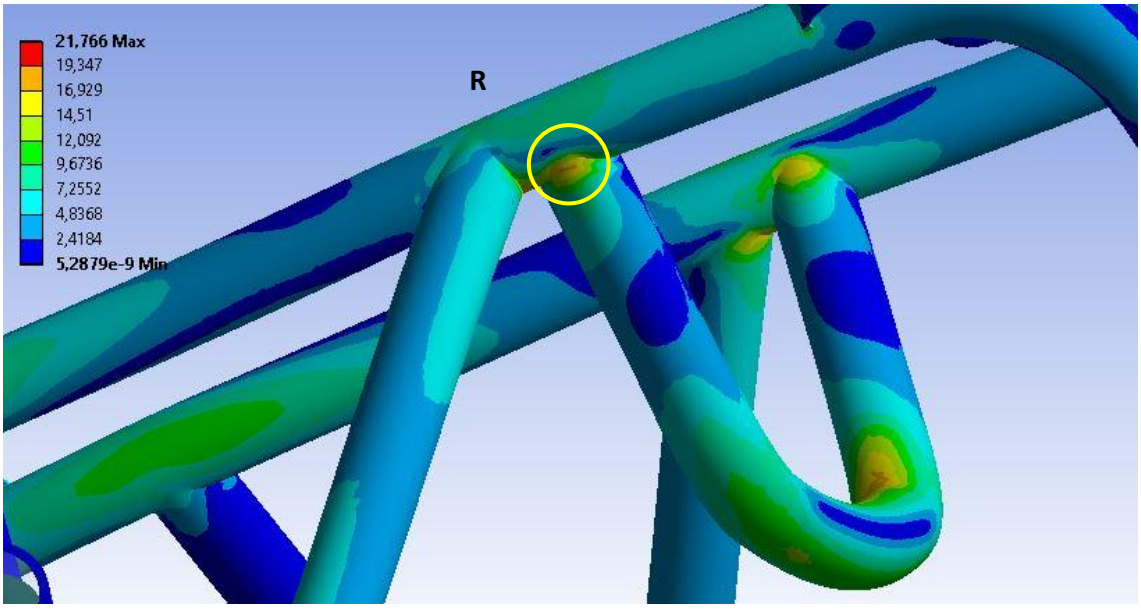

***Figure 7.17**: R position*

- Point S: it is located in the connection between the seat tube and the rear strut (figure 7.18)

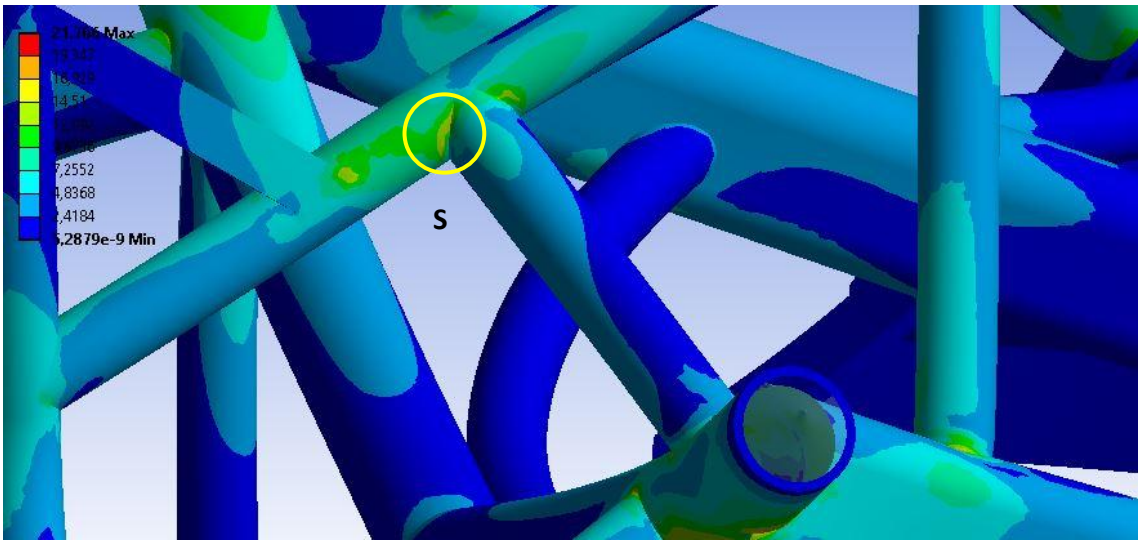

***Figure 7.18**: S position*

For these six points, the K_{Vi} prediction factors were calculated and they are reported in Table 7.4.

Point	σ_{VM} [MPa]	K_V
M	19,62	***5,4***
N	18,01	***5,0***
P	17,88	***5,0***
Q	18,01	***5,0***
R	17,61	***4,9***
S	15,01	***4,2***

***Table 7.4**: K_{Vi} prediction factors*

These prediction factors are useful future analysis, for instance the acquisition of the forces during a match. Their interpretation and future applications are discussed in the next chapter.

CHAPTER 8: DISCUSSION

One of the limitation of this study is that the 3D model used for FEM simulations doesn't perfectly correspond to the real wheelchair used for infield and laboratory tests. The section of the side tube in the model is circular and the real one is oval and the seat tube of the model is shorter than the real one. Moreover, the weld beads weren't modelled and this could influence the peak value of the local stress in the critical points. For instance the value in the M point is amplified by an interference between the axle and main tube. The model was provided directly by the builder and it wasn't so simple to modify it and create paths, which are the best method to study a specific zone. Moreover, the applied boundary conditions don't reflect exactly the real conditions.

The strain gauges were put on the wheelchair 4 months before having the possibility to make simulation with the 3D model. The magnitude of the involved forces and the behaviour of the frame were unknown and the bridges' positions were chosen observing trainings and matches. Moreover, the measurements during the impact tests were influenced by the propagation of shock waves which induce vibrations on the frame. This causes the impossibility to have useful acceleration's data.

8.1 Comparison between experimental and numerical results

With the calculation of the percentage error between the experimental and numerical strain, a correspondence can be verified. For the vertical load configuration, the errors of the two bridges considered are 2,68 % for RFT_BE and 8,47 % for RMT_BE. For the horizontal load configuration, the errors are 23,35 % for RST_BE, 0,32 % for RFT_BE, 4,12 % for RMT_BE and 8,46 % for RMT_AX. Values under 10 % can be considered acceptable, so the only one which doesn't respect this condition is the comparison in RST_BE point. This can be explained by the differences between the 3D model and the real wheelchair, mostly by the different section of the side tube, circular in the model and oval in the reality.

Overall we can say that the 3D model simulation corresponds in acceptable way to the real situation measured by the strain gauges.

8.2 Purpose of this work

The purpose of this work is to formulate a method to study the wheelchair's frame. From the literature, no research works were found which uses strain gauges for infield measurements, in all wheelchair's scope. The idea is to put instrumentation on the wheelchair and recreate different load situation in bench laboratory tests which simulate the infield loads and constraints configurations, for instance during a match situation, in this case a frontal hit. Making various calibrations, as many are the infield load configurations, permits to find calibrations constants for each case and they can be used to obtain the forces' values which the frame is subjected to during the test or a match.

The FEM analysis is needed to validate these measurements and for making a cross check between experimental and numerical results. Moreover, it is necessary to find the most stressed frame's points in order to calculate prediction factors for all these points different depending on the type of load.

These prediction factors are directly in relation with the frame's geometry and its different behaviour to different loads. They can be used to calculate the stress on the critical points during a specific test or during a match.

In Figure 8.1 the stress trend expressed in MPa for the main tube axial bridge obtained from the signal's acquisition of a quarter of a match is reported.

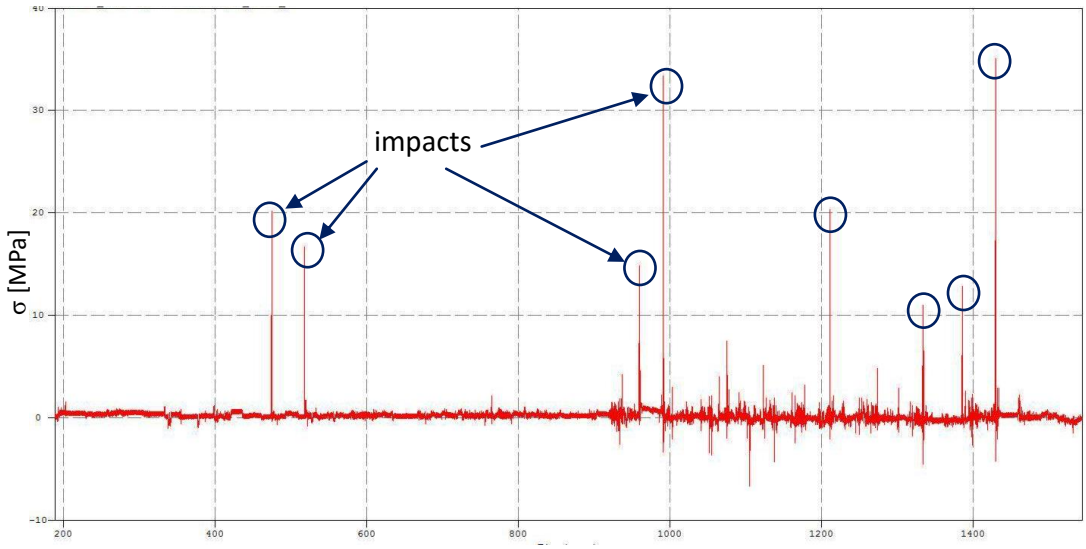

***Figure 8.1**: Axial stress in RMT_AX acquisition during a match*

From this trend, it is possible to obtain a stress spectrum and to recreate a loading history for all the critical points. This can permit to estimate the fatigue limit life and observing if there are yielding zone or crack origin. For instance, in this acquisition the maximum value of σ_N is 35 MPa. Using the K_H factors results:

Points	K_H factors	Local maximum stress [MPa]
A	21,9	***766,5***
B	21,6	***756***
C	8,4	***294***

***Table 8.1**: Local maximum stress in A, B, C in a hit*

The same thing can be done for the vertical load. During the impact test, the maximum value of the flexion stress acting on the main tube is 18,9 MPa, corresponding to a force of 5725 N. By the K_V factors, it's possible to calculate the local maximum stress in the critical points:

Points	K_V factors	Local maximum stress [MPa]
M	5,4	***102,1***
N	5,0	***94,5***
P	5,0	***94,5***
Q	5,0	***94,5***
R	4,9	***92,6***
S	4,2	***79,4***

***Table 8.2**: Local maximum stress in M, N, P, Q, R, S in a landing*

Calculating an estimation of the average number of the hit occurred during a match, all these measurements could permit to predict how many matches the wheelchair could play without having any problem.

This is also useful to study the critical zone with the possibility of redesigned some elements in order to minimize the stress peaks and lighten other part.

8.3 Future improvements

One improvement is certainly to create a model which reflects perfectly the real frame. So it will be possible to remake the FEM analysis and find prediction factors more accurate. Also making other types of calibration and studying of other boundary condition may improve the results. It will be interesting to analyse with FEM an impact, with a mass fastened to the backrest in order to simulate the body of the player.

FEM analysis together with the performance measurements can permit to modify the frame due to make it lighter and realize a more manoeuvrable wheelchair to give to the Italian National Wheelchair Rugby Team.

APPENDIX A: HBM STRAIN GAUGES Y SERIES CATALOGUE [16]

Series Y

with 1 measuring grid / linear SG

LY41
Linear SG
Temperature response matched to steel with α = 10.8 · 10⁻⁶/K (6.0 · 10⁻⁶/°F)

LY43
Temperature response matched to aluminum with α = 23 · 10⁻⁶/K (12.8 · 10⁻⁶/°F)

LY4x
Temperature response matched to customer's choice see page 16

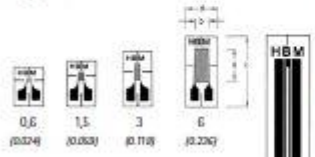

Illustrations show actual size
(Data: grid length in mm/inch)

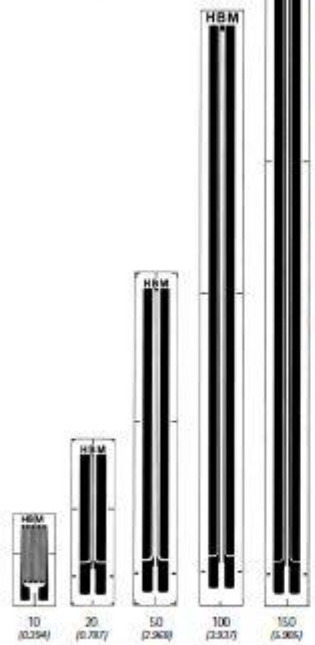

Contents per package: 10 pcs.

Types available ex stock		Variants	Nominal resistance	Dimensions (mm/inch)				Max. perm. effective bridge ex. voltage	Solder terminals [1]
				Measuring grid		Measuring grid carrier			
Steel	Aluminum	Other	Ω	a	b	c	d	V	
1-LY41-0.6/120		1-LY4x-0.6/120[2]	120	0.6 0.024	1.1 0.043	6 0.236	4 0.157	1.5	LS5
1-LY41-1.5/120		1-LY4x-1.5/120	120	1.5 0.059	1.2 0.047	7 0.276	5 0.197	2.5	LS5
1-LY41-3/120	1-LY43-3/120	1-LY4x-3/120	120	3 0.118	1.2 0.047	8 0.315	5 0.197	3.5	LS5
		1-LY4x-3/120A	120	3 0.118	1.2 0.047	8 0.315	5 0.197	3.5	LS5
1-LY41-6/120	1-LY43-6/120	1-LY4x-6/120	120	6 0.236	2.7 0.106	13.9 0.547	5.9 0.232	8	LS5
1-LY41-6/120A		1-LY4x-6/120A	120	6 0.236	2.7 0.106	13.9 0.547	5.9 0.232	8	LS5
1-LY41-10/120		1-LY4x-10/120	120	10 0.394	4.9 0.193	18 0.709	8 0.315	14	LS5
		1-LY4x-10/120A	120	10 0.394	4.9 0.193	18 0.709	8 0.315	14	LS5
1-LY41-20/120		1-LY4x-20/120	120	20 0.787	0.5 0.020	51.8 1.362	8.2 0.323	6.5	LS5
1-LY41-50/120		1-LY4x-50/120	120	50 1.969	0.01 0.031	63.6 2.504	8.2 0.323	12	LS5
1-LY41-100/120		1-LY4x-100/120	120	100 3.937	1 0.039	114.8 4.520	8.2 0.323	19	LS5
1-LY41-150/120		1-LY4x-150/120	120	150 5.906	1.2 0.047	165.6 6.520	8.2 0.323	25	LS5
1-LY41-1.5/350		1-LY4x-1.5/350[3]	350	1.5 0.059	2.3 0.091	8.2 0.323	5.9 0.232	6.5	LS5
1-LY41-3/350	1-LY43-3/350	1-LY4x-3/350	350	3 0.118	2.2 0.098	10.9 0.429	5.9 0.232	9	LS5
1-LY41-3/350A		1-LY4x-3/350A	350	3 0.118	2.2 0.098	10.9 0.429	5.9 0.232	9	LS5
1-LY41-6/350	1-LY43-6/350	1-LY4x-6/350[2]	350	6 0.236	2.8 0.110	13.9 0.547	5.9 0.232	15	LS5
		1-LY4x-6/350A	350	6 0.236	2.8 0.110	13.9 0.547	5.9 0.232	15	LS5
1-LY41-10/350		1-LY4x-10/350	350	10 0.394	5 0.197	18 0.709	8 0.315	24	LS5
		1-LY4x-10/350A	350	10 0.394	5 0.197	18 0.709	8 0.315	24	LS5
1-LY41-3/700	1-LY43-3/700	1-LY4x-3/700	700	3 0.118	2.7 0.106	10.9 0.429	5.9 0.232	13	LS5
1-LY41-6/700		1-LY4x-6/700	700	6 0.236	4.5 0.177	13.9 0.547	5.9 0.232	23	LS5
		1-LY4x-10/700	700	10 0.394	5 0.197	18 0.709	8 0.315	33	LS5
		1-LY4x-3/1000[4]	1,000	3 0.118	2.7 0.106	10.9 0.429	5.9 0.232	16	LS5
1-LY41-6/1000		1-LY4x-6/1000	1,000	6 0.236	4.2 0.165	13.9 0.547	5.9 0.232	27	LS5
		1-LY4x-10/1000	1,000	10 0.394	5 0.197	18 0.709	8 0.315	40	LS5

[1] Solder terminals are not compulsory
[2] With the temperature adaptation for quartz glass / composite (α=6) available ex stock (preferential gage)
[4] Types are only available with matching to aluminum, ferritic or austenitic steel

REFERENCES

[1] International Wheelchair Rugby Federation. IWRF Classification Manual. 3rd Edition; Revised 2015.

[2] International Wheelchair Rugby Federation. International Rules for the Sport of Wheelchair Rugby 2015.

[3] LHV van der Woude, HEJ Veeger, AJ Dallmeijer, TWJ Janssen, LA Rozendaal. Biomechanics and physiology in active manual wheelchair propulsion. *Medical Engineering & Physics* 2001; 23: 713-733.

[4] Y Vanlandewijck, DTheisen, D Daly. Wheelchair Propulsion Biomechanics: Implications for Wheelchair Sports. *Sports Med* 2001; 31(5):339-67.

[5] KT Assato, RA Cooper, RN Robertson, JF Ster. Smartwheels: development and testing of a system for measuring manual wheelchair propulsion dynamics. *IEEE Trans Biomed Eng* 1993; 40: 1320-4.

[6] HEJ Veeger, LHV van der Woude, RH Rozendal. Load on the upper extremity in manual wheelchair propulsion. *J Electromyogr Kinesiol* 1991; 1 (4): 270-80.

[7] HW Wu, FC Su. An instrumented wheel for the kinetic analysis of wheelchair propulsion. *J Biomed Eng* 1998; 120:533-5.

[8] K Roeleveld, E Lute, HEJ Veeger, T Gwinn, LHV van der Woude. Power output and technique of wheelchair athletes. *Adapt Phys Act Quart* 1994; 11(1):71–85.

[9] HEJ Veeger, EM Lute, K Roeleveld, LHV van der Woude. Differences in performance between trained and untrained subjects during a 30-s sprint test in a wheelchair ergometer. *Eur J Appl Physiol Occup Physiol* 1992;64(2):158-64.

[10] HEJ Veeger, LHV van der Woude. Force generation in manual wheelchair propulsion. In: XIII Southern Biomedical Engineering Conference, 1994:779-82.

[11] HEJ Veeger, LHV van der Woude. Force generation in manual wheelchair propulsion. In: H Van Coppenolle, Y Vanlandewijck, J Simons, et al., editors. Proceedings of the First European Conference on Adapted Physical Activity and Sports: a white paper on research and practice; 1994 Dec 18-20: Leuven. Leuven: Acco, 1995: 89-94.

[12] LY Guo, KD Zhao, FC Su, KN An. Moment generation in wheelchair propulsion. *Proc Inst Mech Eng H*. 2003;217(5):405-13.

[13] WJ Rankin, AM Kwarciak, WM Richter, RR Neptune. The influence of altering push force effectiveness on individual muscle demand during wheelchair propulsion. *J Biomech.* 2010; 43(14): 2771–2779.

[14] AJ Dallmeijer, LHV van der Woude, HEJ Veeger, AP Hollander. Effectiveness of force application in manual wheelchair propulsion in persons with spinal cord injuries. *Am J Phys Med Rehabil* 1998; 77 (3): 213-21.

[15] AJ Dallmeijer, YJ Kappe, HEJ Veeger, TW Janssen, LH van der Woude. Anaerobic power output and propulsion technique in spinal cord injured subjects during wheelchair ergometry. *J Rehabil Res Dev* 1994; 31 (2): 120-8.

[16] HBM Strain Gauges Catalogue, 2015

RINGRAZIAMENTI

Ringrazio prima di tutto la mia famiglia, Mauro, Cristina e Luca, perché senza di loro questo traguardo non sarebbe stato possibile, per avermi sostenuto in tutti questi anni e per aver capito i momenti delicati durante la mia carriera.

In secondo luogo ci tengo a ringraziare il prof. Petrone con il quale è stato un piacere lavorare e dal quale ho imparato molto, sia dal punto di vista professionale che umano. Inoltre ringrazio il dott. Giuseppe Marcolin e tutti i miei colleghi del laboratorio di Costruzioni di Macchine del DII per avermi consigliato e assistito durante la realizzazione di questo lavoro e ing. Daniela D'Onofrio della ditta OffCarr per avermi fornito con disponibilità del materiale fondamentale per questo lavoro.

Un grande grazie va anche alla mia allenatrice Federica che ha saputo rispettare pazientemente le esigenze che ha richiesto il conseguimento di questo titolo, soprattutto in un anno come questo così denso di obiettivi.

Ringrazio poi tutta la squadra del Wheelchair Rugby per la disponibilità e la simpatia e per avermi dato la possibilità di lavorare in un ambito che mi entusiasma molto.

E per finire un grande e sentito grazie va a Maria Laura con la quale ho collaborato durante tutta la realizzazione di questo lavoro. Il suo aiuto è stato di fondamentale importanza e insieme siamo riusciti a superare i momenti difficili che si ponevano di fronte, come sensori o stagnature. Ho conosciuto una collega instancabile, ma soprattutto una persona vera con la quale spero di collaborare ancora in futuro.

Francesco